MULTIFUNCTIONAL PROPERTIES OF POLYMER FOAMS AND COMPOSITES

A THESIS SUBMITTED TO
THE GRADUATE SCHOOL OF NATURAL AND APPLIED SCIENCES
OF
MIDDLE EAST TECHNICAL UNIVERSITY

BY

MERVE ÖZKUTLU DEMİREL

IN PARTIAL FULFILLMENT OF THE REQUIREMENTS
FOR
THE DEGREE OF DOCTOR OF PHILOSOPHY
IN
CHEMICAL ENGINEERING

SEPTEMBER 2020

Approval of the thesis:

MULTIFUNCTIONAL PROPERTIES OF POLYMER FOAMS AND COMPOSITES

submitted by **MERVE ÖZKUTLU DEMİREL** in partial fulfillment of the requirements for the degree of **Doctor of Philosophy** i**n Chemical Engineering, Middle East Technical University** by,

Prof. Dr. Halil Kalıpçılar
Dean, Graduate School of **Natural and Applied Sciences** _____

Prof. Dr. Pınar Çalık
Head of the Department, **Chemical Engineering** _____

Prof. Dr. Göknur Bayram
Supervisor, **Chemical Engineering, METU** _____

Assoc. Prof. Dr. Çerağ Dilek Hacıhabiboğlu
Co-Supervisor, **Chemical Engineering, METU** _____

Examining Committee Members:

Prof. Dr. Halil Murat Aydın
Bioengineering, Hacettepe University _____

Prof. Dr. Göknur Bayram
Chemical Engineering, METU _____

Assoc. Prof. Dr. Erhan Bat
Chemical Engineering, METU _____

Assoc. Prof. Dr. İrem Erel Göktepe
Chemistry, METU _____

Assoc. Prof. Dr. Özcan Köysüren
Energy Engineering, Ankara University _____

Date: 16.09.2020

I hereby declare that all information in this document has been obtained and presented in accordance with academic rules and ethical conduct. I also declare that, as required by these rules and conduct, I have fully cited and referenced all material and results that are not original to this work.

Name, Last name : Merve Özkutlu Demirel

Signature :

ABSTRACT

MULTIFUNCTIONAL PROPERTIES OF POLYMER FOAMS AND COMPOSITES

Özkutlu Demirel, Merve
Doctor of Philosophy, Chemical Engineering
Supervisor: Prof. Dr. Göknur Bayram
Co-Supervisor: Assoc. Prof. Dr. Çerağ Dilek Hacıhabiboğlu

September 2020, 158 pages

Polymer foams are low-density materials that consist of solid and gas phases and are used for insulation and transportation applications. This study aims to produce poly(methyl methacrylate) (PMMA) foams with low density and improved thermal and mechanical properties using syntactic foam production and supercritical CO_2 ($scCO_2$) foaming methods.

Syntactic foams were produced dispersing 5, 10, and 15 wt.% hollow glass microspheres (HGMs) in the PMMA matrix. Using different HGM types based on their density, surface coating of the HGMs, and the hybrid syntactic foam approach by dispersing polyhedral oligomeric silsesquioxane (POSS) nanoparticles as a reinforcement material were considered to improve the morphology, density, thermal and mechanical properties. PMMA foams were obtained with $scCO_2$ processing in which CO_2 diffuses and dissolves in the polymer matrix with the aid of high pressure and the releasing of the CO_2 from the matrix forms the voids in the polymer matrix. The effects of foaming parameters: time, temperature, pressure, and venting rate as well as the addition of a CO_2-philic POSS nanoparticles on foam morphology in

terms of pore size and pore density, thermal properties, and density of the foams were investigated.

In syntactic foam studies, the density of the polymer was reduced by 10% with the addition of 15 wt.% high-density HGMs. Higher mechanical properties were also obtained using these HGMs. Surface coating of the HGMs and the hybrid syntactic foam approach by dispersing POSS nanoparticles as a reinforcement material improved the flexural strength by 12% and 15%, respectively. In $scCO_2$ foaming studies, the average pore diameter of PMMA foam, which was processed at 35ºC, 32 MPa for 24 h and depressurized with fast venting rate, decreased from 1.1 to 0.3 µm with the addition of 5 wt.% POSS nanoparticles. PMMA syntactic foams containing 5 wt.% HGM and 5 wt.% POSS, processed with $scCO_2$ at 35ºC, 11 MPa for 24 h and depressurized with fast venting rate, had bimodal pore structure with the ratio of the diameters of the larger pores to smaller pores of 154.

Keywords: Poly(methyl methacrylate), Syntactic Foams, Hollow Glass Microspheres, Supercritical Carbon Dioxide Foaming, Polyhedral Oligomeric Silsesquioxanes

ÖZ

POLİMER KÖPÜKLERİNİN VE KOMPOZİTLERİNİN ÇOKLU FONKSİYONEL ÖZELLİKLERİ

Özkutlu Demirel, Merve
Doktora, Kimya Mühendisliği
Tez Yöneticisi: Prof. Dr. Göknur Bayram
Ortak Tez Yöneticisi: Doç. Dr. Çerağ Dilek Hacıhabiboğlu

Eylül 2020, 158 sayfa

Polimer köpükler, katı ve gaz fazlarından oluşan ve yalıtım ve taşımacılık uygulamaları için kullanılan düşük yoğunluklu malzemelerdir. Bu çalışmada, düşük yoğunluklu ve geliştirilmiş ısıl ve mekanik özelliklere sahip poli(metil metakrilat) (PMMA) köpüklerin sentaktik köpük üretimi ve süperkritik CO_2 ($skCO_2$) köpüklendirme yöntemleri kullanılarak üretilmesi amaçlanmıştır.

Sentaktik köpükler, PMMA matriks içerisinde ağırlıkça %5, 10 ve 15 oranında içi boş cam mikroküreler (HGM'ler) dağıtılarak üretilmiştir. Yoğunluklarına göre farklı HGM tiplerinin kullanılması, HGM'lerin yüzeylerinin kaplanması ve katkı malzemesi olarak polihedral oligomerik silseskuioksan (POSS) nanoparçacıklar dağıtılarak hibrit sentaktik köpük elde edilmesi morfoloji, yoğunluk, ısıl ve mekanik özelliklerin geliştirilmesi için düşünülmüştür. CO_2'nin yüksek basınçta matriks içerisine difüz edip çözünmesi ve CO_2 salınımıyla matriks içerisinde gözeneklerin oluşmasını içeren $skCO_2$ köpüklendirme ile PMMA köpükler elde edilmiştir. Süre, sıcaklık, basınç ve basınç tahliyesi hızı gibi köpüklendirme parametrelerinin ve CO_2 seven POSS nanopartikülleri eklenmesinin köpüklerin gözenek çapı ve gözenek

yoğunluğu gibi köpük morfolojisi, ısıl özellikleri ve yoğunlukları üzerindeki etkileri incelenmiştir.

Sentaktik köpük çalışmalarında, ağırlıkça %15 oranında yüksek yoğunluklu HGM'lerin eklenmesiyle, polimerin yoğunluğu %10 azalmıştır. Daha yüksek mekanik özellikler yine bu HGM'lerin kullanılmasıyla elde edilmiştir. HGM'lerin yüzey kaplaması ve hibrit sentaktik köpük yaklaşımı, eğilme mukavemetini sırasıyla %12 ve %15 artırmıştır. $SkCO_2$ köpüklendirme çalışmalarında, 35ºC, 32 MPa'da 24 saat sürede proses edilen ve hızlı basınç tahliyesi yapılmış PMMA köpüklerin ortalama gözenek çapı, ağırlıkça %5 POSS nanoparçacıklarının eklenmesiyle 1.1'den 0.3 µm'ye düşmüştür. $SkCO_2$ köpüklendirme yöntemi ile 35ºC, 32 MPa'da 24 saat sürede proses edilen ve hızlı basınç tahliye koşulunda geri basınçlandırılan, ağırlıkça %5 HGM ve %5 POSS içeren PMMA sentaktik köpükler, büyük gözeneklerin çapının küçük gözeneklerin çapına oranının 154 olduğu iki farklı gözenek büyüklüğü dağılımlı yapıya sahip olmuştur.

Anahtar Kelimeler: Poli(metil metakrilat), Sentaktik Köpükler, İçi Boş Cam Mikroküreler, Süperkritik Karbondioksit Köpüklendirme, Polihedral Oligomerik Silseskuioksan

To the future

ACKNOWLEDGMENTS

I wish to express my deepest gratitude to,

My thesis advisor Prof. Dr. Göknur Bayram, for her guidance, endless support, motivation, and patience throughout my studies,

My thesis supervisor Assoc. Prof. Dr. Çerağ Dilek, for her guidance, advices, encouragements and insight throughout the research,

My thesis committee members Assoc. Prof. Dr. Erhan Bat and Assoc. Prof. Dr. İrem Erel Göktepe for sharing their invaluable consideration,

Graduate School of Natural and Applied Sciences of the Middle East Technical University for financial support [Grant numbers: BAP-07-02-2014-007-735, BAP-07-02-2017-004- 198 and DKT-304-2018-3729].

Batuhan Demirel, for just being there every time I look at...

My most favorite doctor, Fatma Şahin, who makes me believe in the necessity of going over the Fogler, just kidding, for everything, my most favorite neighbor, Merve Sarıyer, for all the time we shared.My goddess, Seda Sivri, for all the songs we sang, my unbreakable optimist, Ezgi Yavuzyılmaz, for all the advices she gave...

My dear lab mates, Elif Topçuoğlu, Almira Çaldıklıoğlu, Berrak Erkmen, Selin Şahin, Beril Dumanlılar, Yağmur Çulhacıoğlu, Ezgi Gözde who make working cheerful,

All the people who make me feel as I came home every time I encountered in the department, Elif İrem Şenyurt, Aslı Karausta, Nisa Erişen, Soner Yaşar, Nur Ber Emerce, Canan Aksoy, Zeynep İmir, Atalay Çalışan, Mustafa Aslan, Burak Akdeniz, Berkan Atman, Özge Batır, Gülbin Tanrıseven, Arzu Arslan, Zeynep Karakaş, Melis Kargılı, İlker Şener, Çağla Bozcuoğlu, Oğuzhan Sarıyer, Orhun Kahraman, Veysi Helvacı,

My dearest friends, Ayşe Savaş, Gülşah Ercan, Elifhan & Mert Tuzcu, Aslı Ulutürk,

My friends from air, Gülten Kafadar, Büşra Aykaç, Betül Konca, Taner Astarlıoğlu, Derya Kaynar, Gökçe Özgül, Büşra Rakop,

Süleyman Kuşhan, İsa Çağlar, Gazi Saranay, Cemil Araçlı and Mihrican Açıkgöz for their technical help,

My dear father, Ali Ferhat Özkutlu, the most beautiful mom of the world, Gülseren Özkutlu, and my brand new engineer Feridun Can Özkutlu, who always support me and believe in everything I do,

To all the beautiful people of my huge family,

And to the most beautiful cat, Songül.

TABLE OF CONTENTS

LIST OF TABLES

TABLES

LIST OF FIGURES

FIGURES

LIST OF ABBREVIATIONS

ABBREVIATIONS

ABS	Acrylonitrile-butadiene-styrene copolymer
CFCs	Chlorofluorocarbons
DOE	Design of experiment
DSC	Differential scanning calorimetry
EDX	Energy dispersive x-ray
EPR	Ethylene-propylene rubber
FGMs	Functionally graded materials
FTIR	Fourier transform infrared spectroscopy
H	Hollow glass microspheres
HD-HGM	High density hollow glass microspheres
HD-HGM-C	PMMA-coated hollow glass microspheres
HD-HGM-S	Silane treated hollow glass microspheres
HDPE	High-density polyethylene
HGM	Hollow glass microspheres
IB	Octaisobutyl POSS
LD-HGM	Low density hollow glass microspheres
LOI	Limiting oxygen index
MD-HGM	Medium density hollow glass microspheres
MMA	Methyl methacrylate monomer
P	Octaphenyl POSS
PC	Polycarbonate
PCL	Poly(e-caprolactone)
PE	Polyethylene
PET	Poly(ethylene terephthalate)
PLGA	Poly(lactide-co-glycolide)
P_LLA	Poly(L-lactic acid)

PMMA	Poly(methyl methacrylate)
POSS	Polyhedral oligomeric silsesquioxanes
PP	Polypropylene
$ScCO_2$	Supercritical CO_2
SCFs	Supercritical fluids
SEM	Scanning electron microscopy
TGA	Thermal gravimetric analysis
TMS	Octatrimethylsiloxy POSS
USD	United states dollar
UV	Ultra violet
γ-MPS	γ-methacryloxypropyltrimethoxysilane

LIST OF SYMBOLS

SYMBOLS

Tg	Glass transition temperature
a	Mark-Houwink-Sakurada constant
A	Area of the SEM image
D_{av}	Average pore diameter
F	Fast venting rate
K	Mark-Houwink-Sakurada constant
L/D	Length/ diameter
M	Magnification factor of the SEM image
M_v	Viscosity average molecular weight
N	Number of pores on the SEM image
N_v	Pore density
p-value	Probability
S	Slow venting rate
$T_{5\%}$	Temperature at 5% weight loss
T_{max}	Temperature at maximum weight loss
V_{HGM}	Volume fraction of HGMs
wt.%	Weight percent
$[\eta]$	Intrinsic viscosity
η_{inh}	Inherent viscosity
η_{red}	Reduced viscosity
ρ_{HGM}	Density of the HGMs
ρ_P	Density of the polymer
ρ_{theor}	Theoretical density of the composite

CHAPTER 1

INTRODUCTION

Polymer foams are attractive materials for the application field of insulation and buoyancy. Since they have a lower density than their bulk polymers, they are an economical alternative to their bulk polymers. Their fixed shape due to their rigidity leads them to be used in construction, marine, and aerospace applications. Besides, composite formation adds multifunctional properties to polymer foams which widen their application areas. The most common multifunctionalities are fire retardancy, electromagnetic interference shielding and thermal insulation [1]. Nowadays, the polymer foam industry which is frequently mentioned in thermal insulation and transportation is based on polymers such as polyurethane, polystyrene and epoxy. However, during the foaming and applications of these materials, components that are hazardous to human health and environment such as isocyanates, certain hazardous polyols, styrene, cumene and bisphenol A are formed. Therefore, producing thermoplastic foams with the properties of thermosets by a cost-effective method may lead to replacing thermoset foams with their thermoplastic counterparts. This study aims to enhance the mechanical and physical properties of thermoplastic foams and offers an inexpensive production method by using additives in the thermoplastic matrix.

There are several production methods for thermoplastic polymer foams. The extrusion foaming and the foam injection molding methods are the commercial methods in which polymers are blended with a physical foaming agent. When the mixture is heated, the foaming agent evaporates and forms voids in the polymer.

An alternative method for the foaming of thermoplastics is the syntactic foam production method. This method is based on dispersing hollow particle fillers (microspheres or microballoons) in a polymer matrix [2]. The main advantages of syntactic foams are their adjustable properties by changing the type, size, and weight fractions of hollow constituents. Another advantage of these materials is their higher mechanical properties when compared to the other closed-cell foams at the same density level [3]. Production of syntactic foams with low density and high mechanical properties is a challenging task. One important approach is to select the right microsphere type in terms of diameter, density and wall thickness. Besides, the optimum concentration of microspheres in the polymer matrix is also effective on the foam properties. Another approach to improve the properties of the syntactic foams is the surface modification of hollow microspheres which increases the compatibility between the matrix and the microspheres. Recently, syntactic foam studies focus on the production of hybrid syntactic foams with high mechanical properties and low density which are produced by dispersing a reinforcement material and hollow microspheres in the polymer matrix [4-7].

Another method for the production of thermoplastic polymer foams is the batch foaming of polymers with supercritical fluids (SCFs). In this method, a high-pressure vessel is used where polymers are introduced with supercritical carbon dioxide ($scCO_2$) which diffuses and solubilizes in the polymer matrix. After a sufficient amount of time, the pressure of the system is reduced readily and this rapid depressurization produces pores in the polymer [8]. The foaming parameters such as processing pressure, temperature, time, venting rate, and the polymer properties such as molecular weight, density, and presence of the pore inducer material are highly effective on the foam properties.

In this study, poly(methyl methacrylate) (PMMA) was chosen as a matrix material to produce thermoplastic polymer foams. Although based on our knowledge, there has been no industrial production of PMMA foams yet, it is thought that its use as the foam will be advantageous due to its high mechanical properties, high resistance

to UV light and water, low density, and biocompatibility [9]. $ScCO_2$ foaming and the syntactic foam production method were chosen to produce PMMA foams.

With the $scCO_2$ foaming method, PMMA foams with a density of 0.49 g/cm^3 were obtained [10]. In another study, PMMA foams with thermal conductivity of 0.0731 W/mK were also produced [11]. These properties are highly close to the properties of conventional thermal insulation foam materials. In this study polymer foams with small pore size and high pore density were targeted since improved mechanical properties can be obtained with the smaller pores. In syntactic foam studies, PMMA was used as the matrix material only once in 1982 by Kinra and Kerr [12]. Therefore, valuable information can be provided to literature by examining the benign properties of PMMA syntactic foams.

In this study, in order to improve the foam properties, polyhedral oligomeric silsesquioxanes (POSS) nanoparticles were used as reinforcement material in the syntactic foam production method and pore inducer in the $scCO_2$ foaming method. POSSs have inorganic siloxane cage structure with eight organic corner groups, thus they are three-dimensional inorganic/organic hybrid nanostructures. The general formula of the POSSs is $(RSiO1.5)_n$ in which R can be a hydrogen atom or a functional group that can be selected to have desired properties [13]. This unique structure of POSS allows enhancement in the foaming process since R can be chosen as a CO_2-philic group for the $scCO_2$ foaming method or compatible with PMMA for the syntactic foam production method.

This thesis study aims to investigate the PMMA foams which are produced using two different foaming techniques as well as their combination, which are syntactic foam production and batch foaming with supercritical CO_2. This study consists of five parts. In the first part, polymer syntactic foams with three different types of hollow glass microspheres were produced and the effects of microsphere type and the composition on syntactic foam properties in terms of their morphology, density, flexural strength, flexural modulus, impact strength, glass transition temperature and decomposition temperature were investigated. Also, the surface coating of the

microspheres was conducted to increase the compatibility between the polymer and the microspheres. In the second part of the study, hybrid PMMA syntactic foams were produced by using POSS nanoparticles as the reinforcement material and characterized by morphological, mechanical and thermal tests. In the third part, PMMA foams were produced with batch foaming method using $scCO_2$. The effect of process parameters such as pressure, temperature, time, venting rate and concentration of a highly CO_2-philic POSS used as a pore inducing material in the polymer matrix on the properties of foam was investigated. The fourth part includes the combination of these two methods to understand their synergistic effects on the foam properties. For this purpose, PMMA syntactic foams which were produced with hollow glass microspheres (HGMs) were batch foamed with $scCO_2$ to obtain bimodal pore structure. Bimodal pore structure consists of larger and smaller pores which are beneficial for several applications such as thermal and sound insulation and drug delivery. The bimodal pore structure was observed via morphology analysis. The density, thermal and mechanical properties of the foams were investigated. Finally, in the last part the selected specimens from syntactic foam and $scCO_2$ foaming studies were examined in terms of morphology, density, thermal and mechanical properties to understand the effects of the foaming method on the foam properties.

CHAPTER 2

BACKGROUND

2.1 Polymer Foams

Polymer foams are low-density materials that are composed of solid and gas phases. While the solid phase can be produced from thermoset or thermoplastic polymers, the gas phase is constructed by a physical or chemical blowing agent. There can also be a second solid phase that can be added to polymer foams as additives. The most attractive point about the polymeric foams is the reduction of the cost of the raw material due to their low densities especially when they are compared to bulk polymers. Higher volumes of materials can be obtained using a small amount of polymer due to the formation of voids in the matrix. Besides, their high strength to weight ratios, excellent thermal and sound insulation properties, low dielectric coefficients, and high energy or mass absorption capacities make them be used in many applications [14]. The main challenge in polymer foam production is to obtain a foam with low density, low coefficient of thermal conductivity without sacrificing from the mechanical properties [15].

Polymer foams can be classified based on their matrix type as thermoplastic and thermoset foams. Nowadays most of the polymer foam industry mainly depends on thermosets such as polyurethane and epoxy which are known to have adverse effects on the environment and human health [16]. However, thermoplastics foams have gained attention in the last decades. Polymer foams can also be classified based on their nature as flexible and rigid foams and, based on their structures as open-cell foams, where pores are interconnected to each other, and closed-cell, where pores

are independent of each other, their densities as low-density and high-density foams and their pore size as nano-cellular or micro-cellular foams [17].

2.1.1 Brief History of Polymer Foams

The polymer foam industry began with the extrusion foaming of polystyrene which was invented by Munters and Tandberg in 1931. It was followed by the foaming of polyurethane by Dow Chemical Company during the Second World War. At that time, polymer foams were used as coating materials for the protection of the other materials from weather conditions. The first thermoplastic foam was the polyethylene foam which was first introduced by F.L. Johnson in 1941. The insulation of the electrical cables was supplied by polyethylene foams. In 1949 epoxy foam took place in the market for the protection of electronic devices. After that, the foam industry was introduced with syntactic foams by the invention of phenolic microballoons in 1953. After the 1950s development of the foams that could withstand high temperatures gained attention such as silicon foams. Between the 1950s and 1970s, new technologies to produce polymer foams were developed and new types of polymeric materials started to be used as a polymer foam matrix. After the 1980s polymer foam industry focused on the production of environmentally benign polymer foams. Nowadays polymer foam industry uses almost any type of polymers to produce polymer foams with one or combination of several foam production methods [18]. The milestones in the development of the polymeric foams are given in Table 2.1.

Table 2.1 Highlights of polymeric foam developments [18].

Time	Contents	Authors or Companies
1931	Foamed Polystyrene	Munters and Tandberg
1937	Foamed Polyurethane (PU)	Dr. Otto Bayer
1941	Foamed Polyethylene	Johnson, F.L.
1944	Extruded Polystyrene Foam	Dow Chemical
1945	Rigid PU Foam	Germany
1952	Flexible PU Foam	Germany
1954	Expandable Bead	Stastney and Goeth
1959	Rigid PU Foam Produce	ICI
1962	PS Foam Injection Molding	Beyer et al.
1962	Extruded Ethylene Foam	Rubens et al.
1967	Twin Screw for Foam Brt. Pat. 1,152,306	Spa, L. M. P.
1967	ABS foam; Injection Mold	Woollard, D.
1968	Rigid Isocyanurate Foam	ICI
1972	Extruded Propylene Foam	Parrish, R. G. (DuPont)
1982	Accumulator Extrusion	Collins, F. (Valcour)
1984	PP Molded Foam Article	Japan Styrene Paper
1990	PET Foam Extrusion	Shell/Petlite®

2.1.2 Production Methods of Polymer Foams

There are several methods for producing polymeric foams. The production methods are divided into different groups based on the type of blowing agent. Chemical blowing agents are generally used for the foaming of thermosets where curing and foaming occur at the same time. Physical foaming agents can also be used for the foaming of thermosets. However, there are several concerns about the application of physical foaming agents. The mostly used physical foaming agents are chlorofluorocarbons (CFCs). They are known for their harmful effects on the ozone layer depletion [19]. Physical foaming agents are also used for the foaming of thermoplastics. Nevertheless, inert gases such as CO_2 and N_2 as the physical foaming agents have gained attention in the last decades.

For thermosets, the reactive foaming is commonly used where a chemical blowing agent is mixed with the thermoset polymers. The blowing agent and the polymer go

into exothermic reaction and with the help of heat addition, the porous structure is formed due to curing. The most common industrial method for this type of thermoset foams is the slabstock foaming method. In this method, the material mixture is moved by a conveyor where the conveyor goes into the heating unit and forms foam slabs with the dimensions of the walls of the conveyor. This continuous process supports the production of commercial polyurethane foam. The reactive foaming can also be conducted using extrusion, mold or injection molding devices. Conventional polystyrene foam is produced mostly using extrusion foaming or injection molding foaming with reactive foaming method [15].

Foaming of thermoplastics can be conducted via batch foaming, extrusion foaming and foam injection molding processes. Two phenomena are applied for the foaming of thermoplastics with the physical blowing agents. In the first one, the physical foaming agents are mixed with thermoplastics and with the help of heating, these physical agents decompose into the gas phase and form voids in the melted polymers. In the second one, usually, an inert gas such as CO_2 or N_2 is incorporated into the polymer with the aid of pressure and then the polymer is either heated to higher temperatures to form the pores while being depressurized or depressurized directly without heating by releasing the gas to atmospheric pressure which leads to the formation of the voids in the polymer matrix.

Foam extrusion of thermoplastics is a process that allows the foaming of the polymers continuously. The process consists of two steps as pressurization with the blowing gas (generally supercritical CO_2 and N_2) which creates gas/polymer mixture, and depressurization of the gas at the die which forms the pores [20]. In general, conventional extrusion equipment is needed to be adapted to the foaming process with the addition of a supercritical fluid injection system and modification of the screw and die [21]. The main advantage of the foam extrusion process is its continuity which enables it to produce foams in an economical way [22]. Another advantage of the foam extrusion process is that it is possible to create composite foams during the foaming without the pre-compounding processes.

The foam injection molding process is based on the injection of a gas (generally supercritical CO_2 or N_2)-polymer mixture into a mold and the expansion of the polymer by the pressure drop at the cavity [23]. The foam injection molding process ends up with a polymer foam with a specific shape with its pre-determined mold cavity [24]. Production of a polymer foam with the desired shape and the soft-touch surface are the main advantages of this process [25]. When it is compared with the other foaming methods, the foam injection molding process reduces the equipment and operation costs [26]. Besides, the foam injection molding process may improve some mechanical properties such as fatigue life and impact strength [27].

An alternative approach to polymer foam production methods is the syntactic foam production method. In this method, polymers are mixed with the hollow particles generally made from glass or polymer and form a porous structure. In this method the most important factor that affects the foam properties is the type and the concentration of these hollow microspheres.

Batch foaming of polymers with supercritical fluids (SCFs) is another widely used method for producing thermoplastic polymer foams. A high-pressure vessel is used to maintain the required foaming conditions for polymers. During the batch foaming process, a sufficient amount of SCF absorption reduces the glass transition temperature (Tg) of the polymer below the process temperature and generates a liquid polymer solution. This behavior is called the plasticization of the polymer. After the plasticization, the pressure of the system is reduced readily and this rapid depressurization produces pores in the polymer and the system becomes rigid [8]. Among the supercritical fluids, CO_2 is the most commonly used one for polymer processing because of its inexpensiveness and commercial availability [28]. The details of the method and the literature on this topic are discussed in the following chapters.

2.1.3 Applications of Polymer Foams

There are several application areas of polymeric foams. Rigid polyurethane and polystyrene are mainly used as thermal insulation and sound insulation materials in the construction and automotive industries. The rigid polymer foams are also used for packaging and transportation areas. The flexible foams are advantageous when the application requires high strength to environmental impacts. They are mainly used in marine structures, furniture, packages, sporting goods and textiles [19].

Figure 2.1 presents the polymer foam market size in the United States up until today and predictions for the future. In 2020 the polymer foam market had a value of 90.7 billion USD [29]. Also, it is expected that the compound annual growth rate of polymer foams will be 4% higher until 2025. Main consumers of polymer foams are the packaging, automotive, bedding, and furniture industries and these industries are searching for new types of polymer foams with enhanced properties in terms of density, thermal conductivity, and strength. Therefore, the polymer foam industry may consider this demand and put attention in research studies in order to increase their profits.

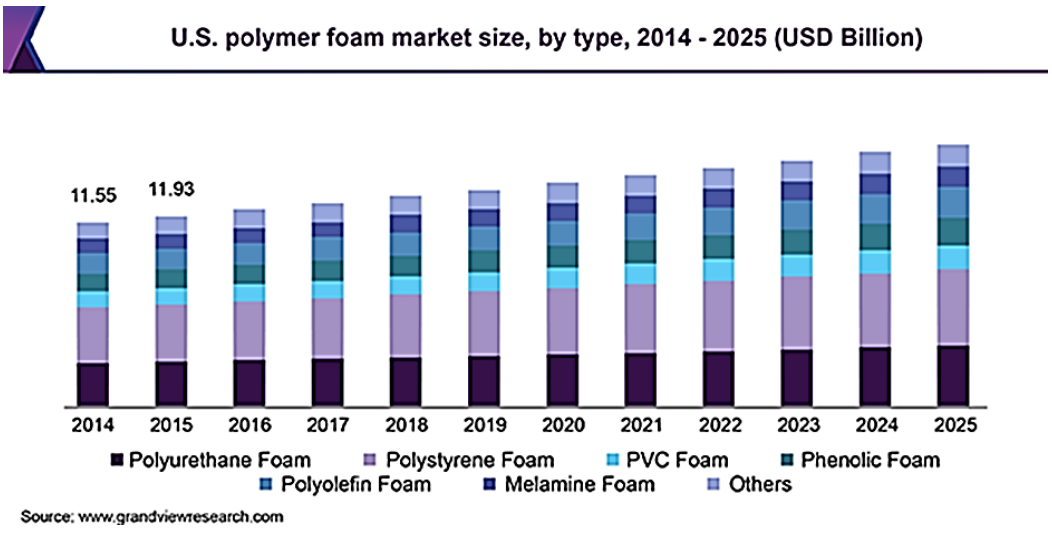

Figure 2.1. U.S. Polymer Foam Market Size [30].

2.2 PMMA and PMMA Foams

PMMA is a thermoplastic polymer which belongs to the acrylic family of resins. The molecular structure of the PMMA is given in Figure 2.2.

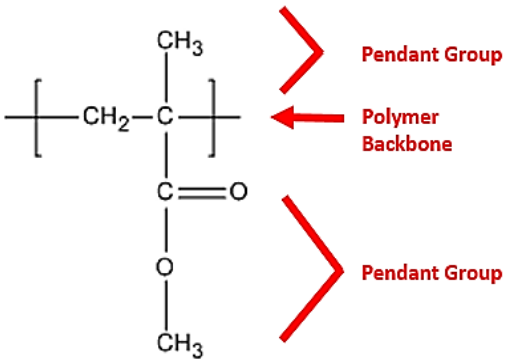

Figure 2.2. The molecular structure of PMMA.

PMMA structure has pendant methyl (CH_3) groups that prevent the polymer chains from rotating around the carbon-carbon bonds and from packing closely in a crystalline fashion. As a result of this behavior, PMMA is a tough and rigid plastic [31]. Also because of these polar carbonyl groups, PMMA has a high resistance to water and some nonpolar solvents [32]. The atactic PMMA is the most commercial one with the glass transition temperature between 100-120ºC. Since it has big side groups and lacks complete stereoregularity, it is an amorphous polymer.

PMMA was discovered in 1877. The first commercial production of PMMA was conducted in 1936 by Röhm and Haas and the very first application of PMMA was the acrylic safety glass. Additionally, Du Pont used PMMA for cast products of rods, tubes and blocks. In modern applications, PMMA is produced mainly from propylene, an organic material obtained from the lighter fractions of crude oil. Propylene and benzene are reacted to form cumene and the cumene is oxidized to

cumene hydroperoxide. This substance is reacted with acid to form acetone and the acetone is converted to methyl methacrylate (CH_2=C[CH_3]CO_2CH_3), the monomer of PMMA. Methyl methacrylate monomers link together with the help of free radical initiators to form solid PMMA. The conventional methods for PMMA production are bulk polymerization and suspension polymerization [33].

PMMA is synthesized from the free radical vinyl polymerization of methyl methacrylate monomer (MMA). This reaction is commonly used for the polymerization of the monomers that contain a carbon-carbon double bond. The reaction starts with an initiator such as benzoyl peroxide. The initiator splits into two pairs which are called initiator fragments that have unpaired electrons. These electrons react with the carbon-carbon bond and form free radicals. This step is called initiation step. The radical then reacts with another monomer and the polymer chain starts to grow which is called propagation step. After that, the chain growth stops and this step is called termination step. The representation of the polymerization reaction of PMMA can be seen in Figure 2.3.

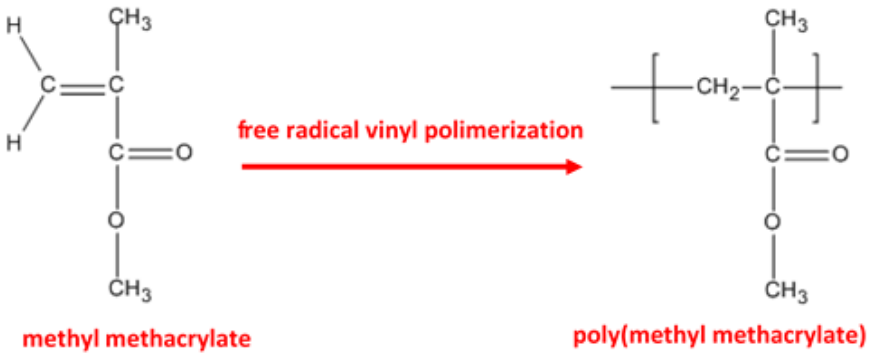

Figure 2.3. Polymerization of PMMA.

PMMA is a low-density polymer with a density between 1.15-1.19 g/cm^3. The outstanding properties of PMMA are its high transparency up to 92% light transmittance, weatherability with low water absorption capacity and high resistance

to UV light and scratching. Besides, it is a non-toxic polymer [9]. These properties make PMMA to be used in aquariums and submarines as transparent glass substitutes, artistic and aesthetic works such as furniture and jewelry design and medical applications such as contact lenses and dentistry implants.

PMMA can be an attractive alternative to be used as a matrix material in the polymer foam applications. Polymer foams which consist of a solid polymer phase and a gas phase, have been widely used in a diverse range of applications for several decades due to their low density. However, their low mechanical properties and low dimensional stability restrict the application area of polymer foams. As an alternative, PMMA is a biocompatible and environmentally stable material with high mechanical properties. Besides, it is suitable to be recycled after use since it is a thermoplastic. Recycling of the material can generate huge profits in long time applications.

As a polymer foam, PMMA has the advantage of having both the unique properties of PMMA and the lightweight of foams. This combination makes PMMA foam to be used in some special applications. Although there is no commercial production of PMMA foams, there are some potential applications of these foams stated in patents and journals. For example, PMMA foam can be used as a part of the reflective sheets for display panels together with the non-foamed PMMA layer. Commercial reflective sheets are made from poly(ethylene terephthalate) (PET) which loses its reflectivity with increasing thickness. However, thick reflective panels are essential for the large size display panels. When using PMMA foam with a plane PMMA layer, light enters through the PMMA layer to the foam layer where light can be reflected out and the reflection effect can be achieved in this way [34].

As a transparent thermal insulation material, foamed polyacrylate plates are widely used for the facade cladding. However, using this material between glass sheets is an expensive method. A cost-effective method is proposed where polypropylene plates with wide chambers filled with PMMA foam can be used as thermal insulators

with relatively high transparency which is 30% higher than conventional substances [35].

Another specific application of PMMA foam has been provided for the packaging industry. In the packaging industry, it is important to produce packaging material with high mechanical and thermal properties with low water absorption capacity by maintaining the cost. Filling the cores of corrugated boards with PMMA foams lead to good thermal insulation property and water resistance. Therefore, this composition can be used for the packaging of valuable products such as electronics [36].

PMMA and other acrylic polymer foams can be used to produce acrylic composite foam board for decorative and aesthetic manner [37].

Functionally graded materials (FGMs) show different composition and structure within the direction of the thickness. The properties of these materials change gradually which make them advantageous in terms of high mechanical properties and thermal stability. FGMs are used in the field of aerospace, electronics, packaging and construction industries. In 2013 a patent was proposed for producing functionally graded PMMA foam which was produced with $scCO_2$ foaming [38].

The other potential applications of PMMA foams are in the area of electromagnetic interference shielding materials [39]. When a conductive nanomaterial is added in the polymer matrix, the foaming process of this composite creates a conductive pathway through the wall of the pores and the polymer can show high electromagnetic interference shielding properties. In addition, PMMA foams can be used as scaffolds in tissue engineering applications [40] since the cell culture can grow in the pores of the biocompatible polymer foam.

2.3 Polyhedral Oligomeric Silsesquioxanes (POSS)

The general formula of $RSiO_{1.5}$ represents the silsesquioxanes where R can be hydrogen, alkyl or alkyl derivatives. Silsesquioxanes can be classified based on their

structures as cage structures, partial cage structures, ladder structures or random structures [41].

Polyhedral oligomeric silsesquioxanes (POSS) have an inorganic siloxane cage structure with organic corner groups and general formula of $(RSiO_{1.5})_n$ where n represents the degree of polymerization. R can be a hydrogen atom or an organic functional group, such as hydroxyl, alkyl, alkylene, epoxide, or acrylate unit. R can be selected to be compatible with polymers, biological systems or surfaces of organic natures. The molecular structure of the POSS is given in Figure 2.4.

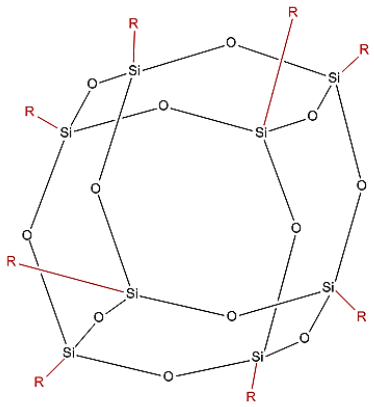

Figure 2.4. The structure of the POSS molecule.

The invention of the complex mixtures of silsesquioxanes was achieved by Meads and Kipping [13]. After that POSS was isolated by Scott in 1946. The POSS molecules were conventionalized by Lichtenhan and his team in 1998, with the foundation of the Hybrid Plastics.

The diameter of the POSS nanostructures is in between 1 to 3 nm. However, they mainly exist in the form of clusters [13]. Due to their small size, POSS molecules can be dispersed in the polymer matrix in a much smaller form than the other nanofillers. Unlike many other nanofillers the shape of the POSS molecule is isotropic that shows the same properties in all directions of the molecule [42]. The

rigid inorganic cage structure of the POSS molecule provides thermal stability and rigidity to the polymer [43].

The addition of POSS nanoparticles can improve the mechanical properties of the polymers if they are homogeneously dispersed and reduced to nano size. They can also act as a fire retardant for the polymer composites depending on the functional group around the silica cage. The formation of a thermally- and oxidatively-stable silicon-oxycarbide ceramic surface during burning, enhances the fire retardancy of polymers [13]. The thermal and mechanical properties of PMMA were enhanced with the addition of POSS in several studies [44-49]. The thermal stability of PMMA was enhanced with the incorporation of octa(3-chloropropyl) POSS and trisilanolphenyl POSS [50] due to the homogeneous dispersion of these particles as a result of their high compatibility with PMMA. In Tanaka et al.'s study PMMA composites with various types of POSS nanoparticles were prepared with the solvent casting method [51]. In this study, while octaisobutyl POSS and octadecyl POSS increased the glass transition temperature, octaphenyl POSS enhanced the loss and storage moduli of PMMA. These enhancements were attributed to the weak interactions between the PMMA and the POSS nanoparticles which caused a plasticizing effect. POSS nanoparticles can be a promising reinforcement material for syntactic foam studies.

2.4 Syntactic Foam Production Method

Syntactic foams are low-density composites that are obtained by dispersing hollow microspheres in a matrix material such as ceramic, metal or a polymer. Polymer syntactic foams are being increasingly used in thermal insulation and transportation. Scanning electron microscopy (SEM) image of vinyl ester syntactic foam is given in Figure 2.5 [52]. The matrix material type, microsphere type and concentration can determine the properties of the syntactic foams. Therefore, it is possible to design a syntactic foam with desired properties. Another advantage of these foams is their low density and moduli that can be higher especially than the closed-cell foams at

the same density level [53]. In general, it is desired to compose syntactic foams with high mechanical properties and low density.

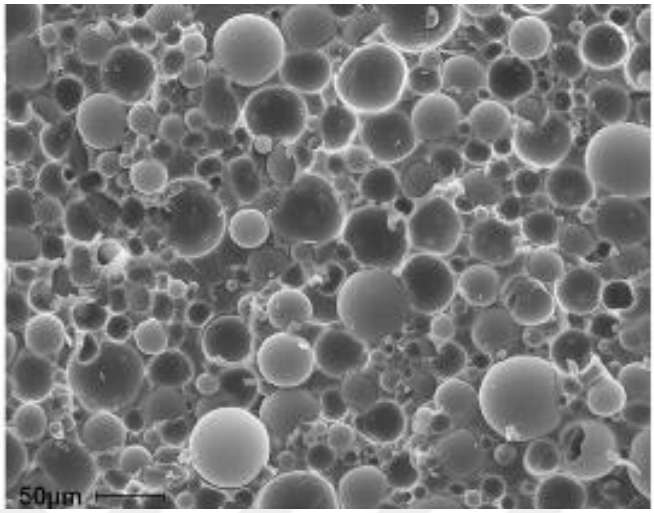

Figure 2.5. SEM images of vinyl ester syntactic foam.

2.5 Supercritical Fluids (SFCs)

Supercritical fluids are gases that differ from the vapors as having a higher temperature than the critical temperatures. In general, if fluid has higher temperature and pressure than its critical temperature and pressure, it is called supercritical fluid [54].

Supercritical fluids have the desired properties of both the liquids and the gases but exist as a single phase. They have high dissolution power provided by their high density and high diffusivity due to their low viscosity which provides sufficient mass transfer through liquids and solids. They also provide a good reduction in surface tension and have gas like compressibility. While a fluid may not dissolve a material at subcritical conditions, the material can be soluble in the fluid at supercritical conditions [55].

SCFs are cost-effective since they can be recovered and reused without any purification step. For this reason, they are environmentally stable and sustainable. SCFs are commercially used in pharmaceutical, cosmetic, food and textile industries. Also, their potential applications have been investigated by scientists in the field of reaction media, synthesis, chromatography, extraction, sterilization, jet-cutting, thin-film deposition and polymer processing [56].

Supercritical CO_2 is one of the most applied supercritical fluid. The advantages of $scCO_2$ such as being non-toxic, non-carcinogenic, non-mutagenic, non-flammable and thermodynamically stable allow it to be used in several applications [56]. The phase diagram of CO_2 is given in Figure 2.6 [57]. The critical pressure and temperature of CO_2 are 7.38 MPa (1070 psig) and 31ºC. Above these values, carbon dioxide will always be in its supercritical state. Since the critical temperature of CO_2 is relatively low, using this substance in SCF applications can provide an economic benefit compared to the other substances [57].

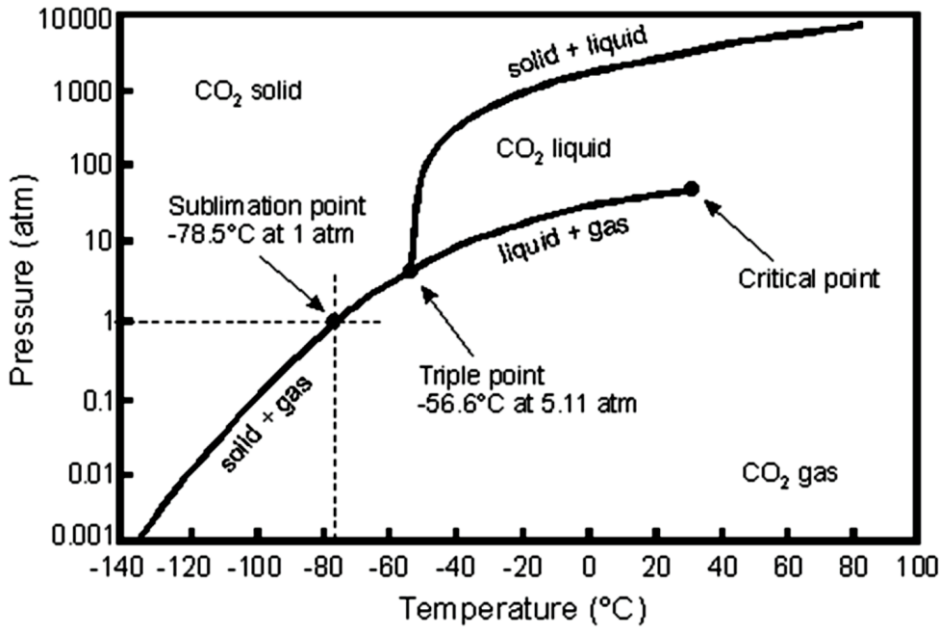

Figure 2.6. Phase diagram of CO_2.

2.6 Supercritical Carbon Dioxide ($scCO_2$) Foaming Method

$ScCO_2$ foaming of polymers gains attention during the last decade. In this method, $scCO_2$ dissolves and solubilizes in the polymer at high pressures. CO_2 absorption into the polymer phase reduces the glass transition temperature (Tg) of the polymer below the processing temperature and plasticizes the polymer. After the plasticization, the pressure of the system is reduced. During this depressurization, due to the decrease in the solubility of CO_2 in the polymer, the polymer-CO_2 mixture becomes supersaturated and bubbles grow from the nucleation sites, forming a porous matrix [8]. The representation of the $scCO_2$ foaming of polymers is given in Figure 2.7.

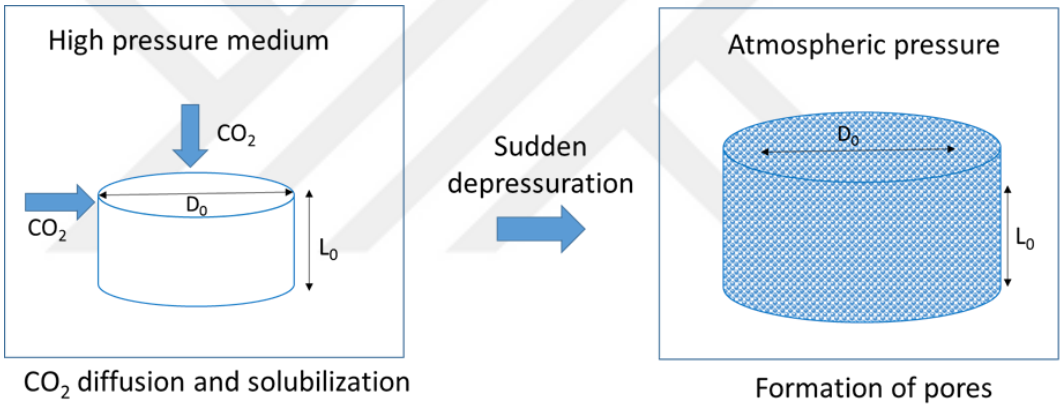

Figure 2.7. Representation of $scCO_2$ foaming.

2.7 Literature Survey

Detailed literature investigation on the selected foaming methods in this study are assessed in this chapter.

2.7.1 Syntactic foam production

The main approach in polymer syntactic foam studies is to obtain syntactic foams with enhanced mechanical and thermal properties and reduced density. Several approaches were considered to obtain foams with low density and high mechanical properties. Matrix selection is the most effective parameter that changes the syntactic foam properties. The most common syntactic foam matrix is epoxy due to its continuing usage in transport vehicles. On the other hand, thermoplastic syntactic foams have several advantages such as ease of production, moldability, recyclability and higher mechanical properties. For example, J-Z Liang selected acrylonitrile–butadiene–styrene copolymer (ABS) as a matrix since there is a high compatibility in terms of interfacial strength between the ABS matrix and glass microspheres. Both the flexural and tensile strengths are enhanced with the incorporation of HGMs into the ABS matrix [58]. Both the density and the thermal conductivity of high-density polyethylene (HDPE) matrix was lowered with the addition of HGMs. In addition, the tensile yield strength and modulus values of the HDPE matrix was also improved. On the other hand, in order to enhance the lowered toughness values of the HDPE, a compatibilizer was used and improved toughness values were obtained [59]. PMMA is a great candidate for the syntactic foam studies due to its relatively low density, low thermal conductivity, remarkable toughness, rigidity and relatively higher energy absorption capacity [9]. The rare properties of PMMA such as high resistance to water, UV light and attractive transparency enlarge its use in several applications such as transportation and thermal insulation. Nonetheless, PMMA is rarely mentioned in syntactic foam applications, for which the addition of suitable hollow microspheres can be useful to provide the desired foam properties. To our knowledge, PMMA was used as a matrix material in syntactic foam studies once in 1982 by Kinra and Kerr [12] and recently by our research group [60, 61] within the scope of this thesis study. As a syntactic foam matrix, PMMA may offer several advantages due to its outstanding properties [9].

Another important parameter that would be effective on syntactic foam properties is the selection of the microsphere type and composition. Since glass has low cost and ease of production, it is the most common hollow microsphere. But the addition of glass reduces the resistance of the matrix to tensile and compression forces [62]. Furthermore, higher percent addition of HGMs, further reduced the strength of the polymer, which also leads to further reduction in the density in several studies [52, 58, 60, 63-66]. In Doumbia et al.'s study, high impact polypropylene (PP) which was composed of PP homopolymer, ethylene-propylene rubber (EPR) and a relatively small portion of polyethylene (PE) homopolymer blend was used as a matrix material and six different hollow microspheres types were incorporated to produce syntactic foams [67]. As a result of the study, four types of microsphere fractured in melt processing. Therefore, the density of the neat polymer increased with the addition of these shattered microspheres. It was found that the microspheres which had higher thickness over diameter ratio had higher resistance to the melt processing. Effects of concentration and the HGM wall thickness on the properties of the vinyl ester matrix were investigated by Gupta et al. It was found that the microspheres with higher wall thickness and low HGM volume fractions resulted in syntactic foams with higher mechanical properties [52]. In Swetha et al.'s study different HGMs based on their densities were used to produce epoxy syntactic foams. High-density HGMs improved mechanical properties up to 30 vol.% incorporation in the matrix. The addition of a higher percentage of HGMs further reduced the density of the syntactic foams [65]. PP syntactic foams were produced with the blending of PMMA microspheres in Mae et al.'s study. Yield stress and modulus values of the syntactic foams were decreased with decreasing relative density [63]. Several studies show that the density [60,65], wall thickness [52, 68], wall thickness over density ratio [67], and the particle size [58, 69] of the hollow glass microspheres significantly affect the mechanical properties. In general, HGMs with high density and high thickness provide enhanced mechanical properties to syntactic foams. Improving the mechanical properties of syntactic foams while maintaining the density is the focus of the current studies.

One approach to improve the mechanical properties of syntactic foam is the surface treatment of HGMs. Enhancing the compatibility between the matrix material and the HGMs by the modification of the surface group of HGMs improves the mechanical properties of the syntactic foams. The coating of HGMs with PMMA increased the mechanical properties of PMMA syntactic foams [60]. Kumar et al. used a silane coupling agent for modification of the hollow microspheres to obtain HDPE syntactic foams with high mechanical properties. Enhanced interfacial bonding between the HDPE and HGM resulted in improved strength for syntactic foams [70]. In Li et al.'s study, styrene-butadiene rubber (SBR) latex coating of the surface of HGMs increased the impact strength of the epoxy matrix, while decreased the bending strength [71]. Improved compatibility between the polymer matrix and glass substances was also obtained in other composite studies. Yi et al. found that PMMA coated glass fibers improved the mechanical properties of acrylic resin [72].

Hybrid syntactic foam production is one of the effective methods to improve the properties of the syntactic foams in which hollow microspheres and a reinforcement material are dispersed simultaneously in the polymer matrix. There are several studies in which fiber reinforcement was carried out to improve the mechanical properties of syntactic foams. One of the most studied reinforcement materials in hybrid epoxy syntactic foams is glass fiber. Studies with enhanced compressive strength [73, 74], compressive modulus [75], flexural strength [76, 77], flexural modulus [78, 79] and impact strength [80] with the addition of glass fiber in epoxy syntactic foams were observed. In addition, fiberglass mesh in epoxy syntactic foams was also enhanced the flexural properties [78]. Also, carbon fiber in epoxy syntactic foams showed improved flexural stiffness, fracture toughness [80], tensile strength and modulus values [81]. Epoxy syntactic foams with the incorporation of short sisal fibers resulted in enhanced storage and loss moduli of these foams [3]. Tensile, compressive and shear properties of the phenolic-amino microspheres syntactic foams were enhanced with the addition of aramid and carbon fibers [82]. On the other hand, since the density of glass fibers is higher than the HGMs, the use of glass fibers increased the density of the syntactic foams [73, 75, 78, 79].

Not only the fibers but also the nanomaterials are incorporated in the syntactic foam matrix for the enhancement of the mechanical and thermal properties of the syntactic foams. With the addition of a small amount of nanomaterial, the properties of the syntactic foams are enhanced without increasing the density. Hybrid epoxy syntactic foam with nanoclay nanoparticles showed higher flexural strength [4, 5], tensile strength [6], toughness [7], loss and storage moduli [5]. In addition, nanoclay improved the compressive and flexural strength and storage modulus of cyanate ester syntactic foams [83]. Using carbon nanofiber also exhibited higher tensile strength, tensile modulus [84] and glass transition temperature [85] of epoxy syntactic foams. Phenolic resin syntactic foams with hollow carbon microspheres and carbon nanofibers resulted in higher flexural strength and fracture toughness [86]. Among the studied nanoparticles, nano-silica, carbon nanotubes [87], and graphene platelets [62] enhanced the compressive properties. It can be concluded that the hybrid syntactic foam approach is highly effective in the enhancement of the mechanical properties of the syntactic foams.

2.7.2 $ScCO_2$ foaming

Studies on $scCO_2$ foaming are focused on the controlling of the foam morphology in terms of pore diameter and pore density as well as the mechanical, thermal, and physical properties of the foams. The process parameters such as time, temperature, pressure and venting rate were found to be highly effective on the properties of the polymer foams [88]. Experimental and modeling studies with PMMA showed that high pressure [10, 89, 90, 91, 92], and fast venting rate [94] resulted in polymer foams with smaller pores and higher pore density. In general, small pore size and high pore density are beneficial for obtaining polymer foams with higher mechanical properties and a lower coefficient of thermal conductivity [95]. Besides the optimization of the process parameters, one of the most popular approaches to obtain small pore size is the addition of nanoparticles in the polymer matrix. These nanoparticles can reduce the critical free energy for nucleation, thus, enhance the

pore formation. The higher number of pores also triggers the formation of smaller pores [96]. Another advantage of using nanoparticles is that depending on the type of nanoparticles, several properties such as electrical conductivity and electromagnetic interference shielding can be added to polymer foams [97]. There are several examples of $scCO_2$ processing of PMMA composite foams produced with the addition of carbon nanotubes [11, 97-105], montmorillonite [106], silica [14, 96, 107, 108], graphene oxide [109-111], nanoclay [112], graphene [39, 113-115], graphene nanoribbon [116] and two-layer hydroxide [117] The general conclusion which can be drawn from these studies is that the addition of nanoparticles reduces the pore diameter of the PMMA foams and increases the pore density.

To enhance the affinity of nanoparticles to CO_2, surface treatment with fluorine groups was considered. It was observed that the nanoparticles which were modified with fluorine groups interacted with CO_2 in advanced levels, and these groups have further enhanced the pore density by decreasing the energy barrier for the pore formation and decreased the pore size [96, 107, 108]. Although the fluorine group is one of the most preferred groups for enhancing the interactions with CO_2 in $scCO_2$ foaming studies, they are known for its harmful effects on human health and the environment. Instead of surface treatment with fluorine groups, a fluorinated pore nucleating agent which can be solubilized in $scCO_2$ due to their compatible structure with carbon dioxide has been studied for once in the literature. A CO_2-soluble pore nucleating agent, trifluoropropyl POSS was used to achieve $scCO_2$ foaming of highly crystalline (>30 %) poly(L-lactic acid) (P_LLA) [118].

The structure of POSS nanoparticles which consist of silica cage structure with the groups linked to the silica atoms allows obtaining the desired properties for polymers by changing those groups [119]. This special structure of the POSS materials can be very advantageous in the $scCO_2$ foaming process since groups linked to the silica atoms can be chosen as CO_2-philic types. POSS nanoparticles were used twice in $scCO_2$ foaming studies. In one of them, Costeux and Zhu examined the effects of methacryl POSS on $scCO_2$ foaming [120]. However simultaneously they used a copolymer in the polymer matrix and also they carried out post foaming process. The

synergistic effect of these parameters allowed the authors to obtain PMMA foams with the average pore sizes below 100 nm. In the second study as mentioned above, trifluoropropyl POSS, which was earlier proven as CO_2-philic [121] was used for $scCO_2$ foaming of P_LLA [118]. In the study, foams with 40% porosity were obtained with polymers processed at 40°C, 21 MPa, and for 24 h. At the same foaming condition, no pores were obtained neither in the pure P_LLA matrix or the one with octamethyl POSS which is known to be not CO_2-philic [122]. There are three advantages of using POSS substances in materials that are to be foamed by $scCO_2$. First, the compatibility of the polymer with CO_2 significantly increases, which can allow the supercritical process to be carried out at lower pressures, temperatures and shorter saturation times. The second advantage is that during the supercritical process these substances are dissolved in $scCO_2$ and can be regained at the end of the process. These two advantages provide the energy and material savings of the process. Finally, as the third advantage, they can also provide control of the pore size growth and thus smaller pores and an increased number of pores can be obtained.

In the $scCO_2$ foaming method, pore size is the most effective parameter that determines the mechanical and thermal properties of the polymer foams. Usually, small pore size results in superior mechanical properties and a lower coefficient of thermal conductivity [95]. On the other hand, larger pores offer reduced mass density. The bimodal pore structure is defined as a porous structure that consists of two types of pores in a single foam matrix as a larger and smaller one. Usually larger pores exist in the diameter range of μm and smaller pores in the diameter range of nm. The unique bimodal cell structure provides several advantages such as reduced mass density that is obtained due to the larger cells and improved mechanical properties that resulted from the smaller cells [123]. In addition, different pore sizes can absorb the different frequencies of sound, therefore bimodal foams can be used in sound absorption applications. The bimodal cell structure is highly effective to improve their performances and expand their applications. To achieve a bimodal porous structure, several techniques were improved. Xin et al., fabricated poly(lactide-co-glycolide) (PLGA) scaffolds that had bimodal pore structure

including macropores and micropores that enhanced the nutrient transfer and cell adhesion to be used in biological applications. Combination of the particle leaching technique and the $scCO_2$ foaming process was used to obtain bimodal structure [124]. NaCl particles were mixed with the polymer and after $scCO_2$ processing, the NaCl particles were leached out with distilled water. As a result of the study, bimodal pore structure was achieved. The smaller pores were obtained from the $scCO_2$ processing and the larger pores were obtained from the leaching of NaCl particles. In Ma et al.'s study, a two-step batch depressurization process was used to obtain bimodal polycarbonate (PC) foams. The bimodal foams had enhanced tensile properties compared with the unimodal foams [123]. For this purpose, PC specimens were exposed to supercritical CO_2. The vessel was depressurized to an intermediate pressure and then maintained at the intermediate pressure for 1 h. After that, the vessel was completely depressurized. The two-step depressurization process was also used for obtaining a bimodal pore structure in poly(e-caprolactone) (PCL) by Solerno et al. [125].

In the case of smaller pores, the most popular approach to reduce the pore size and increase the pore density is the addition of a nanomaterial into the polymer matrix. These nanoparticles reduce the activation energy during the cell formation and enhance the higher number of cells in the matrix. The higher number of cells also leads to smaller pore size [96]. POSS nanoparticles have a siloxane cage structure with the linked R groups. If these R groups were chosen as CO_2-philic, it would further enhance the foam morphology by triggering the CO_2 diffusion.

In this study, we aim to produce PMMA foams with a bimodal pore structure. In order to achieve this morphology, HGMs in the diameter range of 8.6-23 μm were used. The formation of larger pores during the depressurization is attributed to the CO_2 diffusion in the matrix towards the voids already existing between the matrix and HGM surfaces in the composite due to their incompatibility with each other [60]. Formation of smaller pores, on the other hand, is attributed to the $scCO_2$ process in which bubbles grow from the nucleation sites, forming a porous matrix. Therefore, two types of pore size distribution were obtained in the polymer matrix. In order to

enhance the foam morphology, octatrimethylsiloxy POSS which is known to be highly CO_2-philic [126] was used.

2.8 Motivation of the Thesis Study

Today, materials such as epoxy and polyurethane are known to have negative effects on the environment and human health. As an alternative to these polymers, PMMA is a biocompatible and environmentally stable material. It is also suitable for recycling since it is a thermoplastic polymer. The main motivation of this study is to develop a more environmentally friendly foam by applying technical and auxiliary methods that are also environmentally and human health-friendly which do not require separation processes and do not spread volatile organic components. Another motivation is to produce PMMA foams with reduced density and higher mechanical properties, and thus durability compared to commercial foams that can have potential to be used in thermal insulation and transportation fields. For this purpose, PMMA foam was produced by using syntactic foam production and $scCO_2$ foaming methods as well as a combination of them. In addition, reinforcement of the matrix was considered to enhance the foam properties. Therefore, the aim of the study is to compare the effects of different foaming methods, and using nanoparticles on the morphology, density, mechanical and thermal properties of the PMMA foams.

In the literature, there is only one study where this highly advantageous thermoplastic polymer was used as matrix material in syntactic foam studies [12]. Starting from this fact, in this study PMMA was used as the matrix material for syntactic foam studies. The main purpose is to decrease the density of the PMMA without causing a significant loss in the mechanical properties. For this purpose, the effect of HGM density and concentration, and the surface modification of HGMs on the PMMA syntactic foam properties were investigated for the first time. To our knowledge, PMMA hybrid syntactic foams, and the addition of POSS nanoparticles as reinforcement materials have never been studied in literature before.

In the recent thermodynamic studies, it has been found that octatrimethylsiloxy POSS is completely dissolved in supercritical CO_2 with the highest solubility among all the CO_2-philic POSS types [126] due to the rotational flexibility of the siloxane groups and low cohesive energy density, thus weak solute-solute interactions [127]. However, no application of octatrimethylsiloxy POSS in supercritical technologies has yet been found. Thanks to its high solubility in CO_2, its use in this field can provide significant advantages, particularly in reducing energy consumption and in the process of dissolution and recovery with the supercritical fluid, thereby reducing material costs.

In this context, one of the motivations in this study is to reduce the pore size of PMMA foams to the nano level by using CO_2-phillic octatrimethylsiloxy POSS nanoparticles for the first time as a pore inducing agent in the polymer. Nanopores are known to have higher performance in thermal insulation and higher mechanical properties. CO_2-philic POSS nanoparticles can also provide the foaming of the polymer at milder conditions.

In the literature, fluorine modification of pore inducing materials was carried out to enhance the interaction with CO_2 [96, 107, 108]. The POSS used in this study do not contain fluorine groups and therefore is more environmentally friendly. The individual and the synergistic effects of the process parameters as well as the concentration of this additive on the foam morphology were investigated using design of experiment analysis. The two-factorial design method was used to understand the significance of the process parameters on the foam morphology in terms of average pore diameter.

In the final stage of the thesis study, the syntactic foams which were produced with melt blending of PMMA and HGMs in an extruder were processed with supercritical carbon dioxide to obtain bimodal pore structures. The main motivation to carry out these experiments is to obtain a PMMA foam with the advantages of these two foaming methods.

CHAPTER 3

EXPERIMENTAL

3.1 Materials

3.1.1 Poly(methyl methacrylate) (PMMA)

Commercial PMMA (Altuglas V825-T) is a product of Altuglas International, a subsidiary of Arkema, France. In this study, PMMA was used as the matrix material and supplied by Hayim Pinhas A.Ş., Turkey. It has a polydispersity of 2.1 and molecular weight (Mw) of 95,000 g/mol [128]. The viscosity average molecular weight of the PMMA is 77,857 g/mol which was obtained using the Ubbelohde method and the Mark-Houwink-Sakurada constants [129]. Properties of the PMMA from the manufacturer data are given in Table 3.1.

Table 3.1 Properties of PMMA, Altuglas V-825T from the manufacturer data.

Property	Value
Density	1.19 g/cm^3
Melt Flow Index	2.8 g/10 min
Flexural Strength	103 MPa
Flexural Modulus	3300 MPa
Compressive Strength	117 MPa
Impact Resistance	11 kJ/m^2
Light Transmittance	98%
Glass transition temperature	108ºC
Fire Resistance	HB class

3.1.2 Hollow Glass Microspheres (HGMs)

In this study, three different types of HGMs based on their densities were used. Low-density HGM (LD-HGM), HGS-21 is a product of Larand Chemical Corporation, USA and was supplied by Konuray A.Ş., Turkey. Medium-density HGM (MD-HGM), K-37 and high-density HGM (HD-HGM), iM30K are products of 3M, USA and obtained from Kemiropa A.Ş., Turkey. The properties of HGMs from the manufacturer data are given in Table 3.2.

Table 3.2 Properties of the hallow glass microspheres from the manufacturer data.

HGM type	**Density (g/cm^3)**	**Particle size (μm)**	**Crush Strength (MPa)**	**Thermal Conductivity (W/mK)**
LD-HGM	0.12*	70	9.48	0.036
MD-HGM	0.37**	45	20.68	0.124
HD-HGM	0.60**	18	193.05	0.200

* Bulk density
**True density

3.1.3 Polyhedral Oligomeric Silsesquioxanes (POSS)

In this study, three different types of POSS based on their functional group were used. Octaphenyl POSS (in powder form with the molecular formula of $C_{48}H_{40}O_{12}Si_8$), octaisobutyl POSS (in powder form with the bulk density of 0.63 g/cm^3 and the molecular formula of $C_{32}H_{72}O_{12}Si_8$) and octatrimethylsiloxy POSS (in powder form with the bulk density of 0.66 g/cm^3 and the molecular formula of $C_{24}H_{72}O_{20}Si_{16}$) were purchased from Hybrid Plastics, USA. The molecular structure of these POSS can be seen in Figure 3.1.

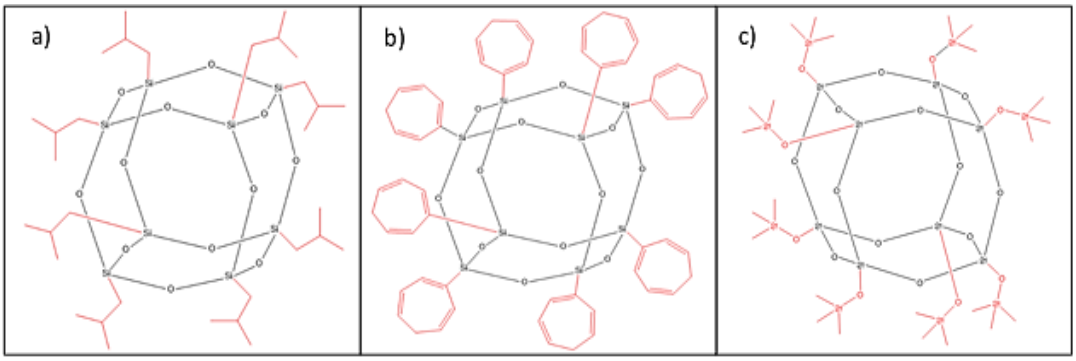

Figure 3.1. Molecular structure of a) octaisobutyl POSS b) octaphenyl POSS and c) octatrimethyl siloxy POSS.

3.1.4 Carbon Dioxide (CO_2)

Carbon dioxide (99.9%) was obtained from Linde Gas, Turkey and used in the $scCO_2$ experiments.

3.1.5 Chemicals Used for the Surface Treatment of HGMs

In order to carry out the silanization process of HGMs, γ-methacryloxypropyltrimethoxysilane (γ-MPS) ($C_{10}H_{20}O_5Si$) and methanol were purchased from Dynaslan, Netherlands and Sigma Aldrich, USA, respectively. The molecular structure of the silane coupling agent is given in Figure 3.2.

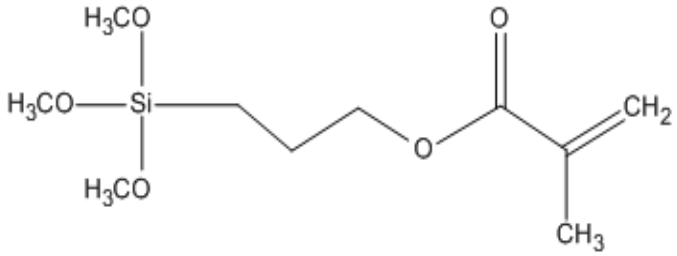

Figure 3.2. Molecular structure of γ-methacryloxypropyltrimethoxysilane.

3.2 Experimental Method

3.2.1 Melt Blending in Extruder

PMMA syntactic foams, PMMA-POSS composites and hybrid PMMA syntactic foams were produced using a co-rotating Thermo Prism TSE 16 TC twin-screw extruder with the L/D ratio of 24:1. The parameters of the extrusion process are given in Table 3.3.

Table 3.3 Parameters of the extrusion process.

Parameter	**Value**
Screw Speed	80 rpm
Zone 1 Temperature	235ºC
Zone 2 Temperature	235ºC
Zone 3 Temperature	235ºC
Zone 4 Temperature	245ºC
Zone 5 (Die) Temperature	245ºC
Feed rate	17 g/min

PMMA pellets were dried at 90ºC for 4 h before the extrusion process. During extrusion, PMMA pellets were fed to the extruder through the main feeder. In order to produce syntactic foams, HGMs were fed to the extrusion through the side feeder. For the production of PMMA-POSS composites and PMMA hybrid syntactic foams, POSS nanoparticles were manually added to the extruder from the hopper since the amount of the nanoparticles was small to be processed with the feeders. The amount of POSS that should be added to the extrusion process at each minute was calculated to obtain the desired composition. The melted composite that is coming out from the die goes into the cooling process through a water bath, stretching and cutting processes via chopper to obtain composite pellets. A photograph of the twin-screw extruder is given in Figure 3.3.

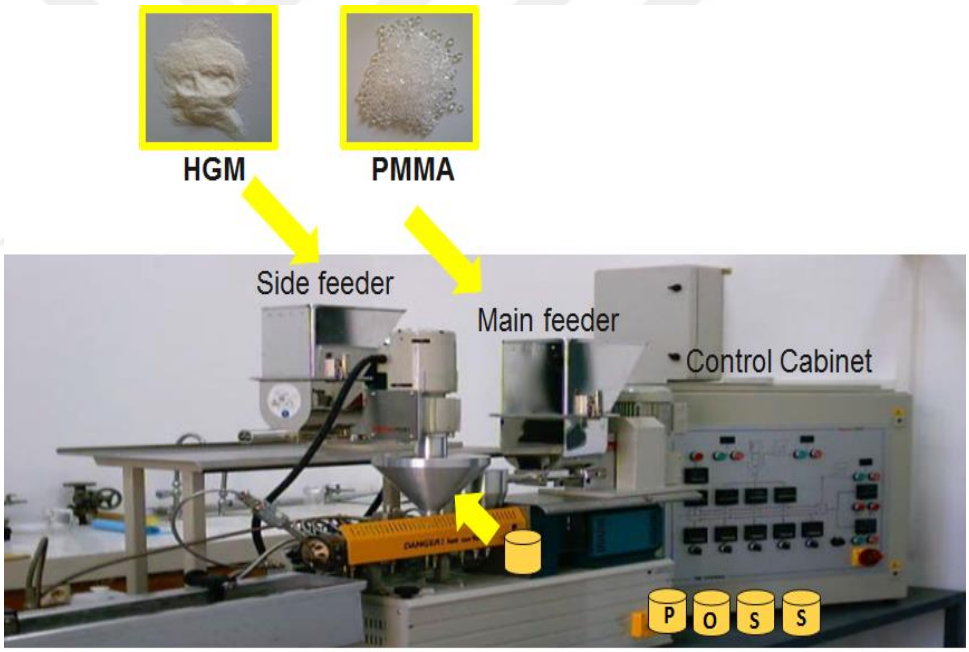

Figure 3.3. A photograph of the twin screw extruder.

The composition of the neat polymer and the composites obtained from the extrusion process and the abbreviations of them are given in Table 3.4.

Table 3.4 Composition of the composites and their abbreviations.

Sample Code	HGM amount (wt.%)	POSS amount (wt.%)
PMMA	-	-
PMMA/LD-H5	5	-
PMM/LD-H10	10	-
PMMA/LD-H15	15	-
PMMA/MD-H5	5	-
PMM/MD-H10	10	-
PMMA/MD-H15	15	-
PMMA/HD-H5	5	-
PMM/HD-H10	10	-
PMMA/HD-H15	15	-
PMMA/HD-HC15	15	-
PMMA/HD-HS15	15	-
PMMA/IB0.25	-	0.25
PMMA/IB0.5	-	0.5
PMMA/IB1	-	1
PMMA/IB3	-	3
PMMA/P0.25	-	0.25
PMMA/P0.5	-	0.5
PMMA/P1	-	1
PMMA/P3	-	3
PMMA/H5/P0	5	-
PMMA/H5/P0.25	5	0.25
PMMA/H5/P0.5	5	0.5
PMMA/H5/P1	5	1
PMMA/H10/P0	10	-
PMMA/H10/P0.25	10	0.25
PMMA/H10/P0.5	10	0.5
PMMA/H10/P1	10	1
PMMA/H15/P0	15	-
PMMA/H15/P0.25	15	0.25
PMMA/H15/P0.5	15	0.5
PMMA/H15/P1	15	1
PMMA/TMP0.5	-	0.5
PMMA/TMP5	-	5
PMMA/H5/TMP0	5	-
PMMA/H5/TMP5	5	5
PMMA/H15/TMP0	15	-
PMMA/H15/TMP5	15	5

In this table, LD, MD, HD and H represent the low-density, medium-density, high-density and HGMs, respectively. The HC and HS represent the PMMA coated HGMs and the silane treated HGMs, respectively. The IB, P and TMS are the abbreviations of the octaisobutyl POSS, octaphenyl POSS and octatrimethylsiloxy POSS, respectively. When the letter H is used without LD, MD or HD in front of it, it is the high-density HGMs.

3.2.2 Injection Molding

The neat polymer and the composite pellets were injection molded to rectangular prism specimens with the dimensions of 80x10x4 mm^3 using a DSM Xplore Micro 10 cc injection molding device. The dimensions were selected based on the standard test methods for the impact test and flexural test according to ISO 179 and ISO 178, respectively. Process parameters for the injection molding were mold and melting barrel temperatures of 98ºC and 235ºC, respectively and maximum applied pressure of 1.3 MPa. A photograph of the injection molding device is given in Figure 3.4.

Figure 3.4. A photograph of the DSM Xplore, laboratory-scale micro injection molding.

3.2.3 Compression Molding

The neat polymer and the PMMA syntactic foam pellets were compression molded to obtain disk shape specimens with a diameter of 50 mm and thickness of 2 mm. These specimens were used in the thermal conductivity measurements. The parameters of the compression molding process can be seen in Table 3.5.

Table 3.5 Processes parameters for compression molding.

Parameters	Pre-heating	Heating	Cooling
Temperature (ºC)	190	190	25
Pressure (bar)	30	120	1
Time (min)	15	7	5

3.2.4 Surface Treatment of HGMs

Surface treatment of the HGMs were carried to enhance the mechanical properties of the PMMA syntactic foams. For this purpose, two different treatments were carried out as silanization of HGMs and coating of HGMs with PMMA. In the silanization process, 30 wt.% γ-MPS - methanol solution was prepared for the silanization of HGMs [130]. 60 g HD-HGM was added into 200 ml of this solution and sonicated in an ultrasonic bath (Bandelin Sonorex) at 80°C for 1 h. After that HGMs were filtered and dried at 100°C for 66 h until the weight of the HGMs did not change.

In the coating process, 4 wt.% PMMA-acetone solution was obtained with the 1 h of sonication process. 100 ml of this solution was mixed with the 60 g of HD-HGMs at room temperature. After 1.5 h, the HGMs were filtered and dried at 90°C for 3 h. The agglomerates of HGMs were smashed into smaller particles using a muller. Finally, the HGMs were sieved using a 100 μm mesh sized sieve.

3.2.5 $ScCO_2$ Process

In $scCO_2$ foaming studies, a high-pressure stainless steel vessel (Micro Reactor model 4592, Parr Instruments, USA) was used. The heating of the vessel was achieved using an electrical heating jacket. The reactor is equipped with a thermocouple to control the temperature and a pressure transducer to monitor the pressure. Teflon sheets with appropriate dimensions were placed into the vessel to form individual sections inside the vessel to prevent the sticking of several specimens to each other. PMMA composite specimens were placed into these sections. Before the experiment, CO_2 was first sent to the syringe pump (model 260D, Teledyne ISCO, USA). Inside the syringe pump, CO_2 was compressed and liquid CO_2 at high pressures was obtained. Then the liquid CO_2 was supplied to the vessel. The schematic representation of the experimental set-up is given in Figure 3.5 [118].

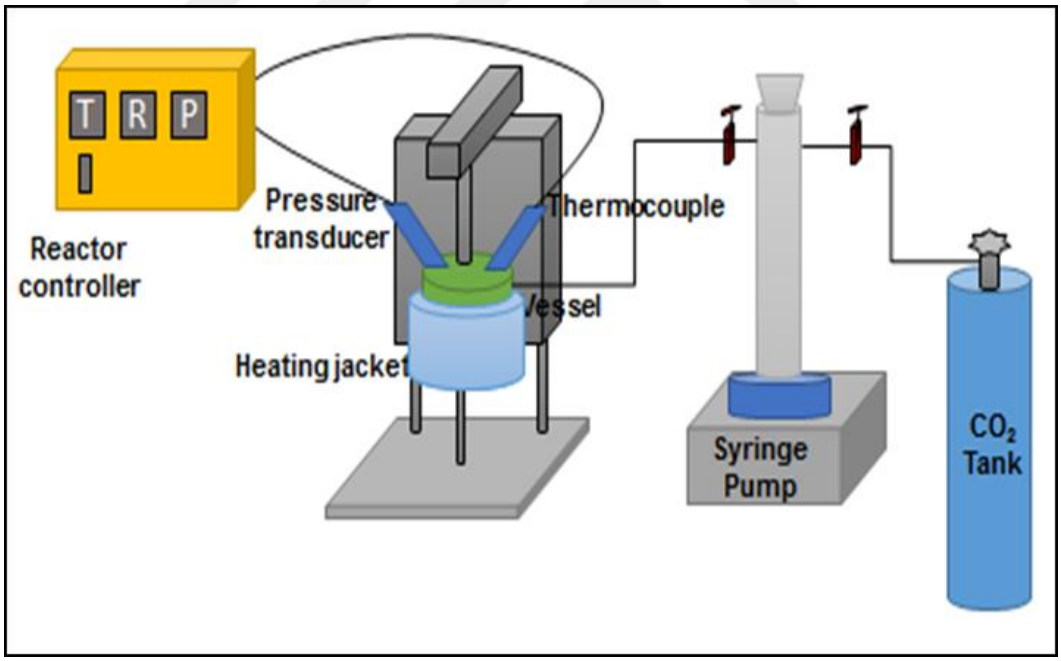

Figure 3.5. Experimental setup of the $scCO_2$ processing.

During the experiments, the pressure of the system did not always remain constant due to the variations in the temperature and the absorption of CO_2. The variation in

the pressure within +/- 1 MPa was accepted for validation of the experiment. However, if the variation was greater than this range then the experiment was repeated. At the end of the process, the system was depressurized with an adjustable venting rate. Foamed samples were not subjected to post foaming process.

3.3 Characterization Methods

3.3.1 Density Measurements

The bar-shaped specimens which were obtained from the injection molding machine were used to measure the densities of the PMMA, PMMA composites and syntactic foams. The densities were determined by the division of the weights of the specimens to the volumes of the bar-shaped specimens. The average of five measurements was considered to calculate the density of the PMMA, PMMA composites and syntactic foams. The highest standard deviation for the density was determined to be smaller than 1%.

The rule of mixture approach was considered to calculate the theoretical densities. The rule of mixture equation which was used to calculate the theoretical densities is given in Equation (1) [60]:

$$\rho_{theor} = \rho_{HGM}.V_{HGM} + \rho_{P}.(1 - V_{HGM}) \quad (1)$$

where ρ_{theor}, ρ_P and ρ_{HGM} are the theoretical density of the composite, densities of the polymer and the HGM (g/cm^3), and V_{HGM} is the volume fraction of HGMs in the composite, respectively [67].

The densities of the foams produced via $scCO_2$ experiments were obtained by the water displacement method. Foam specimens were immersed in water in a 100 ml measuring cylinder at 20°C and the displacement of the water was recorded. Densities were calculated by dividing the weight of the specimen by the volume of the displaced water. The average of four measurements with their standard deviations was reported.

3.3.2 Morphological Analysis

3.3.2.1 Scanning Electron Microscopy (SEM) Analysis

The morphology of the PMMA composites and PMMA syntactic foam specimens were examined using a QUANTA 400F Field Emission and a Tescan Vega 3 SEM. The surface of the PMMA composites which was fractured from flexural analyses was used for the SEM analysis. In the case of PMMA foams which were obtained from $scCO_2$ processing, the samples were fractured in liquid nitrogen. The specimens were mounted on stubs and sputter-coated with Au/Pd to make the surface of the specimens conductive before the analyses. Energy Dispersive X-ray (EDX) analyses were applied on some of the specimens to understand the dispersion of the POSS nanoparticles in the PMMA matrix.

3.3.2.2 Pore Size Measurements

The average pore size of the foams which were obtained from $scCO_2$ processing was obtained by image analysis using ImageJ software. The diameters of the pores were measured using ImageJ tools, then the measured data were analyzed in Excel. Specimens that had complete foaming were taken into account in pore size measurements. These samples were identified easily by observing the central part of the samples through the SEM images since the partially foamed samples had pores only at the outer regions but not in the center. The number of pores that were considered to calculate average pore size was between 40 and 2000 depending on the size of the pores on the observed area.

3.3.2.3 Pore Density Calculation

Pore density calculations were carried out using Equation (2) [131].

$$N_v = \left(\frac{\mathrm{n}}{\mathrm{A}}\right)^{3/2} . \left(\frac{\rho_s}{\rho_f}\right) \quad (2)$$

In this equation N_v is pore density, n is the number of pores in the SEM image, A is the area of the SEM image and ρ_s and ρ_f are the density of the solid and the foam, respectively.

3.3.3 Mechanical Characterization

3.3.3.1 Flexural Test

Flexural properties of the PMMA, PMMA-POSS composites, and the PMMA syntactic foams were determined using a Shimadzu Universal Testing Machine. The bar-shaped specimens were used to conduct the flexural test according to ISO 178 standard. Analysis was carried out using a 100 kN load cell and with a crosshead speed of 2 mm/min. The average of the five measurements with their standard deviations was reported.

3.3.3.2 Impact Test

Impact strength values of the PMMA, PMMA-POSS composites and the PMMA syntactic foams were determined using a Ceast Resil Impactor equipped with a hammer of 7.5 J, according to ISO 179.

3.3.3.3 Shore D Hardness Test

The hardness of the specimens was measured using the Shore D scale durometer, TH21 according to ASTM D2240. The test was applied to the selected specimens of PMMA syntactic foams, PMMA-POSS composites, PMMA hybrid syntactic foams and PMMA foams which were obtained from the $scCO_2$ processing as well as the

neat PMMA. Before the measurements, the surface of the specimens was rubbed with sandpaper in order to obtain smooth surfaces which are stated in ASTM D2240.

3.3.4 Thermal Characterization

3.3.4.1 Thermal Gravimetric Analysis (TGA)

The thermal degradation behavior of the neat PMMA, PMMA composites and PMMA foams were obtained with a Shimadzu, DTG-60H Thermal Gravimetric Analyzer under the nitrogen atmosphere. The experiments were carried out with a heating rate of 10 ºC/min and from 25ºC to 800ºC. Based on the analysis the temperature at 5 wt.% loss and the degradation temperatures were determined. The temperatures at the maximum weight loss were obtained from the first derivative of the TGA curves.

3.3.4.2 Differential Scanning Calorimetry (DSC) Analysis

The glass transition temperatures (Tg) were obtained using a Shimadzu DSC-60A Differential Scanning Calorimeter. Analyses were carried out under a nitrogen atmosphere with a heating rate of 10ºC/min. Two heating runs were carried out for the neat PMMA, PMMA composites and PMMA syntactic foams. The first run was applied from 25ºC to 250ºC. After that the specimens were cooled to 25ºC, the second run was performed from 25ºC to 400ºC. The PMMA foams which were obtained with $scCO_2$ processing were heated from 25ºC to 400ºC and the Tg values were determined from this run.

3.3.4.3 Thermal Conductivity Measurements

The thermal conductivities of the neat PMMA, PMMA-POSS composites and PMMA foams were obtained using an Anter Unitherm™ Model 2022 Thermal

Conductivity Meter according to ASTM E1530. The experiments were carried out at 30ºC using the disk shape test specimens with a diameter of 50 mm and thickness of 2 mm. The analyses were conducted at the General Directorate of Mineral Research and Exploration Laboratories, Ankara, Turkey.

3.3.5 Limiting Oxygen Index (LOI) analysis

The Limiting Oxygen Index (LOI) value is the minimum oxygen concentration in a mixture of O_2 and N_2 which satisfies the combustion of a polymer. The bar shape specimens with the dimensions of 4 mm x 10 mm x 80 mm were burned according to ASTM-D2863. The burning was conducted under the predetermined oxygen concentration until the 50 mm or less of the specimens burned in 180 s without extinguishing. LOI analyses were conducted using a Dynisco Limiting Oxygen Index Equipment in order to observe the effects of pore formation, HGM and POSS addition into the PMMA matrix on the flame retardancy of PMMA.

3.3.6 Ash Content Measurement

The ash content of the syntactic foams and the hybrid syntactic foams were obtained according to the ASTM D5630-13 and the average of three measurements and the standard deviations were calculated. These values corresponded to the total weight percentages of the HGMs and POSS in the composite and provided information about the validity of the targeted HGM concentrations in PMMA syntactic foams.

3.3.7 Viscosity Average Molecular Weight Measurement of PMMA

The viscosity average molecular weight of PMMA was measured by using an Ubbelohde viscometer. For this purpose, PMMA was dissolved in acetone with different concentrations at 25°C and the time for the flowing of this solution through the capillary of Ubbelohde was measured. The time measurements were carried out

three times and the averages of the time were used in the calculations. Huggins-Kraemer plot for PMMA in acetone is given in Appendix A. The intersection of reduced viscosity (η_{red}) and inherent viscosity (η_{inh}) gave the intrinsic viscosity ([η]) of PMMA in acetone. The viscosity average molecular weight of PMMA was obtained from Equation (3);

$$[\eta] = K M_v{}^{a} \quad (3)$$

where K and a are the Mark-Houwink-Sakurada constants for specific polymer and solvent solutions which are equal to 0.000096 dl/g and 0.69, respectively for PMMA in acetone at 25°C [132].

3.3.8 Fourier Transform Infrared Spectroscopy (FTIR) Analysis

FTIR analysis was carried out to investigate the chemical structure of the neat and the surface-modified HGMs. For this purpose, samples were analyzed using a Shimadzu IR Prestige-21 FTIR Spectrophotometer in the wavenumber range of 400-4000 cm^{-1}.

3.3.9 Design of Experiment (DOE)

The effects of the parameters of the study which are process temperature, pressure, time, venting rate, the concentration of HGMs, and the concentration of POSS nanoparticles in the composites, on the foam morphology were analyzed with DOE. A full factorial design method based on the two-level, the two-factorial design was applied. The factors are the parameters that were aimed to be investigated, and the levels are the upper and lower limits for these parameters that were selected based on the literature on neat PMMA and PMMA composite foaming [10, 90, 94, 111] and the process limits of the experimental setup. The lower level and upper level values of process time were 2 h and 24 h, while those of process temperature were 35ºC and 100ºC, respectively. Both levels are above the critical temperature of CO_2

(31.1 ºC), while the upper level is close to the glass transition temperature of PMMA (116 ºC). For pressure, 11 MPa was the lower level, which is higher than the critical pressure of CO_2 (7.4 MPa) and 32 MPa was the upper level, which was decided based on the pressure limit of the vessel (34 MPa). The lower and upper levels of depressurization rate were about 0.007 MPa/s and about 0.41 MPa/s respectively, which were referred to the slow and fast venting rates. The lower levels of the process parameters selected in this study allow foaming to be carried out still at supercritical conditions, yet a more economical supercritical process can be designed in case foaming were effectively achieved at these mild processing conditions. These values can be seen in Tables 3.6. and 3.7. Average pore size and pore density were determined to be the values that were affected by the parameters which are the most effective factor on both mechanical and thermal properties of foams which were obtained with $scCO_2$ processing. In order to evaluate the design of the experiment analyses, "JMP Statistical Software" was used. The software proposed the number of experiments that should be conducted for DOE which is equal to the number of factors to the power of the number of levels. The significance of the effects of the parameters on the pore morphology was determined based on the p-values of the parameters that were obtained from the JMP statistical software.

Table 3.6 Levels for the $scCO_2$ foaming process of PMMA-POSS composites.

Parameters	**Lower limit**	**Upper limit**
Temperature (ºC)	35	100
Time (h)	2	24
Pressure (MPa)	11	32
Venting Rate	Slow	Fast

Table 3.7 Levels for the $scCO_2$ foaming process of PMMA-HGM-POSS composites.

Parameters	**Lower limit**	**Upper limit**
Time (h)	2	24
Pressure (MPa)	11	22
HGM concentration (%)	5	15
POSS concentration (%)	0	5

CHAPTER 4

RESULTS AND DISCUSSION

The main aim of the thesis study is to reduce the density of the PMMA without sacrificing the mechanical properties. For this purpose, syntactic foam production and $scCO_2$ foaming methods were performed. The effects of different foaming techniques on the properties of the PMMA foams are discussed in four main parts in this chapter. In the first part, PMMA syntactic foams were produced using extrusion process. The effects of the HGM density, concentration, and surface modification on the properties of syntactic foams were examined in terms of morphology, density, thermal and mechanical properties. In the second part, the PMMA-POSS composites with two types of POSS were prepared to investigate the effects of POSS types and concentration on the properties of PMMA. Then the POSS that resulted in more enhanced properties were used to produce PMMA hybrid syntactic foams. PMMA hybrid syntactic foams were produced by dispersing both the selected POSS and HGMs to improve the mechanical properties of the syntactic foams while maintaining the density reduction and thermal properties. The third part includes the results of the $scCO_2$ foaming of the PMMA and PMMA-POSS composites. The effects of foaming parameters and a CO_2-phillic POSS concentration on the morphology in terms of average pore size and pore density, thermal properties and density of the foams were examined. In the fourth part, the $scCO_2$ foaming of PMMA syntactic foams with HGMs was performed. The effects of process parameters and the concentration of the HGMs and POSS nanoparticles were investigated. Finally, selected foams from these studies were combined and discussed in terms of their morphology, density, thermal and mechanical properties.

4.1 Effects of HGM Density and Surface Modification on the Mechanical and Thermal Properties of PMMA Syntactic Foams

PMMA syntactic foams were produced using different types of HGMs based on their densities and surface modification of HGMs with PMMA coating and silane treatment were considered to understand their effects on the morphology and the properties of the foams such as mechanical properties, density and thermal properties.

4.1.1 FTIR analysis

The silane treatment of the surface of the HGMs was carried out to increase the affinity of HGMs to the PMMA matrix. FTIR analysis was conducted to understand the success of the silanization process. The FTIR spectrum of the silane treated HGMs is given in Figure 4.1.

The silane-modified HGMs shows the characteristic peaks of the γ-methacryloxypropyltrimethoxysilane (γ-MTP) which are the absorption bands at 2945 and 2840 cm^{-1} (stretching of C–H bonds in alkyl and methoxy groups, respectively) and the bands at 1450 cm^{-1} (bending of C–H in CH_2 and CH_3 bonds) [132]. The band at 1718 cm^{-1} indicates that the hydrogen bonding between silanol groups of γ-MPS and glass [133]. Therefore, it can be concluded that the surfaces of the HGMs were treated with the silane coupling agent. A detailed explanation of the silanization steps is given in Appendix Part B.

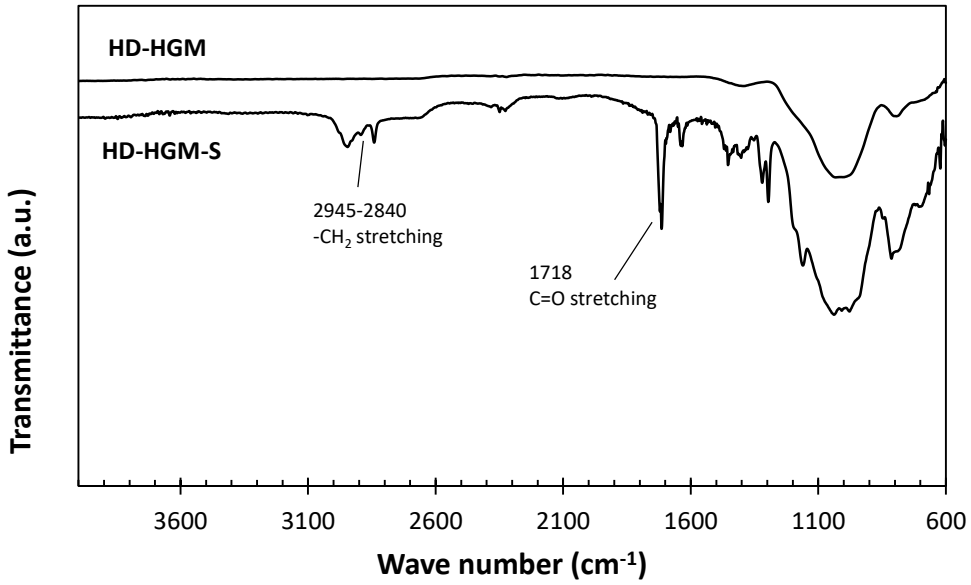

Figure 4.1. FTIR spectra of the HD-HGM-S with and without silane treatment.

The surfaces of the HD-HGMs were coated with PMMA to enhance the mechanical properties of the HGMs by increasing the compatibility between the HGM and PMMA. Figure 4.2 shows the FTIR spectra of the coated and uncoated HD-HGMs. The characteristic stretching peak of soda-lime-borosilicate glass is between 980 and 1040 cm^{-1} and attributed to the Si-O-Si stretching vibration in the spectrum of the uncoated HGMs. The characteristic peaks of PMMA in the spectrum of PMMA coated HGMs: C=O stretching of the acrylate carboxyl group at 1728 cm^{-1}, C–H bending vibration of the methyl group at 1435 cm^{-1} [134] and C-H bending at 972 cm^{-1} [135] represents that the surface of the hollow glass microspheres was successfully coated with PMMA.

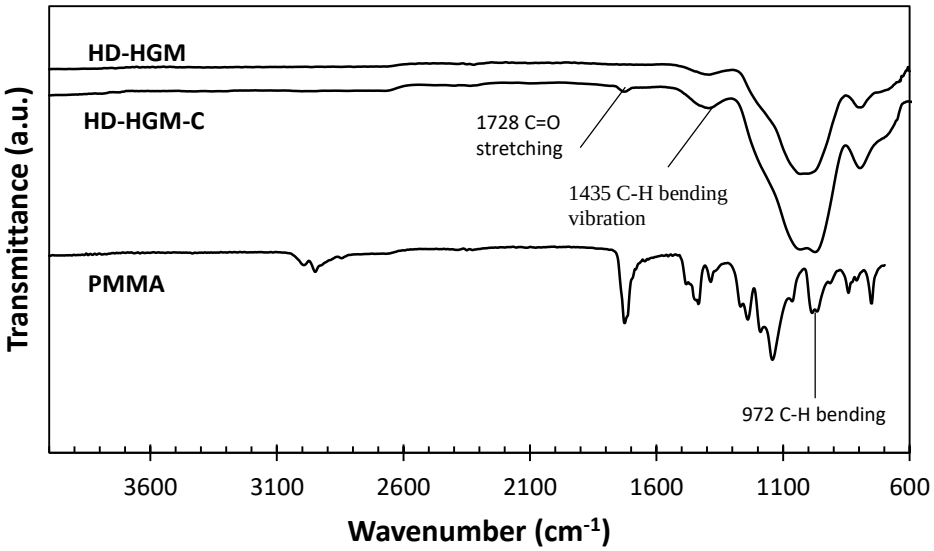

Figure 4.2. FTIR spectra of as received HGM, PMMA-coated HGM and the neat PMMA.

4.1.2 Morphological characterization

The SEM images of the flexural fractured surfaces of the PMMA syntactic foams with LD-HGMs, MD-HGMs, HD-HGMs, PMMA-coated HGMs (HD-HGM-C) and PMMA-silane-treated HGMs (HD-HGM-S) are represented in Figure 4.3.a-e, respectively. According to the images, HGMs were dispersed in the PMMA matrix homogeneously in all the syntactic foams prepared with the as-received and surface-modified HGMs. The LD- HGMs were shattered during the melt processing as can be seen in Figure 4.3.a. On the other hand, the MD-HGMs and HD-HGMs preserved their integrities (Figure 4.3.b and c). The voids between the hollow microspheres and the polymer matrix, as well as the spherical cavities which were formed due to the debonding of the HGMs during the fracturing process can be seen in Figures 4.3.b, 4.3.c and 4.3.e. This was due to incompatibility between the as-received HGMs and also silane-treated HGMs [60].

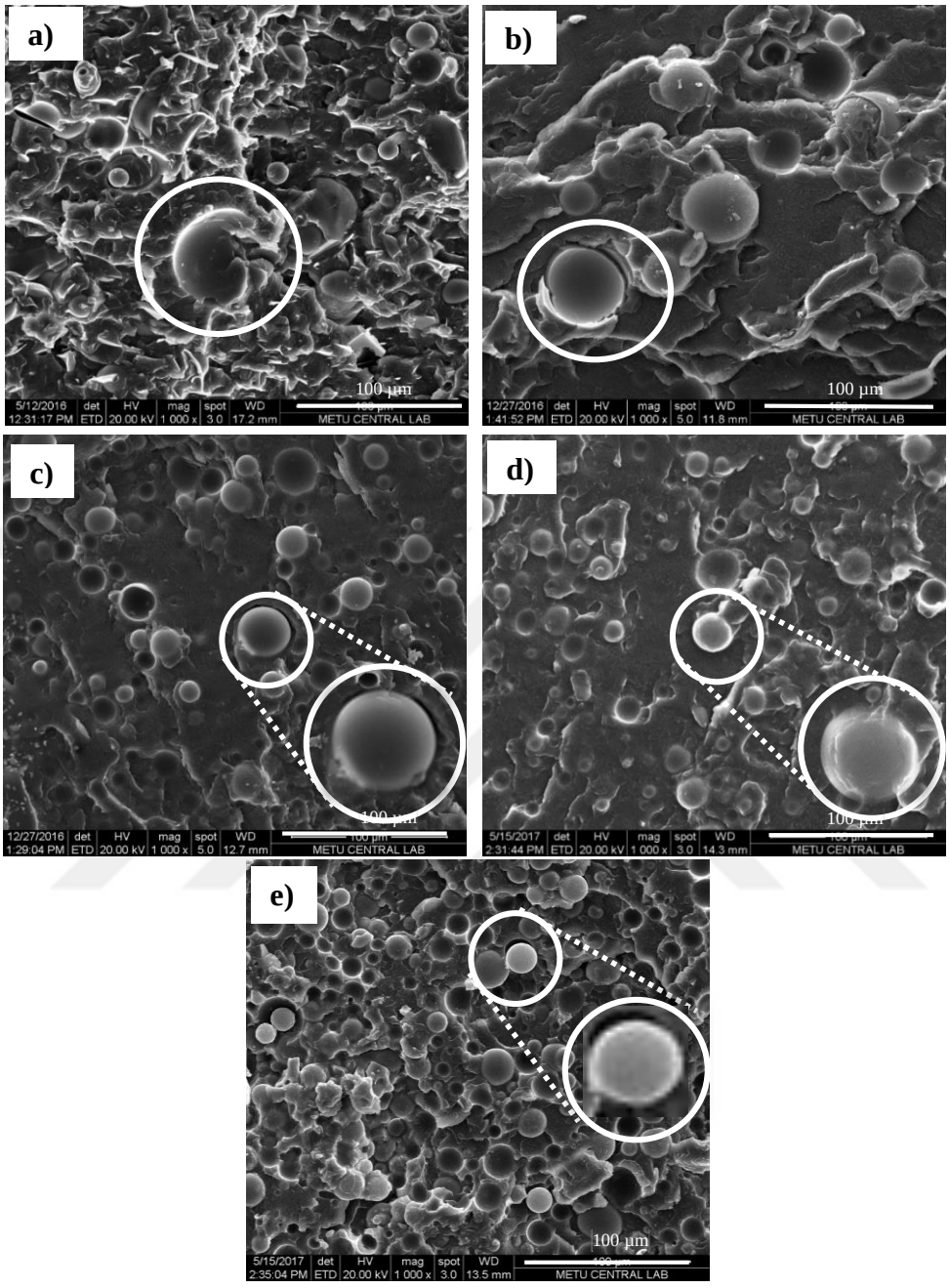

Figure 4.3. SEM images of PMMA syntactic foams with 15% a) LD-HGM, b) MD-HGM, c) HD-HGM, d) HD-HGM-C and e) HD-HGM-S. The white circle indicates the fractured LD-HGM in Fig.4.3.a, the voids between the uncoated HGMs and PMMA in Fig. 4.3.b, 4.3.c and 4.3.e, the coated HGMs embedded into the PMMA matrix in Fig.4.3.d.

On the other hand, the SEM image of the syntactic foam with silane-treated HGMs showed that HGMs were slightly agglomerated compared to the syntactic foams produced with the as-received or PMMA coated HGMs. These slight agglomerates of HGMs can be due to the higher amount of silane coupling agent which may have resulted in unreacted hydroxyls on the HGM surface [136].

The enhanced compatibility between the HD-HGMs and the PMMA matrix can be observed from the SEM image of the fracture surface of the 15% coated HD-HGM syntactic foams (Figures 4.3.d) where the voids between the PMMA and the HD-HGMs surfaces were eliminated.

4.1.3 Mechanical characterization

The effects of HGM type and weight percentage on the mechanical properties of PMMA syntactic foams were investigated with flexural and impact tests. The flexural strength of the PMMA and PMMA syntactic foams are given in Figure 4.4. The results are also given in Table C.1 in Appendix Part C.

The flexural strength of the PMMA was decreased with the incorporation of HGMs. Higher percent incorporation of HGMs further reduced the strength. This can be due to the restricted load transfer from the matrix to the hollow glass microspheres since there were voids between them. The flexural strength of the syntactic foams with HD-HGM had the highest strength, followed by composites with MD-HGM and LD-HGM. It can be concluded that increasing HGM density increased the flexural strength. This can be explained by the higher crush strength of the HD-HGM (Table 3.2). Reduction in the flexural strength, tensile strength, or compressive strength of vinyl ester [137], PP [67] and epoxy [65,68] with the incorporation of hollow microspheres were also reported in several studies. Doumbia et al. defined the decreased mechanical properties with the lowered mobility of polymer chains, while Swetha et al. and Gupta et al. defined with the reduced content of the load-bearing

matrix. Based on Figure 4.4, it can be said that the incorporation of the silane-treated HGMs decreased the flexural strength of PMMA more than as-received HGMs. The reason for decreasing strength can be the formation of HGM agglomerates due to the preference of HGMs to each other more than to the PMMA matrix. On the other hand, the coating of the HGMs with PMMA led to improved mechanical properties. Syntactic foam with 15 wt.% coated HD-HGM had 12% higher flexural strength than the syntactic foam with 15 wt.% uncoated HD-HGM. However, the flexural strength of the syntactic foam with 15 wt.% coated HD-HGM is still lower than that of the neat PMMA [60].

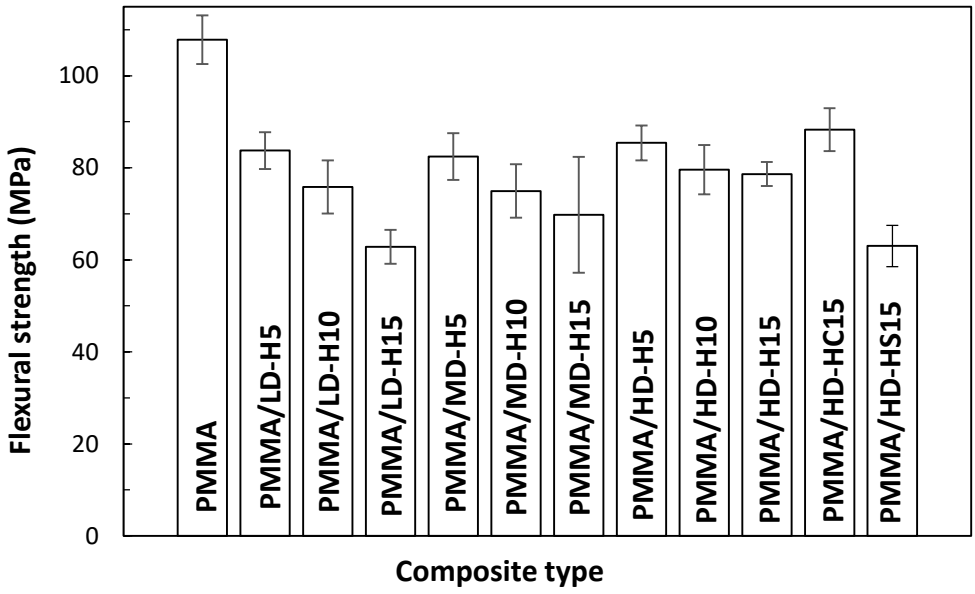

Figure 4.4. Flexural strength of the neat PMMA and the PMMA syntactic foams.

Flexural moduli of PMMA and syntactic foams are given in Figure 4.5. The flexural modulus values are also given in Table C.1 in Appendix Part C.

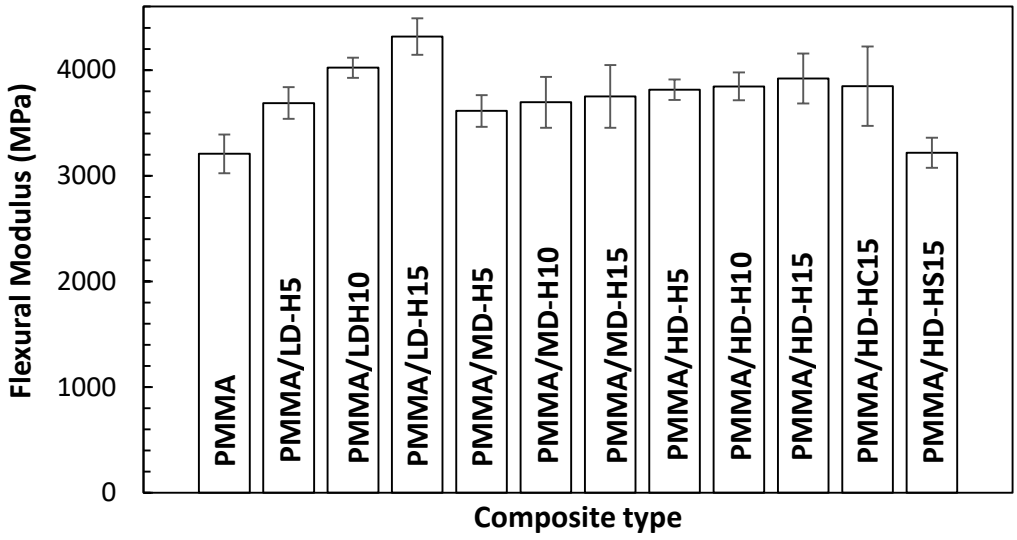

Figure 4.5. Flexural modulus of the neat PMMA and the PMMA syntactic foams.

Figure 4.5 shows that the flexural modulus of PMMA was enhanced with the incorporation of HGMs. This can be due to the rigidity of HGMs. The shattering of the LD-HGM during melt processing led to higher modulus of the syntactic foams with LD-HGM than those with MD-HGM and HD-HGM. This was due to the increasing number of glass particles in the PMMA matrix. Restriction of the movement of the PMMA chains due to the presence of the particles enhanced the flexural modulus of the composites [60]. The smaller particle size of the HD-HGMs (Table 3.2) resulted in more number of particles in the PMMA matrix when it is compared with the other HGMs at the same concentration. The higher flexural moduli of the HD-HGM composites than the MD-HGM composites were attributed to the presence of a higher number of HGMs inside the PMMA matrix. Tagliavia et al. also stated that among the vinyl ester syntactic foams with four different types of HGMs, the composites with the high-density HGMs had higher modulus [137]. On the other hand, the silane treatment of the HGMs resulted in lower flexural modulus. The lower modulus of PMMA/HD-HS15 composite can be caused by the presence of the silane coupling agent. Kanie et al. also explained the decreasing flexural

modulus in PMMA with the increasing γ-MPS content by the increased space between molecules or the increased flexibility of the PMMA chains [138]. The presence of silane groups at the PMMA-HGM interface can form weak interactions between the PMMA matrix and HGM which allow PMMA chains to move more easily than those in the rigid PMMA-as received HGM matrix. The coating of the surface of the HGMs with PMMA did not improve the flexural modulus of the PMMA syntactic foam. This can be due to the dominant contribution of the existence of HD-HGMs in the matrix at a 15% loading level than the contribution of the interactions at the interface. The PMMA matrix with the addition of uncoated and coated HGMs had similar rigidity.

The impact strength of the PMMA and the PMMA syntactic foams is given in Figure 4.6. The impact resistance values of the PMMA and the PMMA syntactic foams were also given in Table C.1 in Appendix Part C.

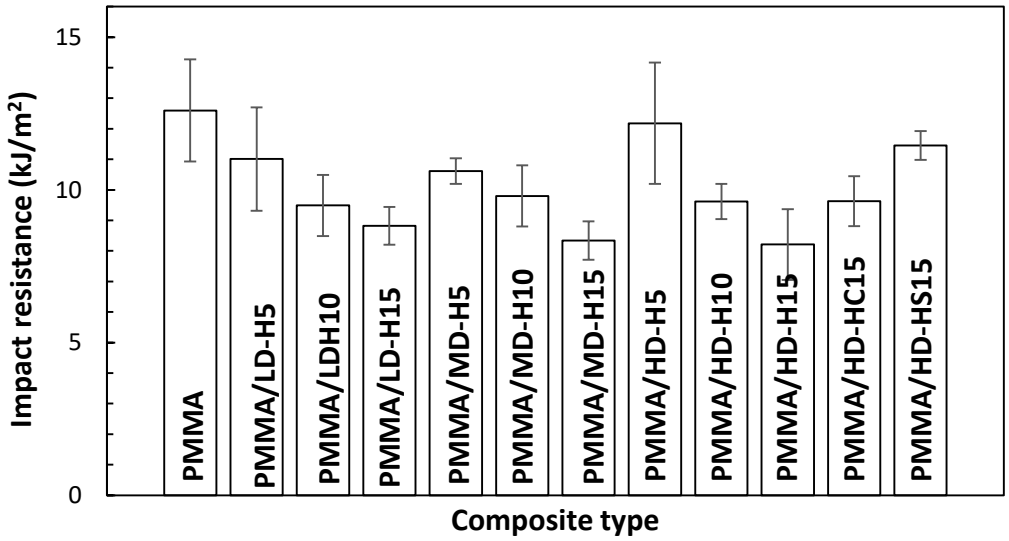

Figure 4.6. Impact resistance of the neat PMMA and the PMMA syntactic foams.

With the introduction of HGMs to the PMMA matrix, the impact strength values were decreased due to the insufficient load transfer. Based on the figure it can be

said that the volume fraction of HGMs is highly effective on the impact strength of the syntactic foams. The highest impact strength values belonged to the PMMA 5 wt.% HGM composites for each HGM type. The addition of a higher amount of HGM, further decreased the impact strengths of the composites. The creation of more stress around the interface of these HGMs during the impact loading caused a reduction in the impact resistance. PP and ABS syntactic foams with HGMs showed lower impact strength values than those of the neat polymers [67, 139]. In addition, among the PP syntactic foams with different HGMs, the high-density HGMs resulted in higher impact strength than the syntactic foams with the lower density HGMs. PMMA/HD-H5 syntactic foam had the highest impact strength among the syntactic foams of this study. This can be explained with the greater crush strength of the HD-HGMs than the MD-HGMs and LD-HGMs [67]. The silane treatment may cause enhanced flexibility in the matrix [138], thus an improvement in the impact strength was obtained. A 17% greater impact resistance was obtained with the incorporation of 15 wt.% surface coated HGMs than the incorporation of 15 wt.% HD-HGMs [60]. The crush strength (resistance to impact loading) of the HGMs may have also improved with the coating of the HGMs with PMMA.

4.1.4 Density measurements

Table 4.1 represents the measured and theoretical densities of PMMA syntactic foams. The density of the neat PMMA was calculated as 1.20 ± 0.003 g/cm^3. The rule of mixture was used to conduct the calculation for the theoretical density values. The theoretical densities of the syntactic foams with the surface treated HGMs cannot be calculated since the bulk density of the surface-treated HGMs is unknown. Syntactic foams with surface modified HGMs were prepared only at the concentration of 15 wt.% and their densities are represented in Table 4.1. All syntactic foams had lower densities than the neat PMMA except for syntactic foams with LD-HGMs. The shattering of these HGMs during the melt processing due to high shear loading caused an increment in the density. The incorporation of MD-

HGMs up to 15 wt.% in the PMMA matrix did not significantly decrease the density of the PMMA. However, theoretical densities of the MD-HGM syntactic foams were lower than the measured densities of them. This can be due to the partial shattering of the HGMs during the melt processing. The highest density reduction was observed in the syntactic foams of HD-HGMs. This can be due to the highest crush strength of these HGMs among the as-received HGMs [60]. In Doumbia et al.'s study, PP syntactic foams with the addition of low-density HGMs, increment in the density of the neat polymer was observed. In addition, they also found out that the highest reduction in the density was obtained with the addition of high-density hollow glass microspheres [67]. The density of the HGMs is the most effective parameter which determines the density of the syntactic foams. The syntactic foams obtained with modified HGMs resulted in a slight increase in the density compared to the as-received HGMs. This can be due to the slight increase in the density of the HGMs with the modification process.

Table 4.1 Densities of the PMMA syntactic foams and the neat PMMA.

Composite/ HGM%	% Ash content			Measured density			Theoretical density		
	5%	10%	15%	5%	10%	15%	5%	10%	15%
PMMA/ LD-H	5.04 ± 0.49	8.59 ± 0.42	11.98 ± 0.08	1.23 ± 0.002	1.25 ± 0.003	1.28 ± 0.008	0.83	0.68	0.58
PMMA/ MD-H	6.64 ± 0.02	12.67 ± 0.05	12.49 ± 0.05	1.15 ± 0.002	1.13 ± 0.002	1.13 ± 0.006	1.04	0.93	0.94
PMMA/ HD-H	8.73 ± 0.06	11.56 ± 0.07	14.13 ± 0.22	1.12 ± 0.001	1.09 ± 0.003	1.07 ± 0.003	1.10	1.08	1.05
PMMA/ HD-HC			14.75 ± 0.28	-	-	1.08 ± 0.002	-	-	-
PMMA/ HD-HS	-	-	-	-	-	1.09 ± 0.002	-	-	-

4.1.5 Thermal Characterization

Thermal degradation plots of the syntactic foams and the neat PMMA matrix are given in Figure 4.7. According to the figure, the thermal degradation behavior of

PMMA did not significantly change with the addition of HGMs. Temperatures at 5 wt. % loss and maximum weight loss are given in Table 4.2. In Lin et al.'s study, HGMs with four different densities were incorporated in epoxy and it was found that the incorporation of the three types of HGMs with lower densities reduced the temperature at 5 wt. % loss of epoxy [140]. According to Table 4.2., the incorporation of HGMs in PMMA led to a slight reduction in the temperature at 5 wt. % loss of PMMA independent from the HGM density. On the other hand, the temperatures at maximum weight loss of syntactic foams were almost the same as that of the neat PMMA. The composite with silane treated HGMs resulted in slightly increased thermal stability which may be due to the condensation between the silanol groups of the silane coupling agent and the surface hydroxyl groups of the HGMs [130].

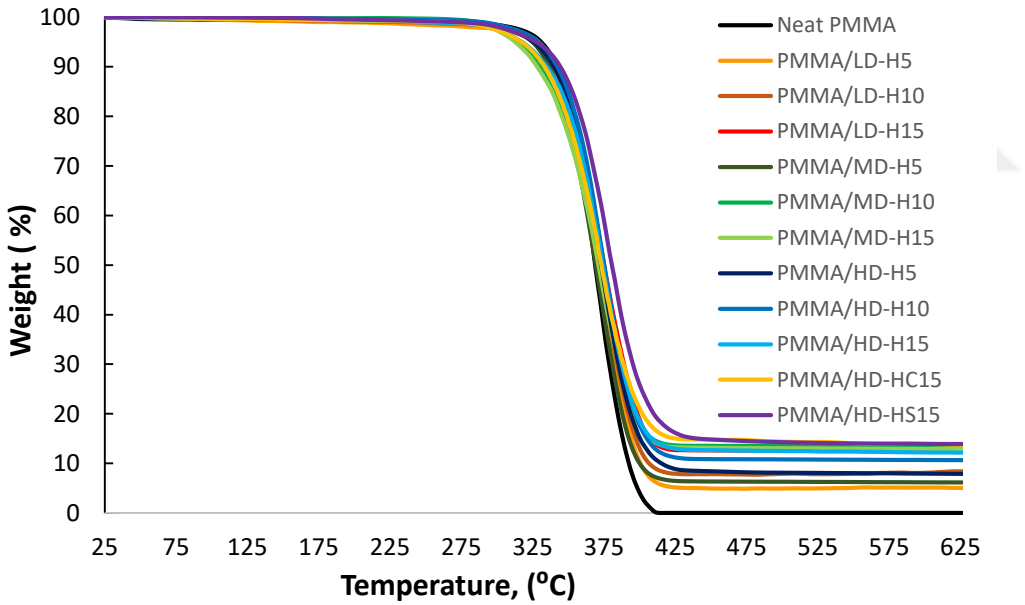

Figure 4.7. TGA curves of the PMMA syntactic foams and the neat PMMA.

The glass transition temperatures of the PMMA syntactic foams and the neat PMMA which were determined using differential scanning calorimetry analyses are also represented in Table 4.2. The addition of HGMs did not significantly change the

glass transition temperature of the neat PMMA. In addition, it was observed that the glass transition temperatures of the syntactic foams with the surface modified HGMs also remained at a similar value to that of the neat PMMA [60].

Table 4.2 Temperatures at 5% weight loss (T5%), temperatures at maximum weight loss (T_{max}) and glass transition temperatures of the PMMA syntactic foams and the neat PMMA.

Sample	**$T_{5\%}$ (ºC)**			**T_{max} (ºC)**			**T_g (ºC)**		
PMMA	331			371			116		
Syntactic Foam	HGM %			HGM %			HGM %		
	5%	10%	15%	5%	10%	15%	5%	10%	15%
PMMA/LD-H	327	329	325	370	374	375	115	115	115
PMMA/MD-H	325	316	313	376	374	375	117	117	116
PMMA/HD-H	325	329	318	375	377	375	117	116	115
PMMA/HD-HC	-	-	317	-	-	373	-	-	114
PMMA/HD-HS	-	-	327	-	-	378	-	-	114

The thermal conductivities of the PMMA syntactic foams and the neat PMMA were measured at 30ºC (± 2ºC) and are given in Table 4.3. The thermal conductivities of the neat PMMA and syntactic foams of PMMA/LD-H15 and PMMA/HD-H15 were found as 0.14, 0.13 and 0.12 W/mK, respectively. The thermal conductivity of PMMA/HD-HC15 was also measured and found as 0.15 W/mK [60]. The stable thermal conductivities may result from the small concentration of HGMs (up to 15 wt.%) in the PMMA matrix. In Zhu et al.'s study, the addition of 60 vol.% HGMs slightly reduced the thermal conductivity of the polymer. They explained the reduction in the thermal conductivity with both the presence of HGMs itself and the formation of voids between the matrix and the surface of the hollow glass microspheres [141].

Table 4.3 Thermal conductivities of the PMMA syntactic foams and the neat PMMA.

Sample	Thermal Conductivity (W/mK)
PMMA	0.14
PMMA/LD-H5	0.12
PMMA/LD-H10	0.12
PMMA/LD-H15	0.13
PMMA/HD-H5	0.12
PMMA/HD-H10	0.13
PMMA/HD-H15	0.12
PMMA/HD-HC15	0.15

In this part of the thesis study, three types of HGMs based on their densities were used to produce PMMA syntactic foams at 5, 10 and 15 wt.% concentrations. While the melt processing caused the deformation of the low density HGMs, the medium and the high density HGMs preserved their integrities in PMMA matrix. The addition of medium and high density HGMs resulted in the reduction in the density of the PMMA and higher percent addition of the HGMs further decreased the density. However, the addition of the HGMs also decreased the mechanical properties of the PMMA. As a result of the study, it was found that incorporation of the high density HGMs resulted in greater density reduction and higher mechanical properties than the incorporation of the medium and low density HGMs. The coating of the HGMs with PMMA enhanced the compatibility between the PMMA matrix and HGMs which can be observed by the morphology analyses. Thus, flexural and impact strengths of the PMMA syntactic foams were improved with the addition of PMMA coated HGMs. On the other hand, the silane treatment did not improve the mechanical properties. The thermal properties of the PMMA did not significantly change with the addition of HGMs.

4.2 Effects of POSS Nanoparticle Reinforcement on the Properties of PMMA Hybrid Syntactic Foams

Hybrid syntactic foams consist of HGMs and a reinforcement material which were dispersed in the polymer matrix. In this work, hybrid syntactic foams were produced to improve the mechanical properties of the PMMA syntactic foams without sacrificing the density. For this purpose, first PMMA-POSS composites were produced using two different types of POSS as octaphenyl and octaisobutyl POSS at the weight percentage of 0.25, 0.5, 1 and 3% to understand the effect of POSS type and concentration on the PMMA properties. After that, the particles of the selected POSS type were dispersed in the PMMA matrix together with the HGMs. In this part of the thesis study, the effects of the POSS nanoparticles on the morphology, density, mechanical and thermal properties of the syntactic foams were evaluated. In addition, the effects of the HGM and the POSS concentration on the properties of PMMA were assessed.

4.2.1 Characterization of PMMA-POSS Composites

4.2.1.1 Morphological characterization

SEM analyses were conducted to investigate the morphologies of the PMMA-POSS composites. The flexural fractured surface of the neat PMMA (Figure 4.8.a) and PMMA-POSS composites are given in Figure 4.8.

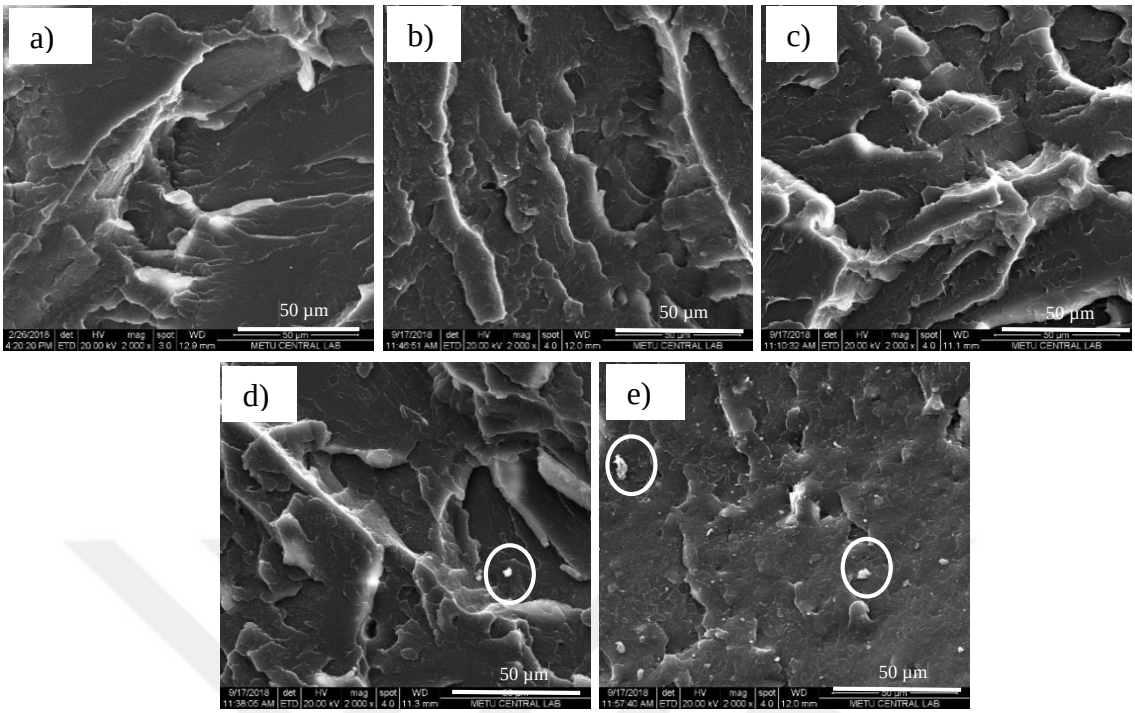

Figure 4.8. SEM images of the fractured surface of a) neat PMMA, and PMMA composites with b) 0.25% octaisobutyl POSS, c) 0.25% octaphenyl POSS, d) 1% octaisobutyl POSS and e) 1% octaphenyl POSS. In Figure 4.8 the white circles indicate the agglomerates of POSS nanoparticles.

The SEM images of the PMMA-POSS composites with the addition of the 0.25 wt% octaphenyl and octaisobutyl POSS (Figure 4.8.b and c) represent that the POSS nanoparticles were homogeneously dispersed due to the compatibility of the selected POSS nanoparticles with the PMMA matrix [51]. On the other hand, the SEM images of the PMMA-POSS composites with 1 wt.% POSS exhibited agglomerates of POSS nanoparticles (Figure 4.8.d and e).

4.2.1.2 Mechanical characterization

The mechanical properties of the PMMA-POSS composites were examined by conducting flexural and impact analyses. Figure 4.9 shows the flexural strengths of

PMMA-POSS composites. Averages of the flexural strength of PMMA-POSS composites and their standard deviations are summarized in Table C.2 in Appendix Part C.

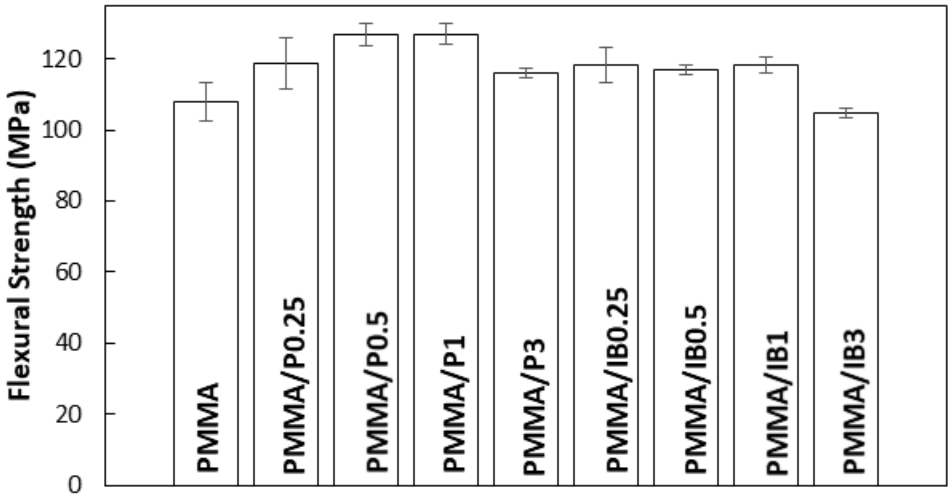

Figure 4.9. Flexural strengths of the neat PMMA and the PMMA-POSS composites.

Figure 4.9 showed that the incorporation of both types of POSS improved the flexural strength of PMMA at the concentration of 0.25, 0.5 and 1 wt.%. However, the addition of a higher amount of POSS nanoparticles at 3 wt.% octaisobutyl POSS decreased the flexural strength of the PMMA due to the POSS agglomerations which were formed at this concentration. The properties of the polymers can be improved by POSS in case they were well dispersed and reduced to nano size. The addition of high concentrations of the POSS nanoparticles in PMMA may result in the insufficient dispersion of the POSS nanoparticles during the extrusion process in which the clusters remained intact. The comparison of the octaphenyl POSS with the octaisobutyl POSS composites represents that the flexural strength of the PMMA composites with octaphenyl POSS resulted in higher strength values. This can be explained by the more favorable compatibility of octaphenyl POSS with PMMA. While octaisobutyl POSS may interact with the polymer due to its long alkyl chain

[51], octaphenyl POSS may interact due to its large and unsaturated bonds [142]. The addition of 0.5 and 1 wt.% of octaphenyl POSS increased the flexural strength of PMMA by 18%. This can be explained with the more favorable interactions of the phenyl groups of octaphenyl POSS with PMMA. In Meth et al.'s study phenyl-modified SiO_2 nanoparticles stabilized a uniform colloidal dispersion in PMMA due to the enhanced affinity of the surface of the SiO_2 nanoparticles to PMMA [143]. n-π interaction between the phenyl ring of polycarbonate and methoxy group of PMMA was indicated by Asano et al. [142]. The addition of 5% modified nanoclay in PMMA matrix enhanced the flexural strength [144]. In this study, 18% improvement in the flexural strength was obtained with the incorporation of just 0.5% octaphenyl POSS [61].

Figure 4.10 shows the flexural moduli of the PMMA-POSS composites. Based on the figure, a slight increase in the flexural modulus of the PMMA was obtained with the incorporation of octaphenyl POSS. On the other hand, the incorporation of octaisobutyl POSS was not effective on the flexural modulus. The interaction between the phenyl groups and PMMA may introduce rigidity to the matrix [142].

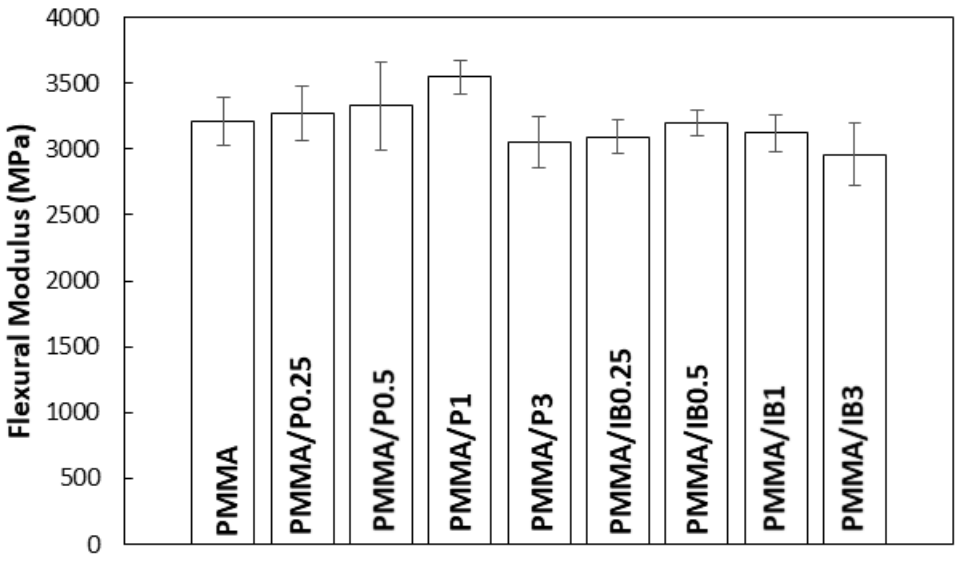

Figure 4.10. Flexural moduli of the neat PMMA and the PMMA-POSS composites.

The impact strength of the PMMA-POSS composites is presented in Figure 4.11. According to the figure, 0.25 and 0.5 wt.% incorporation of POSS in the PMMA matrix improved the impact strength of the PMMA since the homogeneous dispersion of the nanoparticles delayed the formation and distribution of the cracks. Higher percent addition of nanoparticles resulted in the decreased impact strengths that can be caused from the presence of POSS agglomerates. PMMA composites with octaisobutyl POSS and octaphenyl POSS was obtained in Tanaka et al.'s study. The octaphenyl POSS composites showed greater improvement in the thermomechanical properties of the polymer due to the large molecular structure and the unsaturated bonds of the functional groups in the octaphenly POSS [51]. Improvement in the impact strength of the PMMA nanocomposites with the addition of 2 wt.% halloysite nanotubes was obtained in Vuluga et al.'s study [145]. In the present study, the addition of 0.5% POSS nanoparticles enhanced the impact strength of PMMA.

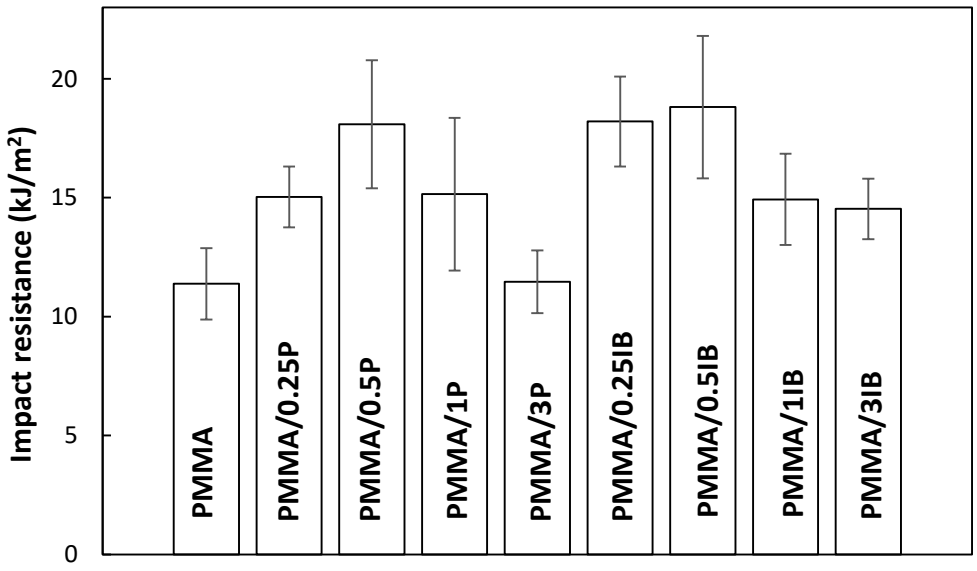

Figure 4.11. Impact strengths of the neat PMMA and the PMMA-POSS composites.

4.2.1.3 Thermal characterization

TGA and DSC analyses were carried out to understand the effects of POSS incorporation in PMMA [61]. The thermal decomposition behaviors of the composites and the neat PMMA are represented in Figure 4.12. The glass transition temperature, the temperature at 5 wt.% loss and temperature at maximum weight loss of the composites are summarized in Table 4.4. According to the TGA and DSC analyses, addition of neither the octaphenyl nor the octaisobutyl POSS was not effective on the temperature at maximum weight loss and glass transition temperature of the PMMA. The decomposition behaviors of the composites during the earlier steps of the thermal degradation were evaluated based on the temperature at 5 wt.% loss values and it was found that the POSS nanoparticles reduced the temperature at 5 wt.% loss of PMMA. PMMA- 3 wt.% octaphenyl POSS composites had the highest reduction in the temperature at 5 wt.% loss values. High thermal conductivity of POSS nanoparticles may lead to this reduction since the POSS nanoparticles may act as heat-dissipating agents during the earlier degradation step of the polymer. There are several studies which resulted in enhanced thermal conductivity of polymers with POSS nanoparticles due to the high thermal conductivity of POSS nanoparticles. Gu et al. found that the addition of aminopropyl isobutyl POSS into bismaleimide diphenylmethane composite increased the thermal conductivity of the neat polymer matrix [146]. In addition, it was found that the methyl methacrylate copolymer composites with monofunctionalized heptaisobutyl methacryl POSS had a higher thermal conductivity than the thermal conductivity of the neat polymer [147].

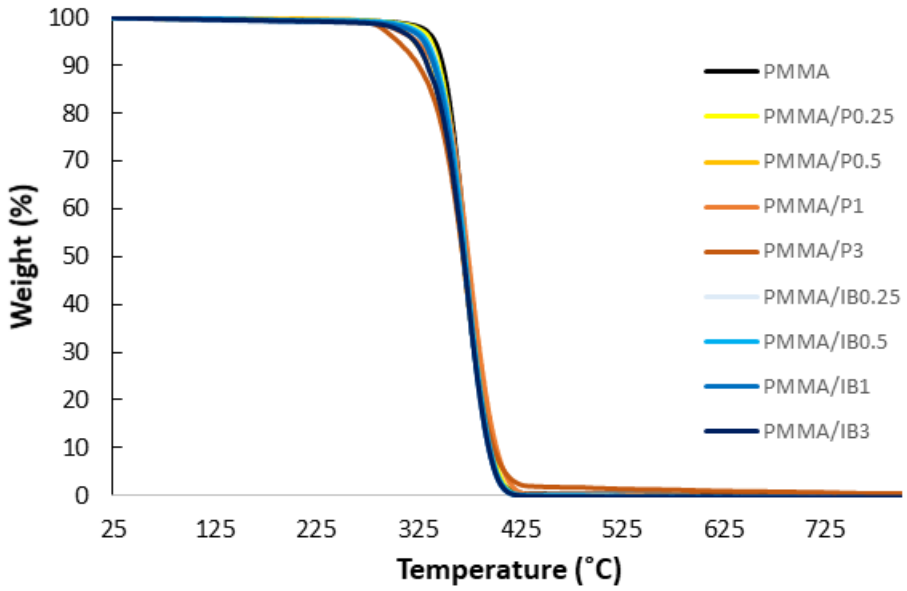

Figure 4.12. TGA curves of the PMMA-POSS composites and the neat PMMA.

Table 4.4 Temperature at 5% weight loss, temperature at maximum weight loss and glass transition temperature of the PMMA-POSS composites and the neat PMMA.

Sample Code	**$T_{5\%}$ (ºC)**	**T_{max} (ºC)**	**T_g (ºC)**
PMMA	341	375	116
PMMA/IB0.25	334	374	117
PMMA/IB0.5	334	375	117
PMMA/IB1	331	376	116
PMMA/IB3	322	376	115
PMMA/P0.25	338	375	119
PMMA/P0.5	321	373	117
PMMA/P1	324	378	118
PMMA/P3	305	371	117

4.2.2 Characterization of PMMA hybrid syntactic foams

In order to produce PMMA hybrid syntactic foams, Octaphenyl POSS was used as the reinforcement material. The selection was made based on the higher enhancement in the flexural strength and the flexural modulus of the PMMA with the incorporation of octaphenyl POSS than addition of octaisobutyl POSS. The concentrations of the POSS nanoparticles were selected as 0.25, 0.5 and 1 wt.% due to the decreased mechanical properties of PMMA with the incorporation of 3 wt.% POSS incorporation in the PMMA-POSS composite studies [61].

4.2.2.1 Morphological characterization

The SEM images of the flexural fractured surface of the hybrid syntactic foams can be seen in Figure 4.13.

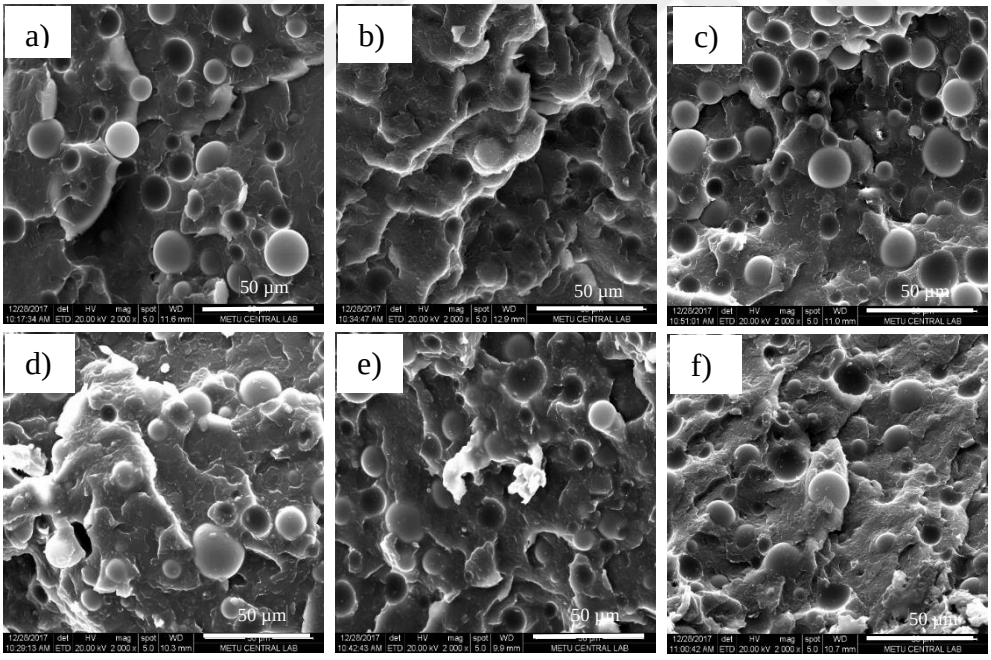

Figure 4.13. SEM images of the fractured surface of a) PMMA/H5/P0, b) PMMA/H10/P0, c) PMMA/H15/P0, d) PMMA/H5/P1, e) PMMA/H10/P1 and f) PMMA/H15/P1.

According to Figure 4.13, HGMs were well dispersed in the PMMA matrix without shattering during the extrusion and injection molding processes. The low compatibility between the HGMs and the PMMA matrix resulted in the debonding of some of the HGMs from the matrix. The SEM images of the hybrid syntactic foams with 1 wt.% POSS (part d, e, and f) show that there are a few POSS agglomerates on both surfaces of the HGMs and in the matrix, while the surfaces of the HGMs in the neat syntactic foams (part a, b and c) are plain. Thus, a slight agglomeration of POSS nanoparticles in the composites with 1 wt.% POSS addition can be indicated. This can be due to the presence of the HGMs which may restrict the dispersion of the POSS nanoparticles during the extrusion process.

4.2.2.2 Mechanical characterization

The effects of POSS incorporation on the flexural and impact properties of the composites were examined by the flexural test. Specific mechanical properties of the composites were obtained by dividing the mechanical properties of a syntactic foam to the density of the syntactic foams. These properties give information about the mechanical properties of a composite by eliminating the effects of density. The specific flexural strength values of the neat PMMA and the PMMA syntactic foams are given in Figure 4.14 which represents that the incorporation of HGMs into PMMA reduced the flexural strength of the PMMA. The reduction in the load-bearing matrix with the addition of HGMs may result in the decreasing flexural strength values [68]. The reduced flexural strength in PMMA [60], PP [67] and vinyl ester [137] matrices with the incorporation of HGMs was also stated in syntactic foam studies [60]. Incorporation of POSS nanoparticles caused slight increase in the specific flexural strength of the 10 and 15 wt.% of HGM syntactic foams. Figure 4.14 shows that the PMMA syntactic foam with 15 wt.% HGM and 0.5 wt.% POSS resulted in the greatest enhancement in specific flexural strength value when it was compared with the PMMA syntactic foams with 15 wt.% HGM. The improvement in the syntactic foam of this composite was 15.4%. This composite was also the

composite which had the greatest density reduction in PMMA. It can be concluded that the addition of POSS nanoparticles enhanced the flexural strength without causing any adverse effect in the density [61].

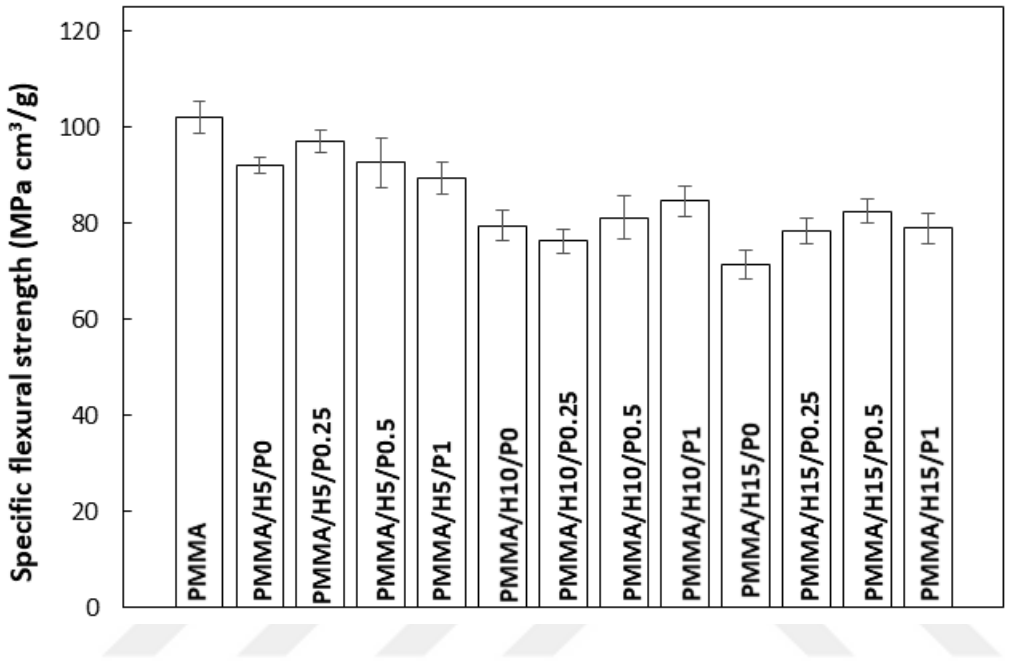

Figure 4.14. Specific flexural strengths of the PMMA hybrid syntactic foams.

According to Figure 4.15 specific flexural moduli of PMMA improved with the addition of HGMs due to the rigidity of the HGMs which restrict the movement of PMMA chains. As explained earlier, increasing HGM concentration further improved the modulus of the PMMA. There are several studies which also showed that the addition of HGM in polymer matrix resulted in the increasing modulus values [67, 137]. Hybrid syntactic foams with the incorporation of POSS nanoparticles resulted in more enhanced specific flexural moduli values for PMMA syntactic foams. On the other hand, the relation between the flexural moduli and the POSS concentration did not follow a trend. The highest enhancement in the specific flexural modulus is obtained with the PMMA syntactic foams with 15 wt.% HGM and 0.25 wt.% POSS which shows 37.6% higher specific flexural strength than the

PMMA [61]. The highest reduction in density was also observed in the PMMA syntactic foams with 15 wt.% HGMs.

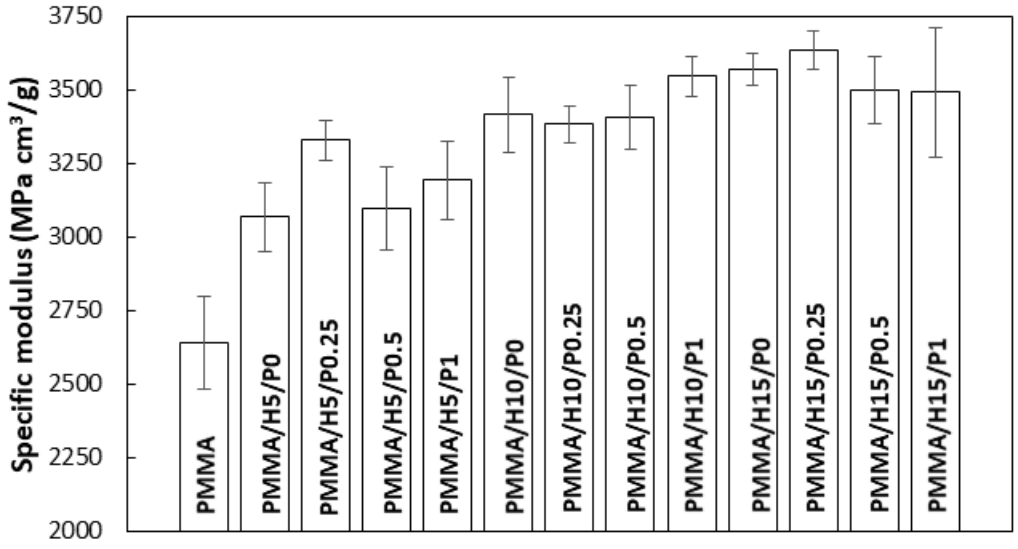

Figure 4.15. Specific moduli of the PMMA hybrid syntactic foams.

Figure 4.16 represents the specific impact strengths of the PMMA syntactic foams. Based on the figure, the incorporation of POSS nanoparticles did not change the specific impact strengths of the syntactic foams except for the syntactic foams with 5 wt.% HGMs. The reason for the unchanged specific impact values can be due to the insufficient dispersion of POSS nanoparticles during the extrusion because of the presence of a higher amount of HGMs. The SEM images of the PMMA hybrid syntactic foams also exhibited the formed agglomerates of the POSS nanoparticles in the syntactic foam matrix (Figure 4.13.d, e and f). On the other hand, the decreasing trend in the impact strength with the incorporation of HGMs was explained before, with the insufficient load transfer between the polymer and the HGMs surfaces [60]. The formation of POSS agglomerates, that were acting as stress concentrated regions, caused a further decrease in the impact strength [61].

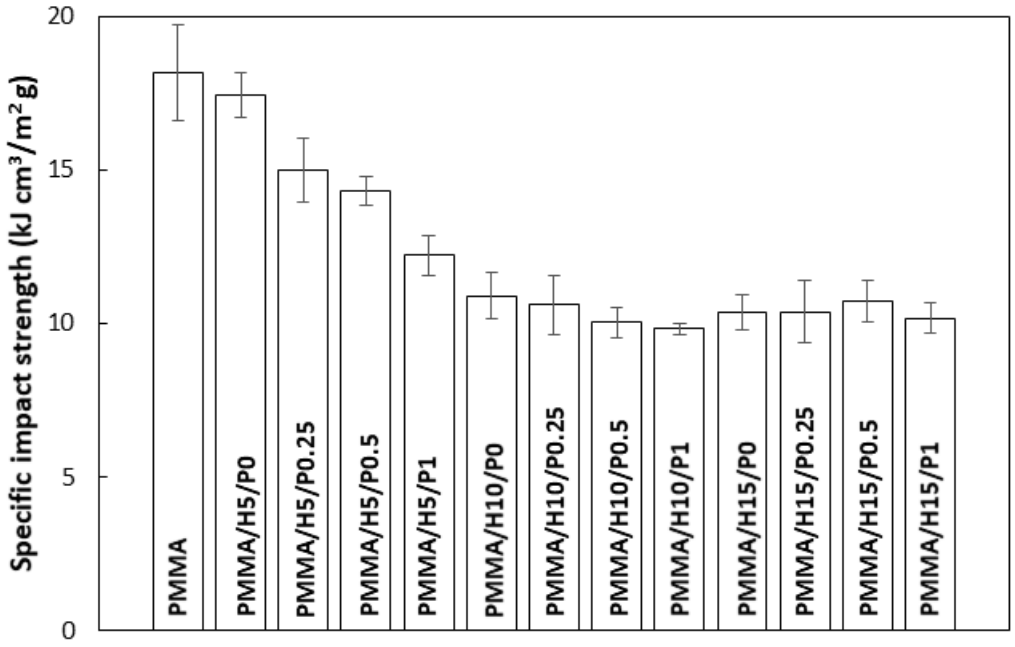

Figure 4.16. Specific impact strengths of the PMMA hybrid syntactic foams.

4.2.2.3 Density measurements

Densities and the ash contents of syntactic foams and the neat PMMA are given in Table 4.5. As explained earlier, density of the PMMA was reduced with the incorporation of HGMs, while higher percent incorporation of HGMs resulted in further reduction in the density. However, the incorporation of POSS nanoparticles did not significantly change the densities of the syntactic foams. This can be explained with the lower percent addition of POSS nanoparticles with a maximum value of 1 wt.%. The highest density reduction was 13.3% which was obtained with the 15 wt.% addition of HGM nanoparticles. The addition of POSS nanoparticles in PMMA resulted in a slight increase in the density. The density reduction in the hybrid syntactic foam with 1 wt.% POSS and 15 wt.% HGM was obtained as 12.5%. The ash contents values represent the amount of HGMs together with the residual amount of POSS nanoparticles in the composites. However, the ash contents of the

hybrid syntactic foams were assumed to reflect the concentration of HGMs, since the concentration of POSS nanoparticles were relatively lower (maximum of 1 wt.%) than the concentration of HGMs. The ash contents of the syntactic foams with different HGM concentrations were different from each other as expected. The ash content values were slightly different from the targeted HGM concentrations but they still approximately represent the values that were targeted. The possible concentration fluctuations in the extrusion process may cause slight differences in the HGM concentrations. In addition, higher percent addition of HGMs resulted in higher ash content values which can be attributed to the preserved integrities of the HGMs during melt processing and addition of POSS nanoparticles [61].

Table 4.5 Densities and ash contents of the hybrid syntactic foams.

Sample Code	**Density (g/cm^3)**	**Ash content (%)**
PMMA	1.20 ± 0.003	-
PMMA/H5/P0	1.13 ± 0.009	6.32 ± 0.02
PMMA/H5/P0.25	1.13 ± 0.006	6.12 ± 0.06
PMMA/H5/P0.5	1.13 ± 0.007	6.61 ± 0.10
PMMA/H5/P1	1.12 ± 0.006	7.24 ± 0.07
PMMA/H10/P0	1.09 ± 0.006	11.50 ± 0.13
PMMA/H10/P0.25	1.08 ± 0.003	11.46 ± 0.11
PMMA/H10/P0.5	1.08 ± 0.004	11.95 ± 0.06
PMMA/H10/P1	1.09 ± 0.008	11.84 ± 0.10
PMMA/H15/P0	1.04 ± 0.004	15.20 ± 0.06
PMMA/H15/P0.25	1.05 ± 0.005	15.22 ± 0.04
PMMA/H15/P0.5	1.05 ± 0.004	14.54 ± 0.11
PMMA/H15/P1	1.05 ± 0.006	15.00 ± 0.08

4.2.2.4 Thermal characterization

Figure 4.17 represents the thermal decomposition behaviors of hybrid syntactic foams. The temperatures at 5% weight loss and at maximum weight loss of syntactic foams which were obtained by TGA as well as the glass transition temperatures

which were obtained by DSC analysis are given in Table 4.6. According to Figure 4.17 and Table 4.6 there is no significant change in the temperature at maximum weight loss and glass transition temperature of the PMMA with the incorporation of both HGMs and POSS nanoparticles. On the other hand, the temperature at 5 wt.% loss of PMMA was reduced with the incorporation of HGMs, while the incorporation of POSS, did not significantly change this value of PMMA due to the relatively lower percent addition of POSS than the HGMs [61].

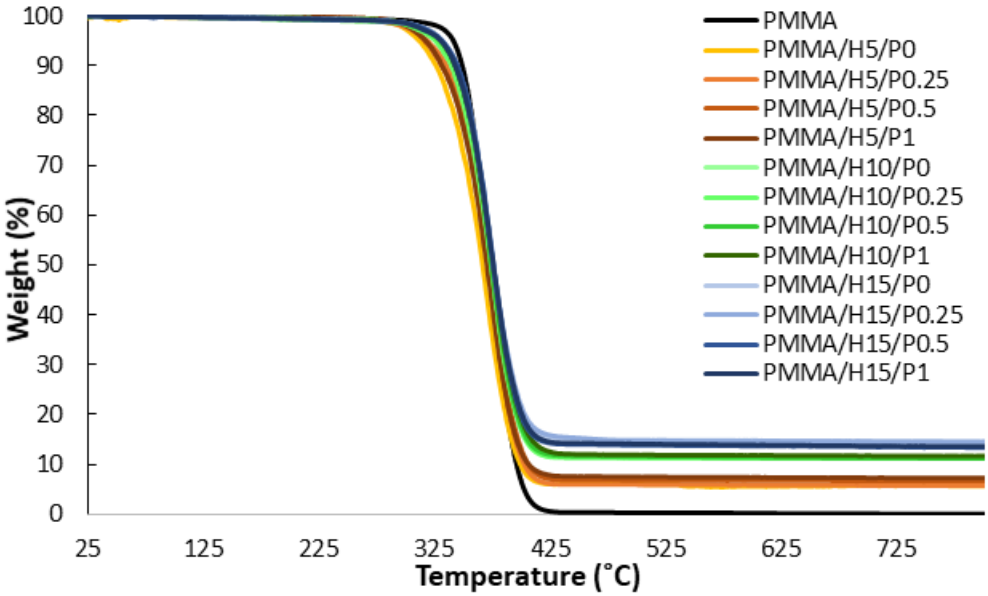

Figure 4.17. TGA curves of the neat PMMA and the PMMA hybrid syntactic foams.

Table 4.6 Temperature at 5% weight loss, temperature at maximum weight loss and glass transition temperature of the neat PMMA and the PMMA hybrid syntactic foams.

Sample Code	**$T_{5\%}$ (ºC)**	**T_{max} (ºC)**	**T_g (ºC)**
PMMA	341	375	116
PMMA/H5/P0	312	369	116
PMMA/H5/P0.25	319	378	116
PMMA/H5/P0.5	317	377	116
PMMA/H5/P1	318	376	115
PMMA/H10/P0	326	377	116
PMMA/H10/P0.25	326	374	116
PMMA/H10/P0.5	330	374	114
PMMA/H10/P1	331	376	115
PMMA/H15/P0	332	375	116
PMMA/H15/P0.25	332	375	117
PMMA/H15/P0.5	332	376	115
PMMA/H15/P1	331	378	117

Table 4.7. represents the thermal conductivities of the PMMA, representative PMMA-octaphenyl POSS composites and PMMA hybrid syntactic foams. The analyses were conducted to investigate the effects of HGMs and POSS incorporation on the conductivity of PMMA. According to the table, incorporation of both the HGMs and the POSS nanoparticles did not significantly change the thermal conductivity of PMMA. The insufficient concentrations of these additives might have caused the unchanged thermal conductivity values [61].

Table 4.7 Thermal conductivities of the neat PMMA, the PMMA-POSS composites and the PMMA hybrid syntactic foams.

Sample Code	Thermal conductivity (W/mK)
PMMA	0.15
PMMA/P0.25	0.16
PMMA/P0.5	0.15
PMMA/P1	0.15
PMMA/H15/P0	0.15
PMMA/H15/P0.25	0.15
PMMA/H15/P0.5	0.15
PMMA/H15/P1	0.14

4.3 Effects of $scCO_2$ foaming parameters and the CO_2-philic nanoparticle addition on supercritical CO_2 foaming of PMMA

In this part of the thesis study, the PMMA foams which were obtained using $scCO_2$ processing are investigated. The effects of process parameters and the addition of CO_2-phillic nanoparticles on the foaming performance and morphologies of the PMMA foams were discussed. PMMA and PMMA-POSS composite foams were produced at the upper and lower experimental conditions of pressure, temperature, processing time and venting rate, based on the two-factorial design.

4.3.1 Morphological Characterization

The CO_2-philic POSS nanoparticles were used in PMMA matrix at 0.5 wt.% and 5 wt.% concentrations to improve the effectiveness of $scCO_2$ foaming and foam morphologies of PMMA. The dispersion of POSS nanoparticles in the PMMA matrix was investigated with the EDX mapping analysis. The SEM image and the EDX mapping of the PMMA-5% POSS specimen for silicon atom are given in Figure 4.18 [148].

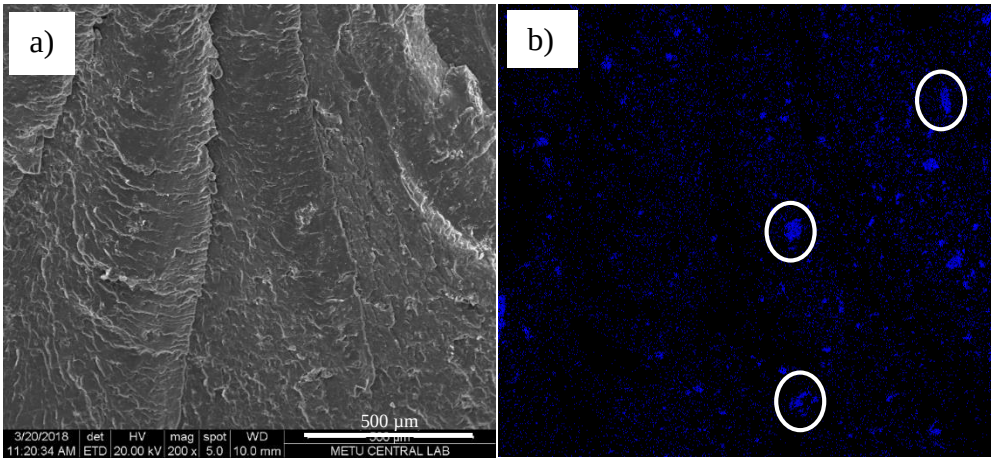

Figure 4.18. a) SEM images of PMMA/TMS5 b) Results of EDX mapping for Si composite. In Figure 4.18 the white circles indicate the agglomerates of POSS nanoparticles.

Figure 4.18 demonstrates that silicon atoms are dispersed homogeneously throughout the PMMA matrix, although they show an indication of some agglomerations indicated by the blue concentrated regions. EDX mapping analysis was also carried out on the foamed specimen to observe if POSS nanoparticles still existed in the foamed matrix after the venting. The SEM images of the PMMA/5% POSS composite foam and EDX mapping result are given in Figure 4.19.

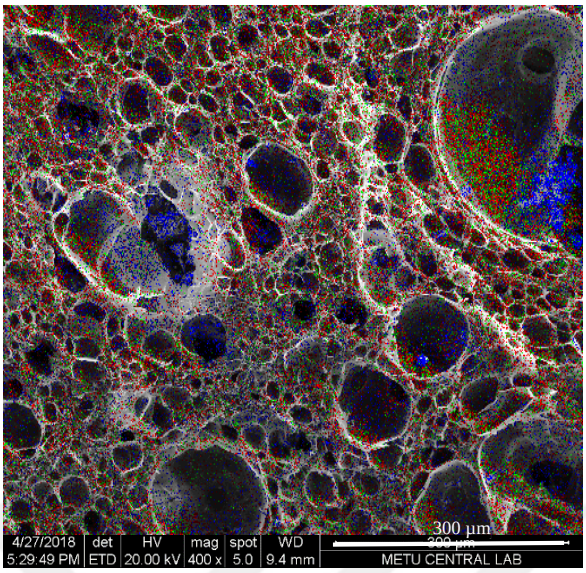

Figure 4.19. Results of SEM images and EDX mapping for PMMA/TMS5 composite foam (blue dots refer to the silicon atoms).

The EDX analysis showed that the agglomerated POSS nanoparticles led to the formation of larger pores as seen in Figure 4.19, showing the larger pores around the blue dots, which correspond to the silicon atoms of POSS nanoparticles. In their $scCO_2$ foaming study of epoxy-multi-walled carbon nanotubes (MWCNTs) composites, Li et al. also found that at high concentrations of MWCNT in epoxy, larger pores were formed around the agglomerates of the MWCNT since the nucleation sites concentrated around them [149]. Although non-uniform pore distribution was observed due to agglomerates, the distribution of the pores size was not considered as bimodal since according to the image analysis, these larger pores occupied maximum 5% of all pores.

The effects of $scCO_2$ process parameters as pressure, temperature, time and venting rate on the foaming performance of PMMA and PMMA-POSS composites were investigated. The morphology of all the neat PMMA specimens and PMMA-POSS composites processed with $scCO_2$ using two-factorial design of experiment were

investigated with SEM analysis. The specimens were categorized based on their foaming performances as given in Table 4.8.

Table 4.8 Foaming performances of the foamed PMMA specimens. Negative signs (-) refer to the partially foamed specimens and positive signs (+) refer to the completely foamed specimens.

Exp. #	Temperature (ºC)	Time (h)	Pressure (MPa)	Venting rate	Neat PMMA	PMMA/ TMS0.5	PMMA/ TMS5
1	35	2	11	slow	-	-	-
2	35	2	11	fast	none	none	-
3	35	2	32	slow	-	-	-
4	35	2	32	fast	-	-	-
5	35	24	11	slow	+	+	+
6	35	24	11	fast	+	+	+
7	35	24	32	slow	+	+	+
8	35	24	32	fast	+	+	+
9	100	2	11	slow	-	-	-
10	100	2	11	fast	-	-	-
11	100	2	32	slow	+	+	+
12	100	2	32	fast	-	-	+
13	100	24	11	slow	+	+	+
14	100	24	11	fast	+	+	+
15	100	24	32	slow	Shape deformation	Shape deformation	Shape deformation
16	100	24	32	fast	Shape deformation	Shape deformation	Shape deformation

* Negative signs (-) refer to partially foamed specimens and positive signs (+) refer to completely foamed specimens.

The highly CO_2-philic nature of the octatrimethylsiloxy POSS nanoparticles may be effective on the foaming performances of the specimens by enhancing the interactions between the CO_2 and the polymer matrix. As seen in Table 4.8, some of the experimental conditions resulted in different foaming performances based on the POSS concentrations of the PMMA-POSS composites. For example, 5% POSS addition resulted in the partial foaming of the specimens at the experimental conditions of 35ºC, 11 MPa, 2 h of processing time and fast-venting rate, while no pore formation was observed in the scCO_2-processed neat PMMA and PMMA-0.5%

POSS composite specimens at these conditions. At the experimental conditions of 100ºC, 32 MPa, 2 h of processing time and fast-venting rate, processing of the PMMA-5% POSS composite specimens resulted in complete foaming, while processing of the neat PMMA and PMMA-0.5% POSS composites resulted in partial foaming. Photographs of these specimens are given in Figure 4.20.

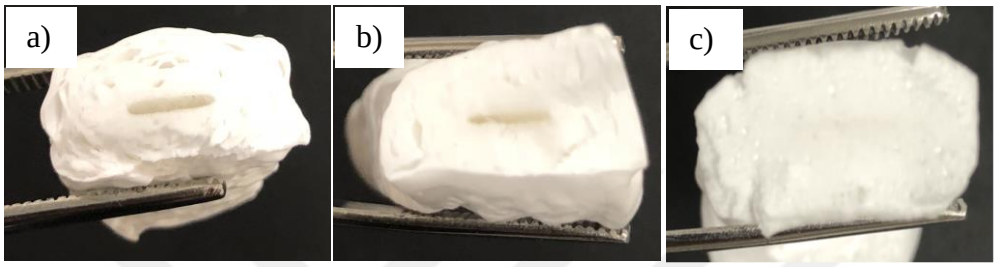

Figure 4.20. The photographs of a) PMMA, b) PMMA/TMS0.5 and c) PMMA/TMS5 composite foams which were processed at 100ºC, 32 MPa, 2 h and fast venting rate.

Figure 4.20 shows that while the neat PMMA specimens had unfoamed region in their central parts, PMMA-TMS0.5 composite specimens had slightly smaller unfoamed regions. However, when the POSS concentration was increased to 5%, the specimens were completely foamed. The addition of a CO_2-philic POSS allowed a more effective scCO_2 foaming of PMMA specimens. Completely foamed specimens can be obtained by using of CO_2-philic POSS at the experimental conditions of 100ºC, 32 MPa, 2 h and fast venting rate.

Since the focus of this study is to obtain completely foamed specimens, further characterizations were performed with the specimens produced at the processing conditions that provided complete foaming. Table 4.9 shows the average pore sizes calculated from the SEM images of the completely foamed specimens. In this table the letter “F” and “S” represent the fast and slow venting rates, respectively.

Table 4.9 Average pore size of the PMMA and PMMA-POSS composite foams.

Experimental conditions	Neat PMMA	PMMA/TMS0.5	PMMA/TMS5
	$D_{av,\mu m}$	$D_{av,\mu m}$	$D_{av,\mu m}$
35°C-24 h-11 MPa-F	2.4 ± 1.9	1.2 ± 1.2	0.6 ± 0.5
35°C-24 h-11-MPa-S	3.4 ± 1.8	1.4 ± 1.3	1.1 ± 1.4
35°C-24 h-32 MPa-F	1.1 ± 1.2	1.7 ± 2.0	0.3 ± 0.6
35°C-24 h-32 MPa-S	12.5 ± 16.1	3.4 ± 1.1	0.8 ± 1.1
100°C-2 h-32 MPa-F	-	-	3.9 ± 5.6
100°C-2 h-32 MPa-S	300.1 ± 105.5	338.3 ± 166.8	16.6 ± 27.3
100°C-24 h-11 MPa-F	66.2 ± 41.7	54.2 ± 23.0	18.1 ± 19.3
100°C-24 h-11 MPa-S	429.3 ± 271.0	344.2 ± 178.8	95.6 ± 51.9

Small average pore size is desirable in polymeric foams for especially transportation and thermal insulation applications since it leads to higher mechanical properties and lower coefficient of thermal conductivity [95]. According to Table 4.9, at each experimental condition, the average pore diameters of foams produced from the PMMA/TMS5 composites were smaller than the foams of neat PMMA and PMMA/TMS0.5 composites. Among all the foams of PMMA-5% POSS composites, the experimental conditions of 35ºC, 32 MPa, 24 h of processing time and fast-venting rate resulted in the smallest average pore diameter of 0.3 ± 0.6 µm. Zeng et al. explained that the reduction of the nucleation free energy activation barrier due to the presence of nanoparticles which act as nucleation sites during the foaming resulted in the change in the morphology of PMMA foam [112]. Here it is believed that the POSS additives act as cell nucleators by reducing the nucleation free energy activation barrier while their CO_2-philic nature enhances the supercritical CO_2 foaming performance further by improving the CO_2-polymer chain interactions in PMMA [148]. The recent studies on P_LLA foaming with supercritical CO_2 using other CO_2-philic POSS types such as fluoroalkyl POSS, isooctyl POSS or methacrylisooctyl POSS as cell nucleators also showed enhancement in the foaming behavior of the polymer, and allowed foaming at low temperatures such as 40ºC, at

which the polymer cannot be foamed without the POSS additives due to its highly crystalline nature [118, 150].

High pore density is another important property of polymer foams, which is favorable for enhanced thermal and mechanical properties [95]. The pore densities of the supercritical CO_2-foamed PMMA and PMMA-POSS composites are shown in Figure 4.21. The results are also summarized in Table D.1 in Appendix Part D.

It was observed that among the foamed specimens processed at the same experimental conditions, the pore densities of PMMA/TMS5 composite foams were higher than those of neat PMMA and PMMA/TMS0.5 composite foams. Increased POSS concentration resulted in the increased pore density and decreased average pore diameter of the foams. These results support that the homogeneously distributed CO_2-philic siloxy-based POSS nanoparticles in PMMA enhanced the supercritical foaming performance of the polymer. The increased cell nucleation sites and improved interactions of the polymer with CO_2 provided by these CO_2-philic nanoparticles overall enhanced the foaming performances of these composites, decreasing the pore size and increasing the pore density [150, 151, 152]. Among all the studied conditions the highest pore density was obtained with the PMMA/TMS5 composite processed with $scCO_2$ at the experimental conditions of 35ºC, 32 MPa, 24 h of processing time and fast venting rate. This was the condition that also provided the smallest average pore diameter in the PMMA-based foams.

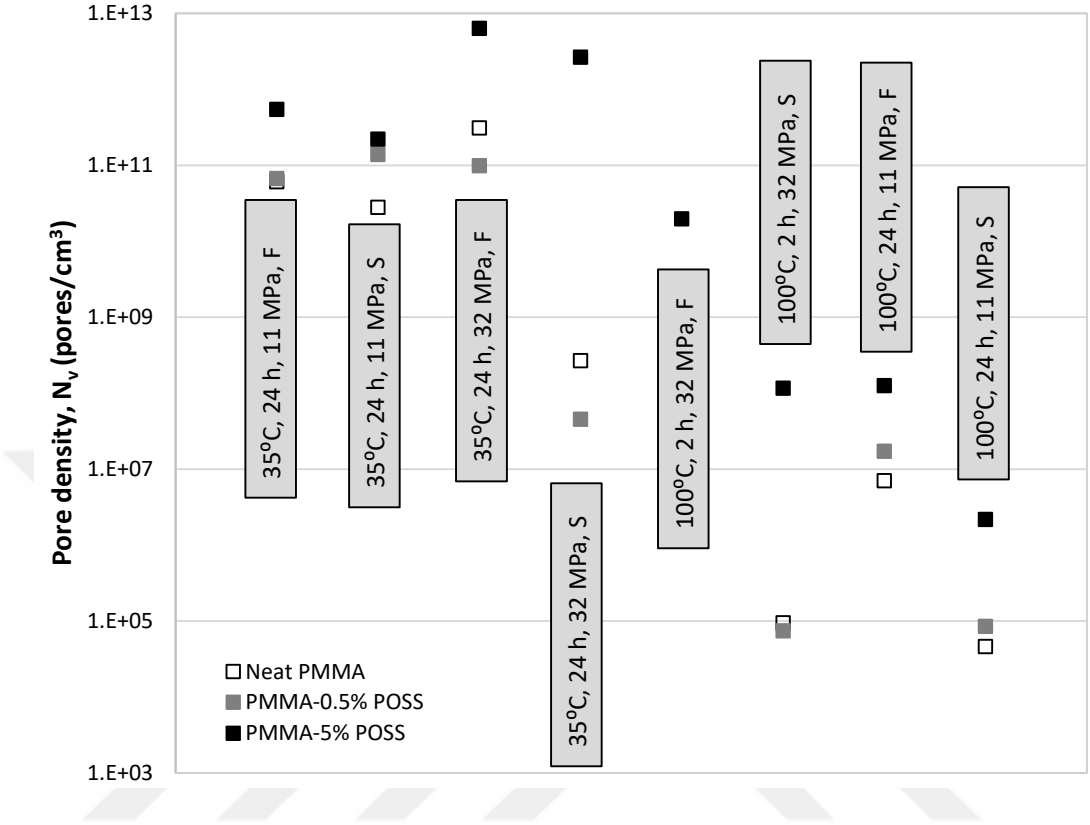

Figure 4.21. Pore density of the PMMA and the PMMA-POSS composite foams.

The effects of POSS concentration on the morphology of the PMMA foams can be shown at each processing conditions (Table 4.9. and Figure 4.21). The representative SEM images of the foams of composites with different POSS concentrations processed at 35ºC, 11 MPa, 24 h and depressurized with fast venting rate given in Figure 4.22 show the effect of POSS concentration on pore density.

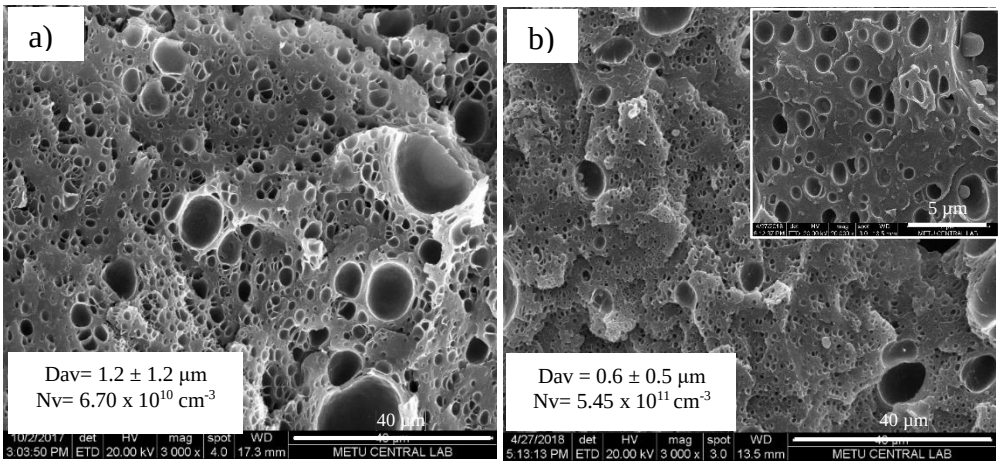

Figure 4.22. SEM images of a) PMMA/TMS0.5 and b) PMMA/TMS5 composite foams which were processed at 35°C, 24 h, 11 MPa, fast venting.

In this study PMMA- 5 wt.% POSS composite foams showed the best results in terms of foaming performance, pore size and pore density. Therefore, the effects of the parameters were evaluated focusing on the composites at this concentration. The temperature is one of the most important parameters on the polymer foam morphology; supercritical fluid processing temperatures closer to the glass transition temperature of the polymer allow more facile processing of the composites. With the PMMA composite specimens processed at 35ºC, 32 MPa, for 2 h and depressurized with slow venting rate, only partial foaming was observed (Table 4.8). Nevertheless, with the specimens processed at the same experimental conditions except for temperature, which was 100ºC, complete foaming was achieved. The complete foaming can be attributed to the high processing temperature enhancing the diffusion of CO_2 among the polymer chains [151], thus improving the foaming performance of the polymer. Increasing processing time to 24 h led to increase in the average pore size up to 100 folds and even shape deformation of the specimens if the process was carried out at high pressure (Tables 4.8. and 4.9.). The effect of high temperature on the foam morphology of the composites processed for 24 h at 11 MPa, depressurized with fast venting rate can be seen in Figure 4.23. The temperature increase led to an increase in the average pore diameter from 0.6 µm to 18 µm. Higher amount of

supercritical fluid incorporation within the polymer is achieved at low temperatures while the increased carbon dioxide dissolution led to formation of smaller pores [152]. On the other hand, the images present the inverse relation between temperature and pore density; as the temperature increases from 35ºC to 100ºC, the pore density decreased by three orders of magnitude, with fewer pores occupying larger area.

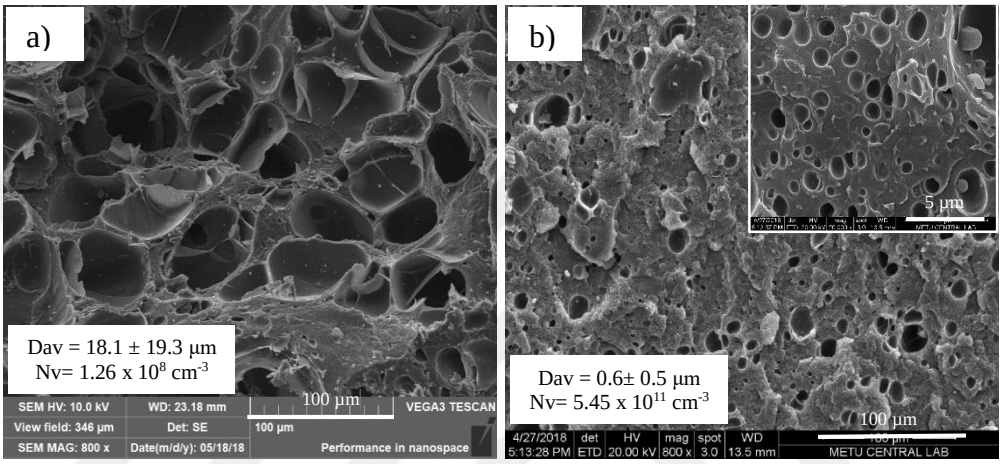

Figure 4.23. SEM images of PMMA/TMS5 foams saturated at 11 MPa, 24 h, fast venting and a)100ºC, b) 35ºC.

The effect of pressure on the foam morphology of PMMA-5% POSS composite was studied with composites processed at 11 MPa and 32 MPa. Pressure was observed to be not as influencing as temperature on the foaming performance of the PMMA-POSS composites. Increasing pressure did not affect the average pore diameter. Its effect was only observed on PMMA-5% POSS composites processed at 100 ºC for 2 h, where lower pressure processing resulted in partially foamed specimens while increased pressure led to complete foaming (Figure 4.24). This is due to the increased concentration of CO_2 in the polymer matrix at high pressures [153]. The increased CO_2 dissolution in the polymer with pressure also manifests itself as the increased pore density of the PMMA-5% POSS composite foams (Figure 4.21).

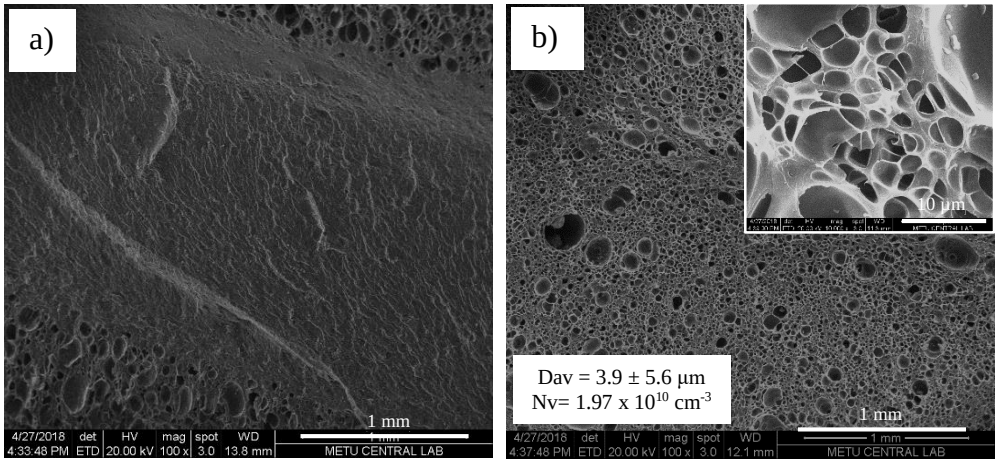

Figure 4.24. SEM images of PMMA/TMS5 foams saturated at 100°C, 2 h, fast venting and a) 11 MPa, b) 32 MPa.

The properties of the polymeric foams also depend on the processing time, which also has a strong influence on foaming performance of the PMMA-POSS composites. The SEM images of the PMMA-5% POSS foams, which were processed at 35ºC, 32 MPa, for 2 or 24 h and vented with slow venting rate are given in Figure 4.25.

When the PMMA-POSS composite was subjected to a sufficient period of time, 24 h, for CO_2 to diffuse and solubilize in the polymer matrix, complete foaming can be achieved since the amount of CO_2 sorption increases. According to Table 4.8 all the 2 h experiments resulted in none or partially foamed region, except the foams processed at the experimental conditions of 100ºC, 32 MPa, and depressurized with both slow or fast venting rate. The increase in the processing time resulted in completely foamed specimens for all the PMMA-POSS composites [148].

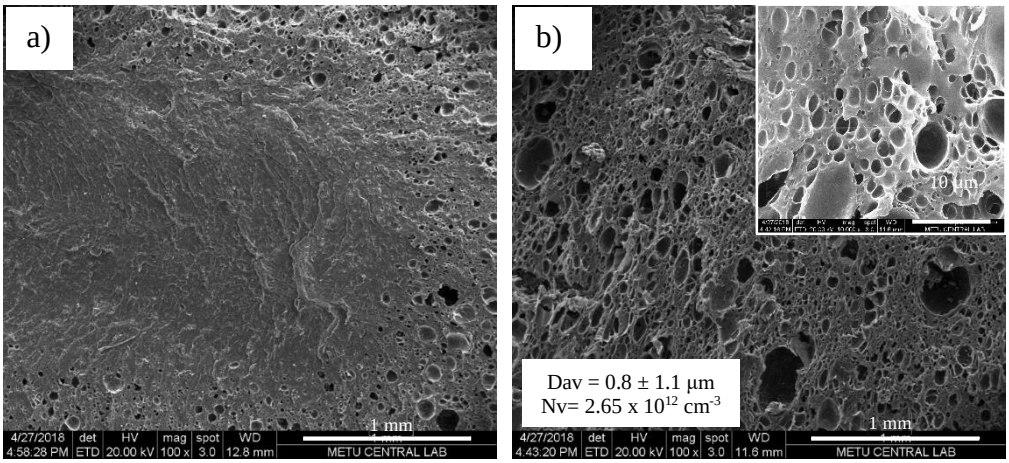

Figure 4.25. SEM images of PMMA/TMS5 foams saturated at 35°C, 32 MPa, slow venting for a) 2 h and b) 24 h.

During the depressurization step of $scCO_2$ foaming, supersaturated polymer/CO_2 mixture is formed while glass transition temperature of the polymer increases due to the decreasing concentration of CO_2 and due to the decreasing plasticizing effect. The nucleation sites develop in these supersaturated regions in the polymeric matrix. The speed of the depressurization is highly effective in the formation of nucleation sites and pore growth. In the present study all the foams that were processed with slow venting rate (about 0.007 MPa/s) had larger pores than their counterparts processed with a fast venting rate (about 0.41 MPa/s) processed at the same temperature and pressure (Table 4.9). In addition, parallel to the increase in the average pore size, the venting rate decrease resulted in the decrease of pore densities of the PMMA-POSS composite foams. Representative SEM images of PMMA/TMS5 composite foams, depressurized with fast and slow venting rates are given in Figure 4.26.a and b, respectively. When the venting rate was decreased to 0.007 MPa/s from 0.41 MPa/s, the average pore diameter increased from about 18 µm to 96 µm. The increase in the average pore size with decreasing venting rate is attributed to the pore coalescence at longer depressurization periods [94].

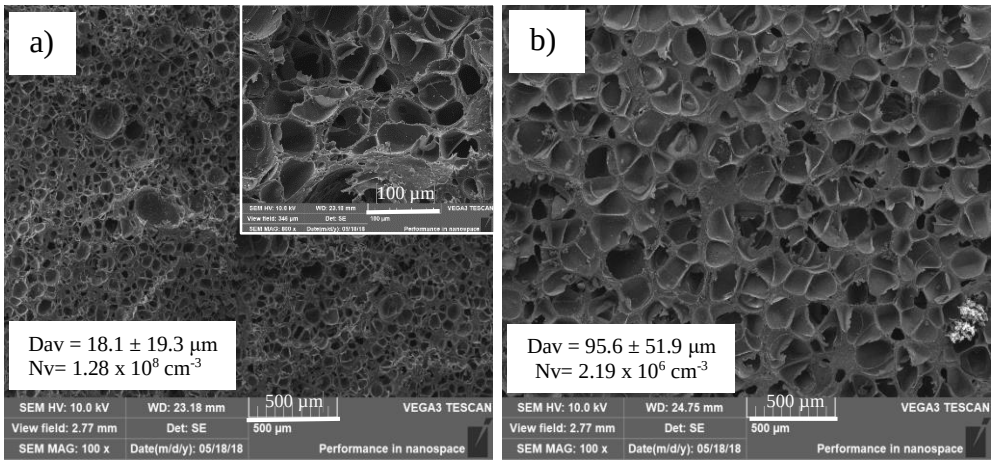

Figure 4.26. SEM images of PMMA/TMS5 foams saturated at 100°C, 24 h, 11 MPa and a) fast venting rate and b) slow venting rate.

4.3.2 Density Measurements

In order to observe the effects of $scCO_2$ processing on the density of PMMA and PMMA composite specimens, density measurements were conducted. The major advantage of the polymer foams is their reduced density which widens the applications of polymers in plethora of area. The effect of $scCO_2$ processing on the density of PMMA and PMMA composite specimens is presented in Figure 4.27. The results are also summarized in Table D.2 in Appendix Part D. The label "100ºC, 2 h, 32 MPa, F" was vertically written to emphasize that the only PMMA-5% POSS specimen was fully foamed at these experimental conditions while the neat PMMA and PMMA-0.5% POSS composite were partially foamed. According to the figure, $scCO_2$ processing reduced the density more than 50% for the composites processed at high temperature or the composites processed at low temperature and high pressure. Generally, the PMMA and PMMA-POSS specimens which were processed at 100ºC had lower density than the specimens processed at 35ºC which is due to the formation of the larger pores at higher processing temperatures.

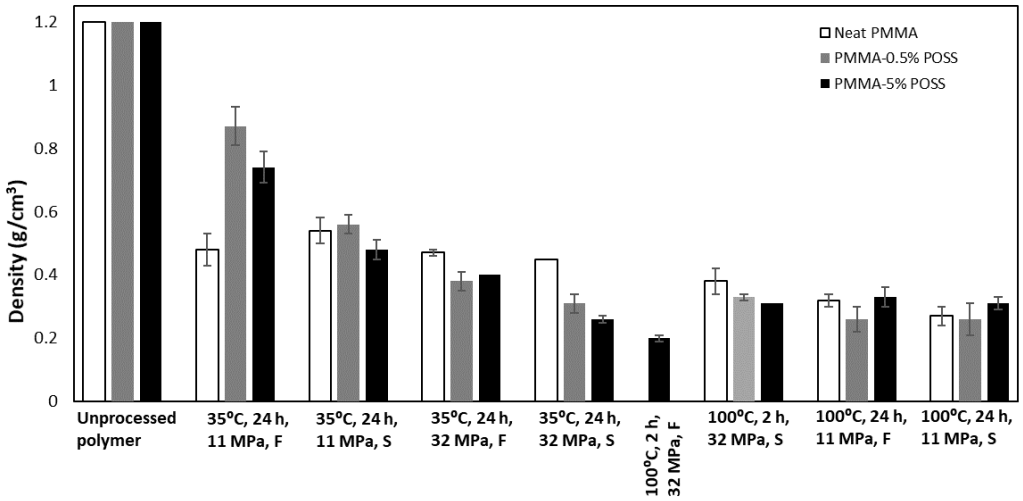

Figure 4.27. Density of the PMMA and the PMMA-POSS composite foams.

4.3.3 Thermal Characterization

In order to investiagate the effects of $scCO_2$ processing on the glass transition temperatures of PMMA and PMMA composite foams, DSC analyses were carried out. The glass transition temperatures (Tg) of the foams are given in Figure 4.28. The results are also summarized in Table E.1 in Appendix Part E.

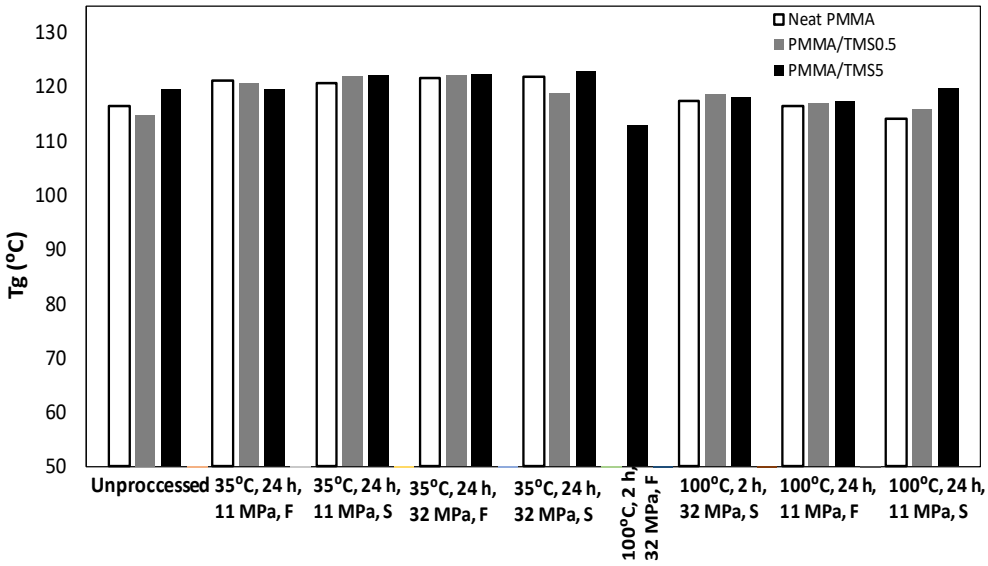

Figure 4.28. Glass transition temperature of the PMMA and the PMMA-POSS composite foams.

$ScCO_2$ foaming process slightly increased the glass transition temperature of the PMMA and PMMA composites when they were processed at 35ºC, high pressure and low pressure and depressurized with slow and fast venting rate. During the foaming process, as CO_2 behaves as a plasticizer, decreasing the Tg of the polymer, possibly the chains of PMMA realign to a more ordered, lower energy state that leads to stronger intermolecular interactions between the chains, increasing the Tg of the polymer [151]. Another reason to this increase might be the formation of the nanoscale pores leading to the confinement of the polymer chains within the cell walls, increasing the Tg of the polymer foam [10]. This effect manifests itself in the foams of PMMA and PMMA-POSS composites processed at 35ºC, 11 MPa, 24 h and depressurized with fast and slow venting rates, which have about an order of magnitude smaller average pore diameter than those processed at 100ºC.

TGA analysis for bulk polymers and foams were also carried out. Figures 4.29 and 4.30 show the thermal degradation of PMMA foams.

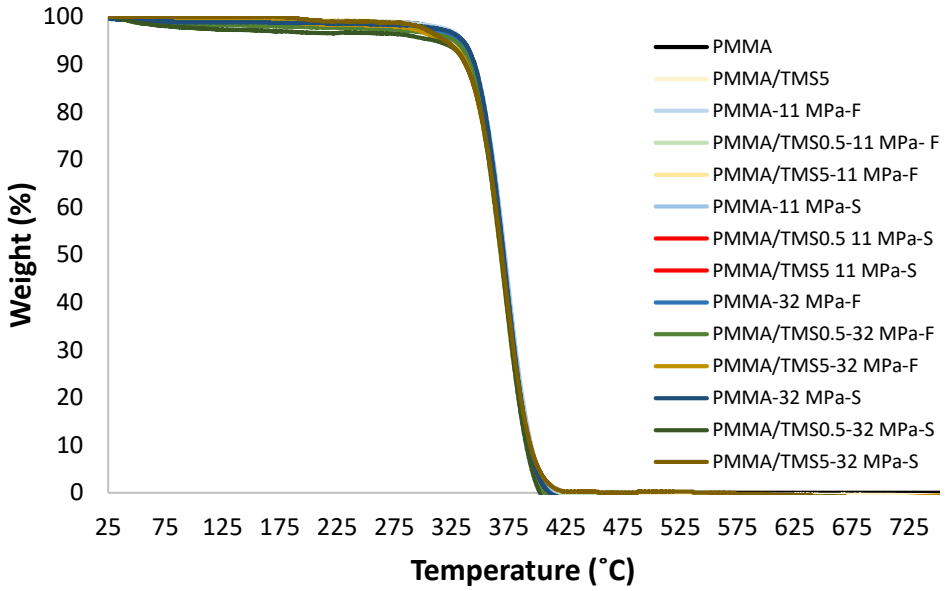

Figure 4.29. Thermal degradation of PMMA foams saturated at 35°C for 24 h.

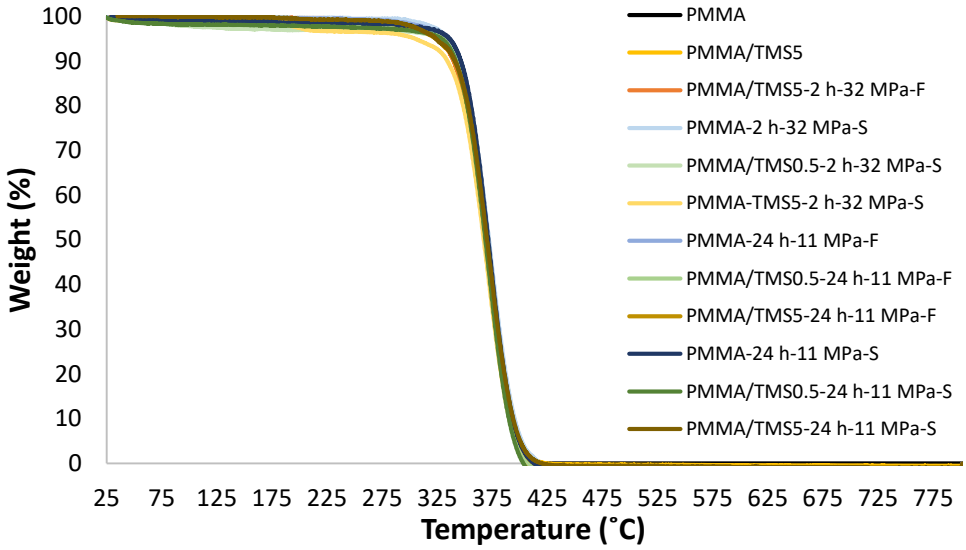

Figure 4.30. Thermal degradation of PMMA foams saturated at 100°C for 24 h.

Figures 4.29 and 4.30 show that foaming process did not change the thermal degradation behavior of PMMA. In order to understand the effects of foaming

process on the earlier steps of the degradation, temperature at 5% weight loss and maximum weight loss were determined and summarized in Table 4.10. The temperature at 5% weight loss and maximum weight loss did not change significantly with the addition of POSS nanoparticles or with the $scCO_2$ processing. This can be due to the low concentration of the POSS nanoparticles in the matrix. The $scCO_2$ processing also did not change the chemical structure of the composites.

Table 4.10 Temperature at 5 wt.% loss and temperature at maximum weight loss values of PMMA foam.

Experimental conditions	Temperature at 5 wt.% loss (ºC)			Temperature at maximum weight loss (ºC)		
	PMMA	PMMA/ TMS0.5	PMMA /TMS5	PMMA	PMMA/ TMS0.5	PMMA /TMS5
Bulk	331	-	328	371	-	372
35-24-1600-F	335	333	322	376	371	373
35-24-1600-S	334	331	326	376	376	375
35-24-4600-F	332	327	316	376	375	372
35-24-4600-S	320	311	335	372	371	373
100-2-4600-F	-	-	326	-	-	374
100-2-4600-S	334	327	305	374	372	371
100-24-1600-F	331	330	324	374	377	374
100-24-1600-S	336	329	324	374	375	376

4.3.4 DOE analysis

The effect of process conditions such as pressure, temperature, processing time and venting rate on the morphology of the PMMA/TMS5 composite foams were investigated using the two-factorial design method. For this purpose, 16 experiments were carried out and the results of the average pore size measurements were entered to the JMP statistical software. The experiments which resulted in partial foaming and shape deformation were excluded from the analysis. A model was fitted to the experimental data based on the standard least squares method by using JMP

software. The software shows the significance of the process parameters on the pore size by calculating the P-values of each parameters and dual combinations of them in the confidence limit of 95%. P-value is defined as the probability; the probability of something to happen by chance. Therefore, when p-value is small it is more likely to define selected data is not obtained by chance [154]. The sorted parameter estimates are given in Table 4.11 based on the p-values and the original JMP output of the table is given in Appendix Part F in Figure F.1. The estimate column represents the coefficient of the terms in the model. Standard error column shows the standard error of the estimate. The ratio of the estimate to its standard error gives the t-ratio. However, when the degrees of freedom are insufficient to estimate error, the JMP software provided the relative standard errors. In that case, the t ratios and p-values are calculated using Lenth's pseudo standard error (PSE). The higher the magnitude of the t-ratio, the more effective the parameter on the results.

Table 4.11 The most effective parameters on the pore size of PMMA/TMS5 composite foams.

Term		**Estimate**	**Relative Std Error**	**Pseudo t-Ratio**	**Pseudo p-Value**
Temperature (°C) (35, 100)	Biased	27.59	0.5	1.58	0.2031
Temperature (°C) * Venting rate (psi/s)		-20.16	0.5	-1.12	0.3377
Time (h) (2,24)	Biased	22.84	0.7	0.93	0.4168
Time (h) * Venting rate(psi/s)		-17.01	0.7	-0.67	0.5483
Venting rate (psi/s) (1,60)		-3.41	0.5	-0.19	0.8609
Pressure (psi) (1600,4600)	Biased	-0.15	05	-0.01	0.9936
Pressure (psi) * Venting rate (psi/s)		-1.78E-15	0.5	-0.00	1.0000
Temperature (°C) * Time (h)	Zeroed	0	0	.	.
Temperature (°C) * Pressure (psi)	Zeroed	0	0	.	.
Time (h) * Pressure (psi)	Zeroed	0	0	.	.

The DOE shows the synergistic effect of the parameters that cannot be observed by direct observation. The regression analysis determined the most effective parameters on the pore size of the PMMA/TMS5 composite foams. This analysis provides the selection of the optimum parameters to obtain the desired average pore size value. The p-values of the parameters and the dual combinations of them have values higher than 0.05 which is the border in the statistics to decide a parameter as significant on the results. Although the parameters are higher than 0.05 they are still close to the value of zero. According to Table 4.11, the most effective parameter on the pore size is the temperature since the p-value of this parameter is smaller than p-values of the other parameters. The positive sign before the estimate of the temperature indicates that the direct ratio between the parameter and the pore size. This result was expected since the PMMA-5% POSS composites processed at 35ºC, 11 MPa, 24 h and depressurized with fast and slow venting rates had more than an order of a magnitude smaller average pore diameter than those processed at 100ºC (Table 4.9). The second effective parameter is the dual combinations of the temperature and venting rate. Although the temperature has a direct relationship with the average pore size, the dual combination with the venting rate has an inverse relationship.

In this part of the thesis study, highly CO_2-philic nanoparticles, octatrimethylsiloxy polyhedral oligomeric silsesquioxanes (POSS) are used to increase the affinity of PMMA to CO_2 during $scCO_2$ foaming. PMMA and PMMA-POSS composite foams were produced at the upper and lower experimental conditions of pressure, temperature, processing time and venting rate, based on the two-factorial design. The foams of PMMA-5% POSS composites exhibited smaller average pore sizes and higher pore densities than the neat PMMA and the PMMA-0.5% POSS composites. It was found that the POSS nanoparticles also improved the foaming performance of the PMMA where completely foamed specimens was obtained with POSS incorporation. The density of the foamed PMMA and PMMA-POSS specimens produced with $scCO_2$ processing was reduced by about 50%, compared to the unprocessed polymer.

4.4 Effects of $scCO_2$ foaming parameters and the CO_2-philic nanoparticle addition on supercritical CO_2 foaming of PMMA Syntactic Foams

The PMMA syntactic foams, which were obtained with the dispersion of HGMs in PMMA matrix, were processed with $scCO_2$ to obtain bimodal-pore structured foams. In order to observe the effects of CO_2-philic nanoparticle on the foaming performance and morphology of the foams PMMA hybrid syntactic foams were also produced and processed with $scCO_2$. The effects of the process parameters and the concentrations of the HGMs and POSS nanoparticles on the morphology, density and thermal properties of the foams were investigated.

4.4.1 Morphological Characterization

The morphologies of PMMA-HGM and PMMA-HGM-POSS composites processed with $scCO_2$ were investigated with SEM analysis. Through these analyses, completely foamed specimens with pore formation throughout the whole matrix and partially foamed specimens with pore formation obtained only at the outer regions were identified. In addition, two types of foaming performances were observed for the completely foamed specimens: some of the specimens had only larger pores and some specimens had bimodal pore structure with the formation of both smaller and larger pores. The foaming performance of the foams are given in Table 4.12.

Table 4.12 Foaming performance of PMMA syntactic foams specimens processed at 35 °C and depressurized with fast venting rate. Positive signs (+) refer to completely foamed specimens, negative signs (-) refer to either partially foamed specimens or specimens with no pore formation.

Exp. #	Time (h)	Pressure (MPa)	HGM amount (wt. %)	POSS amount (wt. %)	Formation of larger pores (8.6 – 188 μm)	Formation of smaller pores (0.02 – 8.4 μm)
1	2	11	5	0	-	-
2	2	11	5	5	-	-
3	2	11	15	0	-	-
4	2	11	15	5	-	-
5	24	11	5	0	+	-
6	24	11	5	5	+	+
7	24	11	15	0	+	-
8	24	11	15	5	+	+
9	2	22	5	0	-	-
10	2	22	5	5	-	-
11	2	22	15	0	-	-
12	2	22	15	5	-	-
13	24	22	5	0	+	+
14	24	22	5	5	+	+
15	24	22	15	0	+	+
16	24	22	15	5	+	+

As seen in Table 4.12, the specimens processed with $scCO_2$ for 2 h, which are represented with two negative signs in both columns in the table, were either not foamed at all, which means either no pores existed throughout their matrices or they were partially foamed, i.e. both larger and smaller pores are observed only in the outer regions of the specimens. The SEM images of one of these composites PMMA-H15-TMS0 processed for 2h, are given in Figure 4.31. In these images while there are no pores formed due to supercritical processing, the HGMs are clearly observed, embedded in the polymer as well as the spherical cavities formed due to the

incompatibility between the HGMs and PMMA leading to detachment of some of the HGMS during the cryogenic fracturing of the specimens [60].

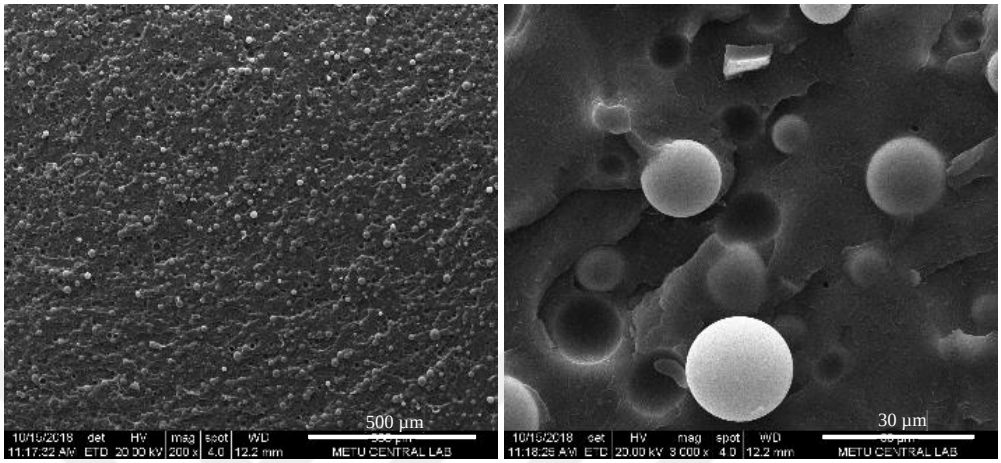

Figure 4.31. SEM images of PMMA/H15/TMS0 composite which processed at 35ºC, 11 for 2 h and depressurized with fast venting rate.

The specimens processed for 24 h were completely foamed with either only larger pores or both larger and smaller pores formed in the matrix based on the content of the CO_2-philic POSS or process pressure, both of which allowed tuning of the foam morphology. The complete foaming is attributed to the sufficient processing time for CO_2 to diffuse and dissolve in the matrix [151]. The completely foamed specimens with only larger pores were PMMA-H5-TMS0 and PMMA-H15-TMS0 syntactic foams, which contain only HGMs and no POSS, and were processed for 24 h at the lower pressure, 11 MPa. The representative SEM image of the scCO_2 processed PMMA-H15-TMS0 syntactic foam is given in Figure 4.32.a, which shows the larger pores grown from the surfaces of the HGMs. The formation of solely larger pores during the depressurization is attributed to the CO_2 diffusion in the matrix towards the voids already existing between the matrix and HGM surfaces in the composite because of their incompatibility with each other [60]. The enlarging voids due to the

CO_2 diffusion formed the larger pores which stabilize during the depressurization with the increasing Tg of the polymer [151].

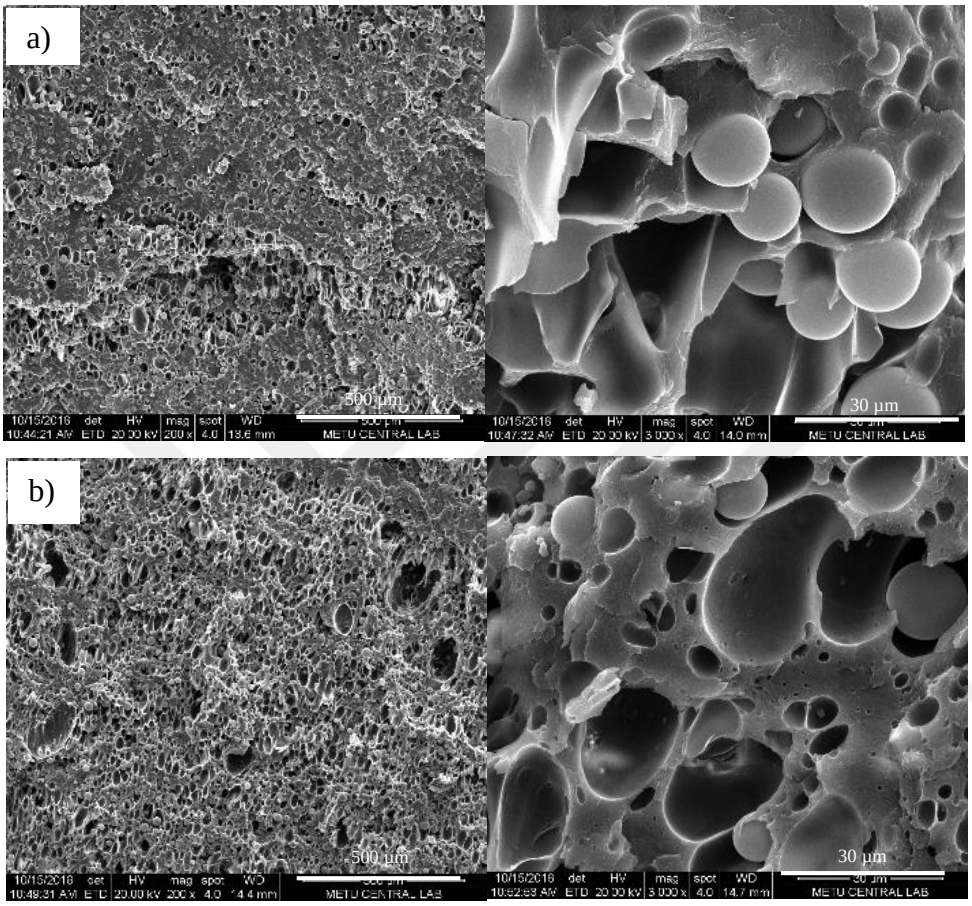

Figure 4.32. SEM images of PMMA-HGM and PMMA-HGM-POSS composite which processed at 35ºC, 11 MPa a) PMMA/H15/TMS0 for 2 h b) PMMA/H15/TMS0 for 24 h c) PMMA/H15/TMS5 for 24 h.

Among the POSS added syntactic foams, PMMA-H5-TMS5 and PMMA-H15-TMS5 foams processed at 11 MPa for 24 h were completely foamed forming a bimodal structure with both smaller and larger pores formed in the matrix. The SEM image of the PMMA-H15-TMS5 foam is given in Figure 4.32.b. The bimodal structure of the polymer is attributed to the highly CO_2-philic nature of the

octatrimethylsiloxy POSS [126] which can affect the $scCO_2$ processing via two ways. Firstly, these nanoparticles behave as nucleation sites and reduce the critical free energy for nucleation; therefore, their existence increase the density of the nucleation sites and enhance the formation of pores [112]. Secondly, they increase the affinity of polymer to CO_2 [118], thus improve the incorporation of CO_2 in the polymer.

After determining the completely foamed specimens, the average pore diameters of these specimens were calculated. Completely foamed specimens which had pores not only at the outer regions but also in the central part of the specimens were considered in pore diameter measurements. Table 4.13 represents the average pore diameters of the composites.

Table 4.13 Average pore size of PMMA composite foams processed at 35°C for 24 h and depressurized with fast venting rate.

Experimental condition	Average pore size (larger pores)	Average pore size (smaller pores)	Pore size of larger pores/ pore size of smaller pores
PMMA/H5/TMS0 11 MPa	40.9 ± 29.0	-	-
PMMA/H5/TMS5 11 MPa	15.4 ± 8.3	0.1 ± 0.1	154.0
PMMA/H15/TMS0 11 MPa	15.6 ± 6.3	-	-
PMMA/H15/TMS5 11 MPa	15.8 ± 6.1	1.0 ± 0.5	15.8
PMMA/H5/TMS0 22 MPa	27.1 ± 16.4	1.6 ± 1.2	16.9
PMMA/H5/TMS5 22 MPa	17.3 ± 12.1	0.5 ± 0.5	34.6
PMMA/H15/TMS0 22 MPa	21.6 ± 9.8	1.0 ± 0.6	21.6
PMMA/H15/TMS5 22 MPa	13.9 ± 5.2	0.2 ± 0.1	69.5

The pores were divided into two groups as smaller and larger ones. 8.6 μm was determined as the minimum value for the pore diameter of the larger pores since the larger pores formed around the HGMs and the lowest value in the particle size distribution of HGMs was 8.6 μm. Therefore, the pores which include an HGM were also considered as larger pores. The pores with diameters smaller than this value were included in the average pore diameter calculation of the smaller pores. According to Table 4.13, the smallest ratio between the average pore diameters of larger and smaller pore was 15.8, which was measured in the PMMA-15H-5P specimen foamed at 11 MPa for 24 hours. This ratio increased up to 154, which was obtained with PMMA-H5-TMS5 specimens foamed at 11 MPa, for 24 h. Bimodal structure of these PMMA composite foams was distinct due to the high difference between the average sizes of the small and large pores. While POSS nanoparticles enhanced the formation of smaller pores at lower pressure of 11 MPa, the smaller pores were formed in the composite foams processed at 22 MPa without the addition of POSS nanoparticles. With increasing process pressure, the increasing concentration of CO_2 in the polymer matrix led to formation of more nucleation sites which grew into smaller pores [153]. POSS nanoparticles affected the average pore diameter of the smaller pores in PMMA-HGM composites processed also at 22 MPa, decreasing this value from 1.6 μm down to 0.5 μm and to 0.2 μm at HGM concentration of 5 and 15 wt.%, respectively. The smallest average pore diameter of 0.1 μm was obtained with PMMA-H5-TMS5 composite processed at 11 MPa, for 24 h. PMMA-POSS composite specimens which contain 5 wt.% of POSS processed at 11 MPa for 24 h had an average pore diameter of 0.6 μm [148]. The presence of HGM particles in this composite decreased the smaller average pore diameter value compared to the foams obtained from the PMMA-POSS composites without HGM. In literature, when clay was used as nanoparticles in polymers, two opposite effects were reported for the transport of CO_2 from the polymer [106]. One was the increase in the diffusion coefficient of CO_2 with clay concentration [155, 156] which was attributed to the partial agglomerations of the clay particles leading to a lower resistance pathway and thus faster CO_2 diffusion out of the polymer nanocomposites.

In this work, the pore size decreasing effect of HGM is attributed to the voids between the HGM and PMMA matrix forming escaping paths for CO_2, leading to a similar enhancing effect on the transportation of the gas from the matrix. This possibly hindered the coalescence of the pores, which in turn allowed formation of smaller pores, similar to pore diameter decreasing effect of rapid depressurization. This effect of HGM was also observed at the higher pressure of 22 MPa, where the average pore diameters of the PMMA-HGM-POSS composites foams decreased with increasing HGM concentration at constant POSS wt.%. In literature, however, slowing effect of clays on the diffusion of CO_2 from the polymer nanocomposites was also reported [157], where clays act as diffusion decreasing barriers. Here, as stated above, in the foams with 5 wt.% POSS, processed at lower pressure (11 MPa) and thus with less CO_2 incorporation, addition of HGM at 5 wt.% to the PMMA-POSS composite decreased the average pore diameter remarkably due to the voids between the polymer and HGMs creating CO_2 escape paths, promoting rapid CO_2 transport from the polymer. However, as the HGM concentration was increased further to 15 wt.%, the average pore diameters of the PMMA-HGM-POSS composites increased from 0.1 μm to 1.0 μm. This shows that, when processed at lower $scCO_2$ pressures, the HGMs in the PMMA-HGM-POSS composites with higher HGM concentrations started to behave as barriers hindering the rapid diffusion and escape of CO_2 from the polymer, allowing the coalescence of the pores during the diffusion of CO_2 from the polymer, thus leading to formation of larger pores. In composites processed at high pressures and thus incorporated with more CO_2, the transport promoting effect of HGMs was more dominant on the composites than their negative effect hindering the CO_2 escape. All these results show that there are indirect relationships between the certain parameters ($scCO_2$ processing pressure, POSS concentration and HGM concentration of the composite) and the average pore diameter of the PMMA-POSS-HGM composite foam. This indicates that a fine tuning of the average pore diameter of these hybrid syntactic foams can be achieved with a thorough evaluation of these relationships and selecting an appropriate set of parameters for the desired pore size.

The pore densities of the completely foamed PMMA-HGM-POSS composites were also strongly affected by the process parameters as shown in Figure 4.33.

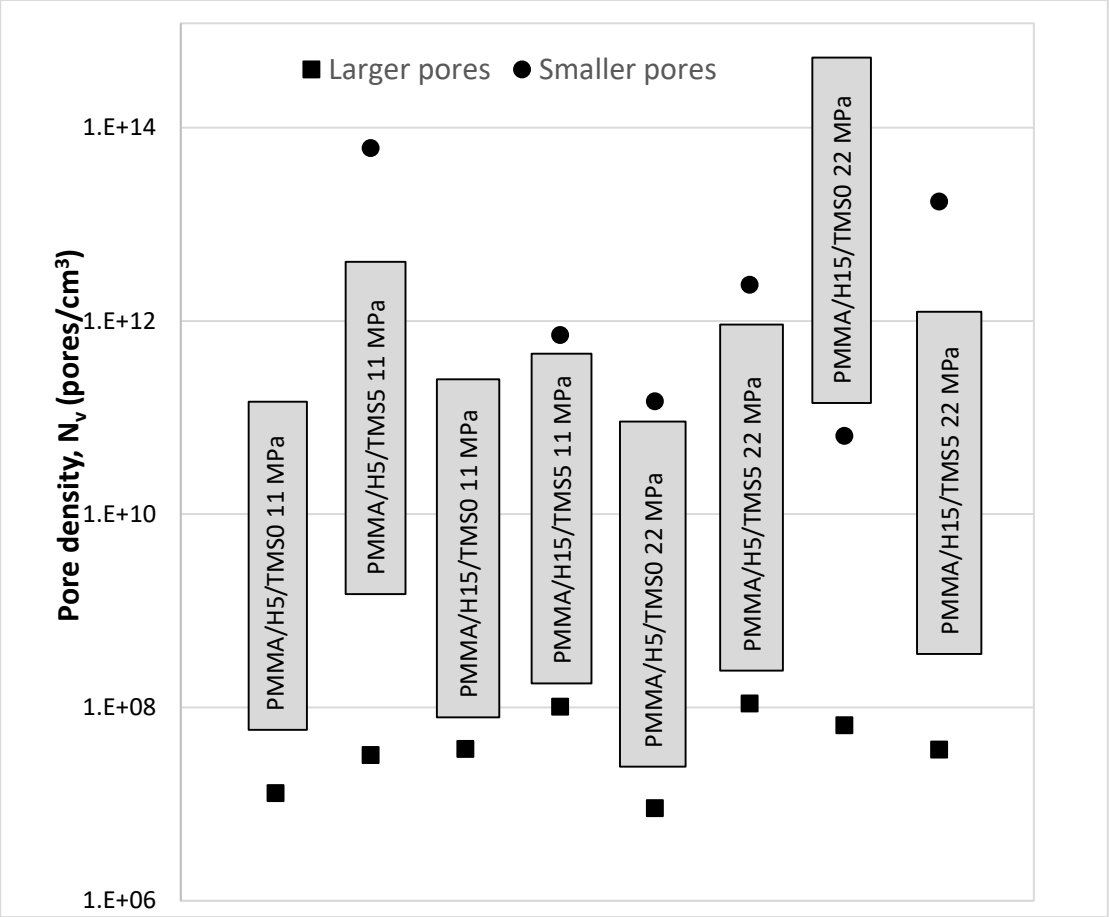

Figure 4.33. Pore density of PMMA composite foams.

For the bimodal composite foams, the pore density of the larger pores of a composite foam was always lower than that of the smaller pores, and the difference between these values was at least three orders of magnitude. This difference was expected since there were less number of larger pores and they occupy larger areas compared to smaller pores. Composites with 5 wt.% POSS nanoparticles had higher pore density of smaller pores than the composites without POSS nanoparticles. In the composites processed at the higher pressure, even though small pores formed, the

incorporation of POSS increased the small pore density by at least an order of magnitude. CO_2-philic nature of these nanoparticles may increase the dissolution and diffusion of CO_2 during processing that may promote the formation of higher number of nucleation cites and thus pores [151]. The HGM concentration increase on the other hand influenced the pore densities similar to its effects on the pore sizes of the composites. When the HGM concentration was increased by 10 wt.% in PMMA-HGM composites, with $scCO_2$ processing at the lower pressure, about 55% decrease in the density of the larger pores was observed. This is due to the corresponding increase in the voids between the HGM and PMMA which formed the larger pores upon $scCO_2$ processing. When these composites were processed at the higher pressure, similarly, density of larger pores increased with HGM concentration. However, this increase was more profound, as it was about an order of magnitude, possibly due to the higher amount of CO_2 incorporation leading to higher number of the voids to grow into larger pores. The concentration of HGMs had also a strong influence on the smaller pore density if these were formed due to cell nucleating POSS particles. However, as in the pore size of the composite foams, they had opposite effects that depend on the processing pressure. Processed at lower pressure, when they existed in the composite at the higher concentration, the barrier effect of HGMs became more profound, slowing the CO_2 escape, leading to the coalescence of the growing pores, corresponding to a decrease in the smaller pore density by two orders of magnitude. When processed at higher pressure, with the higher CO_2 incorporation in the matrix, the CO_2 transport enhancing effect of HGMs became dominant at the higher HGM concentration, hindering the coalescence of the growing pores and thus increased the density of the smaller pores by an order of magnitude. On the other hand, in PMMA-HGM composites processed at the higher pressure, the small pores were formed only due to the higher CO_2 incorporation, and their density decreased with the HGM concentration increase in the composite, showing that their barrier effect became more dominant in the absence of cell inducing agents. The highest pore density of 6.14×10^{13} cm^{-3} was obtained with PMMA-H5-TMS5 composite processed at 11 MPa for 24 h (Figure 4.34). This

composite also had the smallest average pore diameter with the same processing conditions. The pore density of this foamed composite was higher than the PMMA-5 wt.% POSS composite processed at a higher pressure of 11 MPa for 24 h (N_v=5.45x 10^{11} cm^{-3}) [148]. This is consistent with the CO_2 transport enhancing effect of HGMs increasing the smaller pore density that is observed at high pressure.

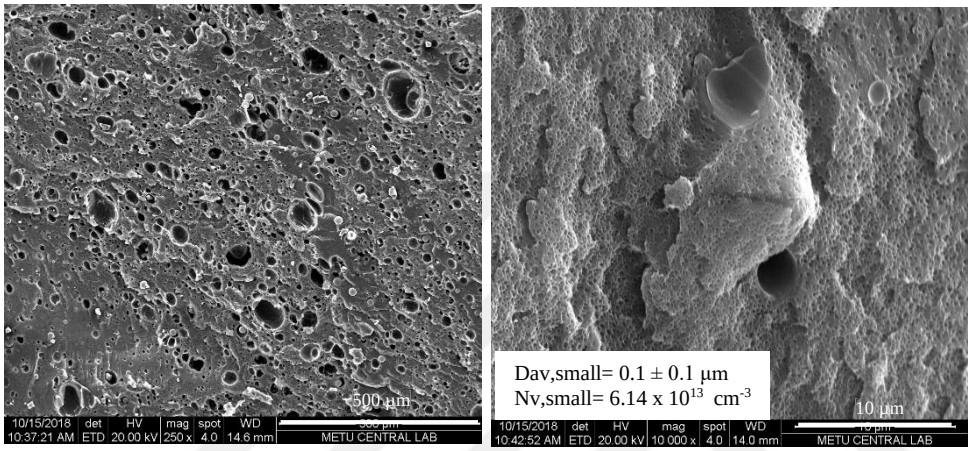

Figure 4.34. SEM images of PMMA/H5/TMS5 composite which processed at 11 MPa and 24 h.

4.4.2 Density Measurement

Densities of composite foams were determined by water displacement method and the results are given in Figure 4.35. The results are also summarized in Table D.1 in Appendix Part D.

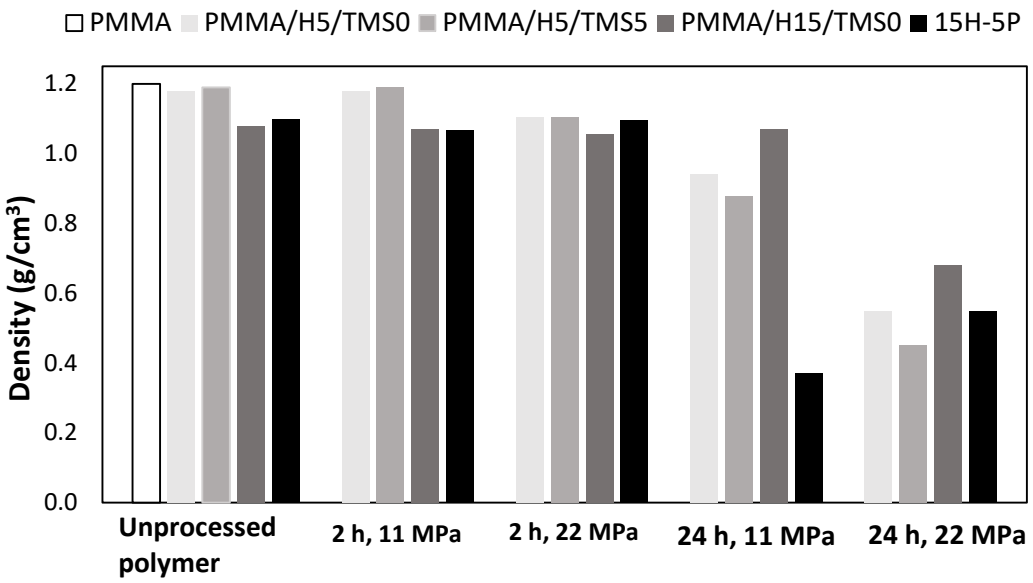

Figure 4.35. Density of PMMA composite foams.

It was observed that the addition of HGM in the polymer matrix decreased the density of the polymer prior to $scCO_2$ processing due to their hollow structure [60, 61]. $ScCO_2$ processing further decreased the density of the specimens upon pore formation if they were completely foamed after being processed for 24 h. The density reduction of these foams was up to about 50 % and the smallest density as 0.37 g/cm^3 was obtained with the processing of PMMA-H15-TMS5 specimen at 11 MPa for 24 h. Even though the porosity of this composite was not as high as its counterpart processed at 22 MPa for 24 h as a result of the HGMs' barrier effect at the lower pressure, its density was less due to its five folds greater pore size. The addition of POSS nanoparticles decreased the density of the completely foamed specimens, due to the cell inducing effect of POSS nanoparticles increasing the pore density of the composite foams. However, they did not decrease the density when the processing time is limited to 2 h. In the presence of POSS in the composites, the opposite effects of HGM depending on the processing pressure manifested itself on the density of the PMMA-HGM-POSS composites.

4.4.3 Thermal Characterization

Thermal characterization of PMMA foams was carried out using TGA and DSC. TGA analysis results for bulk polymer and composite foams which were processed for 24 h are given in Figure 4.36.

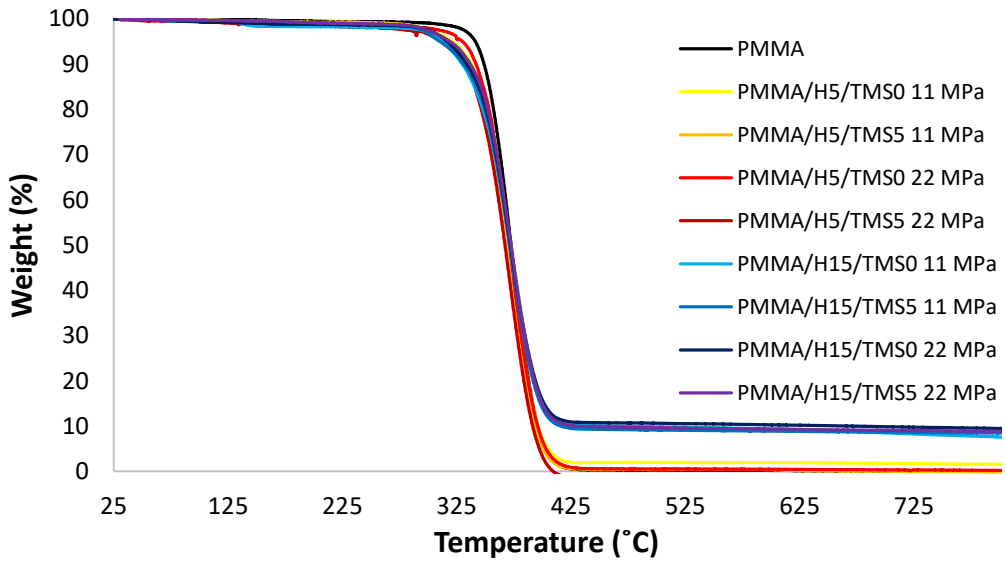

Figure 4.36. Thermal degradation of PMMA composite foams.

Figure 4.36 shows that foaming process did not cause any change on thermal degradation behavior of PMMA. On the other hand, char yield of the composites which is attributed to the HGMs were different from each other due to the different concentration of the HGMs in the composites.

Temperature of 5% weight loss and maximum weight loss as well as the glass transition temperature of the foams are summarized in Table 4.14 which contains the TGA analysis results of fully foamed specimens which were saturated at 35°C for 24 h and depressurized with fast venting rate.

Table 4.14 Temperature of 5% weight loss and temperature at maximum weight loss of PMMA composite foams.

Composite	Temperature at 5% weight loss (ºC)	Temperature at max. weight loss (ºC)	Glass transition temperature (ºC)
PMMA	341	375	116
PMMA/H5/TMS0 11 MPa	321	372	116
PMMA/H5/TMS5 11 MPa	318	372	117
PMMA/H5/TMS0 22 MPa	330	375	117
PMMA/H5/TMS5 22 MPa	312	371	117
PMMA/H15/TMS0 11 MPa	312	373	118
PMMA/H15/TMS5 11 MPa	310	374	118
PMMA/H15/TMS0 22 MPa	317	373	118
PMMA/H15/TMS5 22 MPa	319	374	118

Although the addition of POSS nanoparticles into the PMMA matrix decreased the temperature at 5% weight loss values for both bulk polymer and foams, it did not change the temperature at maximum weight loss values. POSS nanoparticles which act as heating source during the earlier degradation step of the polymer may cause the reduction in the temperature at 5% weight loss. However, for the temperature at maximum weight loss, the addition of POSS did not cause a significant change. The glass transition temperatures of the PMMA-HGM-POSS composite foams were found to be the same with PMMA specimens. This can be explained with the formation of larger pores due to the presence of HGMs. Although the movement of the PMMA chains restricted by the formation of smaller pores, the formation of the larger pores compensated this behavior.

4.4.4 DOE analysis

In order to observe the effects of foaming parameters and concentration of the composites on pore size and pore density, JMP software was used. The selected gain value is the average pore size of the smaller pores. Since there are six foam specimens which had complete foaming for smaller pores, the average pore size of these six foams were inserted into JMP statistical software and a model was fitted to these data based on the standard least square method. JMP software suggests the significance of the process parameters effects on average pore size by calculating the p-value for each parameter and dual combinations of them in the confidence limit of 95%. Table 4.15 shows the sorted parameters estimates based on the p-values. The original JMP output of the sorted parameters are given in Appendix Part F, Figure F.2.

Table 4.15 The most effective parameters on the pore size of PMMA-HGM-POSS composite foams.

Term		Estimate	Relative Std Error	Pseudo t-Ratio	Pseudo p-Value
POSS (%) (0, 5)	Biased	-0.475	0.5	-3.62	0.0305
HGM (%) * Pressure (psi) (1600, 3200)		-0.3	0.5	-2.29	0.0975
Pressure (psi)	Biased	-0.1	0.5	-0.76	0.4964
HGM (%) (5, 15)	Biased	0.075	0.5	0.57	0.6040
HGM (%) * POSS (%)		0.075	0.5	0.57	0.6050
Time (h) (2, 24)	Zeroed	0	0	.	.
HGM (%) * Time (h)	Zeroed	0	0	.	.
Pressure (psi) * Time (h)	Zeroed	0	0	.	.
Pressure (psi) * POSS (%)	Zeroed	0	0	.	.
Time (h) * POSS (%)	Zeroed	0	0	.	.

Based on Table 4.15, it was found that the most effective parameter on pore size is the concentration of POSS nanoparticles since the p-value of this parameter is

smaller than p-values of the other parameters. This is due to the CO_2-philicity of the nanomaterial which makes the matrix more prone to CO_2 thus enhances the morphology. The effects of the POSS concentration is statistically significant since the p-value is lower than 0.05. Based on the signs of the estimates it can be said that the POSS%, HGM% and pressure have inverse ratio with the pore size. Thus it can be concluded that both addition of HGM and POSS nanoparticles enhanced the foam morphology by decreasing the pore size.

4.5 Comparison of the Properties of the PMMA Foam Specimens Produced via Different Foaming Methods

In this part of the thesis study, PMMA foam specimens which are produced with syntactic foam production method and $scCO_2$ foaming method as well as the combination of these two methods were compared to evaluate the performances of the foaming methods. In order to understand the effects of foaming processes, the neat PMMA and PMMA-POSS composites were also compared with the foams. In this scope, the neat PMMA, PMMA-POSS composite (PMMA/TMS5), PMMA syntactic foams (PMMA/HD-H5 and PMMA/HD-H15) which were obtained using melt blending method and the PMMA foams from the $scCO_2$ processing (PMMA foam, PMMA/TMS5 foam and the PMMA/H5/TMS5 foam) which were processed with $scCO_2$ were selected in order to compare the all foaming methods that were performed in this study. Their morphologies, densities, mechanical properties and thermal properties were compared and discussed.

4.5.1 Morphologies of The Selected Specimens

Morphologies of the selected specimens were examined with SEM analysis. The SEM images of the syntactic foams PMMA/HD-H5 and PMMA/HD-H15 can be seen in Figure 4.37 which represents that the homogeneous distribution of the HGMs in PMMA matrix was achieved with the extrusion process. In addition, HGMs were

preserved their integrities during the melt processing. Based on Figure 4.37. a, d, the PMMA and PMMA/TMS5 composite specimens show similar morphology with each other. This can be attributed to the homogeneous dispersion of the POSS nanoparticles in PMMA matrix. When the PMMA foam specimen (Figure 4.37.e) was compared with the neat PMMA sample (Figure 4.37.a), it can be easily seen that the $scCO_2$ foaming process created pores in the PMMA matrix. The average pore size of the neat PMMA foam was larger than the average pore size of the PMMA/TMS5 foam specimen which was the result of using CO_2-phillic POSS nanoparticles. This type of POSS enhanced the affinity of PMMA to CO_2, therefore, the diffusion and concentration of CO_2 in PMMA/TMS5 composite were higher than the neat PMMA during the foaming. Therefore, higher number of pores were formed in the matrix which also led to formation of smaller pores. For the PMMA/H5/TMS5 composite, it can be concluded that the larger pores formed due to the CO_2 diffusion in the matrix towards the voids between the matrix and HGM surfaces. Smaller pores, on the other hand, were obtained due to the presence of POSS nanoparticles. The processing of syntactic foams with $scCO_2$ resulted in a bimodal pore structure with larger and smaller pores in the PMMA matrix.

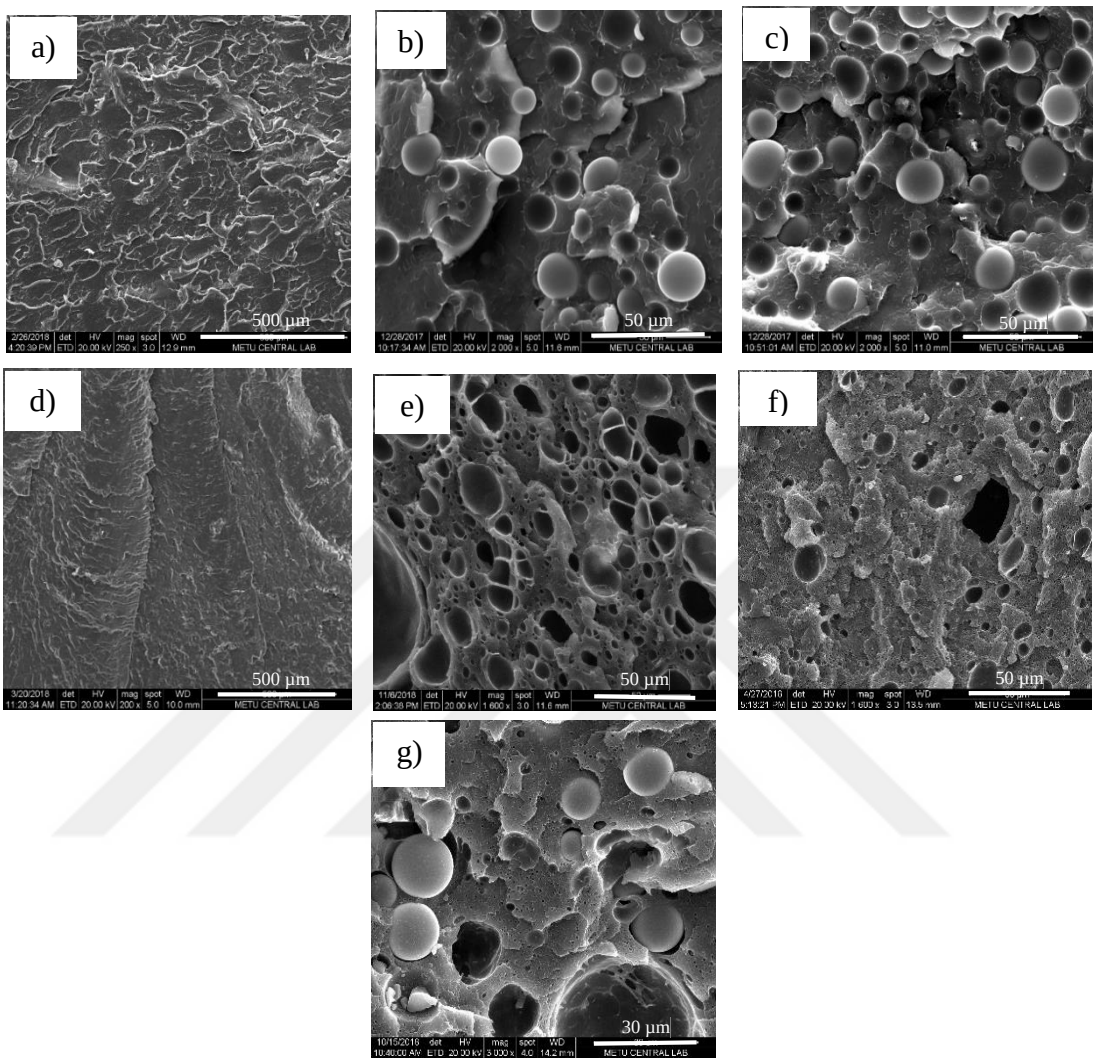

Figure 4.37. SEM images of a) PMMA, b) PMMA/HD-H5, c) PMMA/HD-H15, d) PMMA/TMS5, e) PMMA $scCO_2$ processed foam, f) PMMA/TMS5 $scCO_2$ processed foam, g) PMMA/H5/TMS5 $scCO_2$ processed foam.

4.5.2 Densities of The Selected Specimens

Densities of the composite foams were determined by water displacement method and the results are given in Figure 4.38.

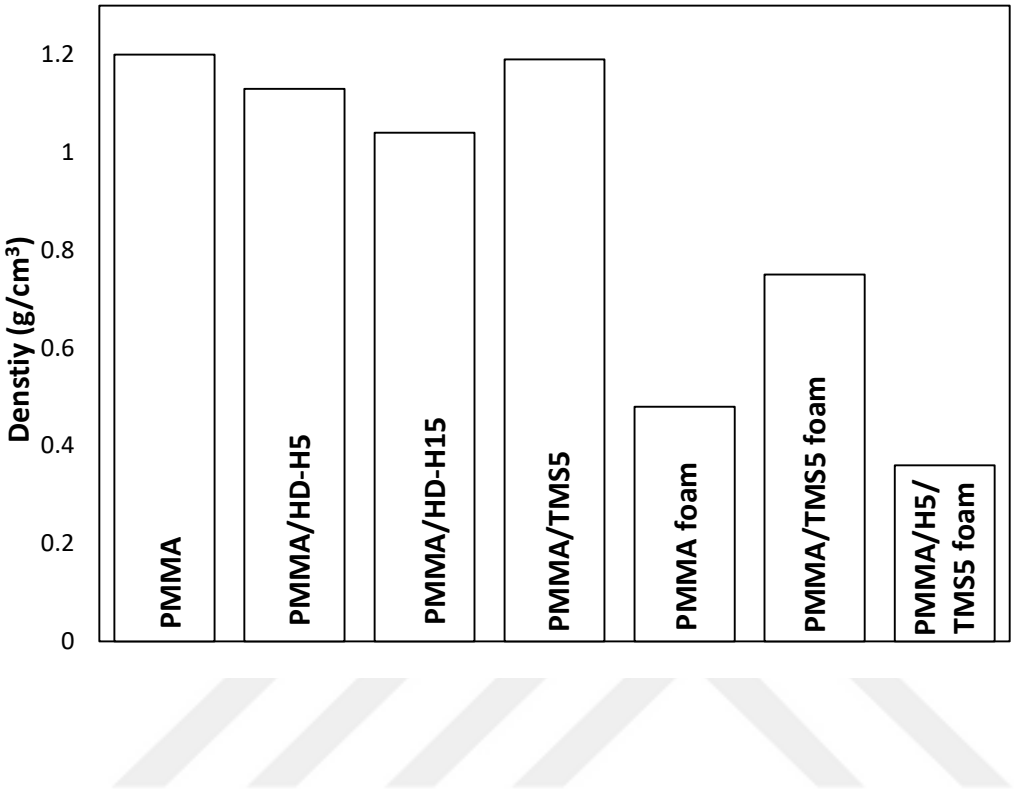

Figure 4.38. Densities of the PMMA, PMMA composites and PMMA foams.

According to Figure 4.38, it was observed that the addition of HGM in the polymer decreased the density of the polymer due to their hollow structures. A higher percent addition of these materials further decreased the density of the polymer. The PMMA/HD-H15 syntactic foam had a 13% lower density than PMMA. The addition of POSS nanoparticles did not change the density of PMMA. Foams obtained by the $scCO_2$ processing were found to be lighter than the PMMA, PMMA/TMS5 composite and syntactic foams with HGMs due to the pore formation in the matrix. The density of PMMA/H5/TMS5 composite foam had the lowest density among all the foams. The reason behind this can be the bimodal pore structure of this specimen consisting of larger pores which are greater than 8.6 μm. The density reduction with the bimodal pore structure is 70% based on the neat PMMA specimen.

4.5.3 Hardness Measurements of the Selected Specimens

The hardness measurements of the selected specimens were evaluated using the Shore D hardness test. The test standard of the Shore D hardness test does not require a specific dimension for the test specimens, thus this measurement can be applicable to all the foams that were obtained during the thesis study including foams of the $scCO_2$ processing. The results of the Shore D hardness test are summarized in Table 4.16.

Table 4.16 Hardness of the PMMA, PMMA composites and PMMA foams.

Composite	Preparation method	Shore D hardness
PMMA	Extrusion	86.8 ± 0.40
PMMA/HD-H5	Extrusion	87.6 ± 0.49
PMMA/HD-H15	Extrusion	87 ± 0.63
PMMA/TMS5	Extrusion	84.6 ± 1.02
PMMA foam	Extrusion + $scCO_2$ processing	80.8 ± 0.75
PMMA/TMS5 foam	Extrusion + $scCO_2$ processing	77.6 ± 0.80
PMMA/H5/TMS5 foam	Extrusion + $scCO_2$ processing	76.2 ± 0.75

According to Table 4.16, PMMA and the PMMA syntactic foams with HGMs have similar Shore D hardness values. However, it was observed that the addition of 5% POSS nanoparticles slightly decreased the hardness of PMMA. This may be attributed to the weak interaction between PMMA and octatrimethylsiloxy POSS nanoparticles. The foams which were obtained by $scCO_2$ processing have lower hardness value than the PMMA and PMMA syntactic foams. This is due to the porous structure of these particles where the presence of pores decreased the resistance of the materials to the applied load. The Shore D Hardness values of the foams that were obtained from the $scCO_2$ processing were slightly lower than the unprocessed polymers, however a great reduction in density up to 69% can be obtained without a vital sacrifice from the mechanical properties with the $scCO_2$ foaming method.

4.5.4 Thermal Properties of the Selected Specimens

Thermal characterization of the selected specimens was carried out using DSC, TGA and LOI analyses. Results of the DSC analyses are given in Figure 4.39.

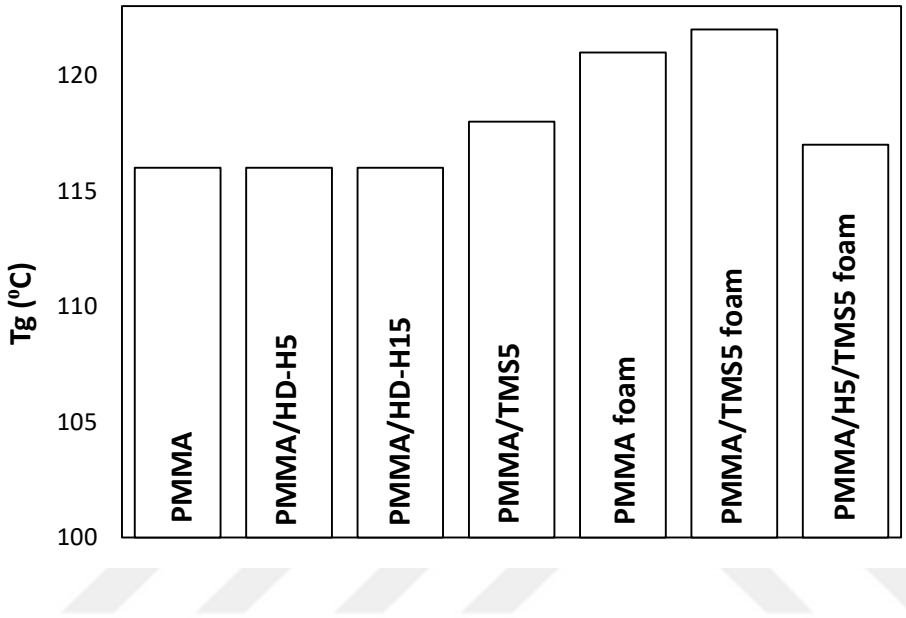

Figure 4.39. Glass transition temperature of the PMMA, PMMA composites and PMMA foams.

The glass transition temperature of PMMA did not considerably change with the addition of neither HGM nor the POSS nanoparticles. On the other hand, the $scCO_2$ foaming process significantly increased the glass transition temperature of PMMA. This can be explained with the pore formation in the matrix. During the foaming process, the chains of the PMMA were realigned in a more ordered state and this led to a reduction in the free volume of the matrix material. The space between the pores had a narrower area since the pores were in the nanometer range, thus the chain mobility was restricted. This resulted in a higher glass transition temperature of the polymer. The PMMA/H5/TMS5 composite foam consisted of also larger pores besides the smaller pores having a bimodal pore structure. The presence of these

larger pores allowed the PMMA chains to move easily in the PMMA matrix, thus Tg of this composite foam was found to be similar to the bulk PMMA.

TGA curves of the polymer composites and foams which were saturated at 11 MPa, 35°C for 24 h and depressurized with fast venting rate are given in Figure 4.40.

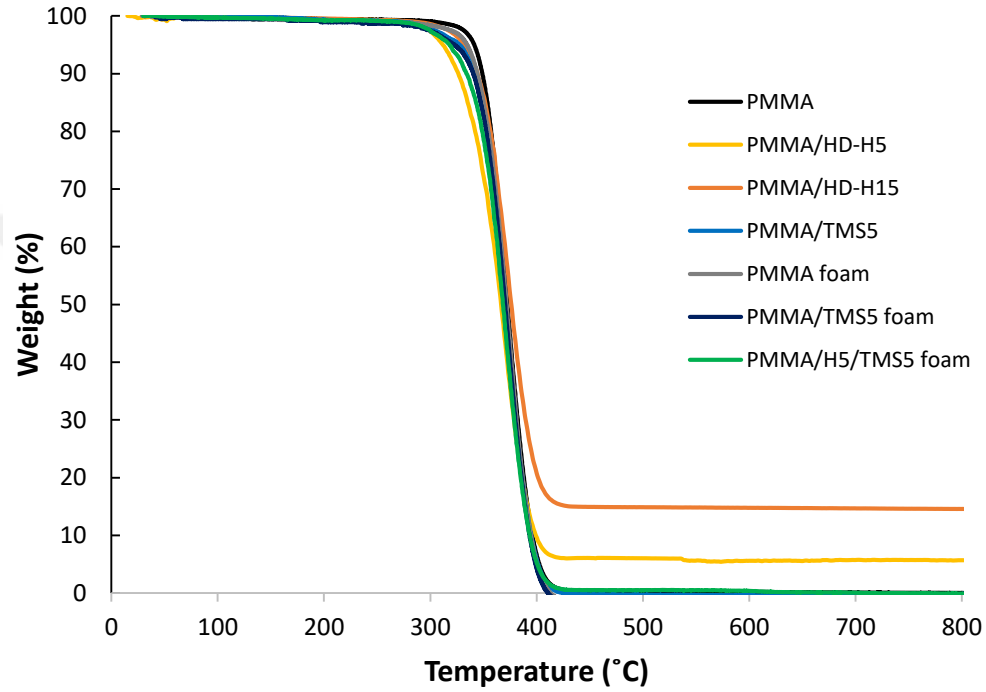

Figure 4.40. TGA curves of the PMMA, PMMA composites and PMMA foams.

Figure 4.40 represents that syntactic foam production method and the $scCO_2$ foaming method and the addition of POSS nanoparticles did not cause any change on the thermal degradation behavior of PMMA. Temperature of 5% weight loss and maximum weight loss of the composites and foams were determined and summarized in Table 4.17.

Table 4.17 Temperature at 5 wt.% loss and temperature at maximum wt.% loss of the PMMA, PMMA composites and PMMA foams.

Specimen	**Preparation method**	**Temperature at 5 wt. % loss (°C)**	**Temperature at max. wt.% loss (°C)**
PMMA	Extrusion	341	375
PMMA/HD-H5	Extrusion	312	369
PMMA/HD-H15	Extrusion	332	375
PMMA/TMS5	Extrusion	328	372
PMMA foam	Extrusion + $scCO_2$ processing	335	376
PMMA/TMS5 foam	Extrusion + $scCO_2$ processing	322	373
PMMA/H5/TMS5 foam	Extrusion + $scCO_2$ processing	318	372

Although the addition of POSS nanoparticles and HGMs into the PMMA matrix decreased the temperature at 5 wt.% loss values for both bulk polymer and foam, it did not change the temperature at maximum wt.% loss values. POSS nanoparticles and HGMs which act as heating sources during the earlier steps of the thermal degradation of the polymer might have caused a reduction in the temperature at 5 wt.% values. The thermal degradation behavior of the PMMA did not change with the addition of HGMs. This can be attributed to the addition of glass particles in the PMMA matrix which has no chemical interaction with the PMMA matrix and shows no degradation under the conditions of the TGA.

In order to see the effects of pore formation and HGM and POSS addition on the flame retardancy behavior of PMMA, limiting oxygen index analyses were carried out. The results can be seen in Table 4.18.

Table 4.18 LOI values of the PMMA, PMMA composites and PMMA foams.

Specimen	Preparation method	LOI (% vol. oxygen)
PMMA	Extrusion	18
PMMA/HD-H5	Extrusion	19
PMMA/HD-H15	Extrusion	20
PMMA/TMS5	Extrusion	20
PMMA foam	Extrusion + $scCO_2$ processing	20
PMMA/TMS5 foam	Extrusion + $scCO_2$ processing	20.5
PMMA/H5/TMS5 foam	Extrusion + $scCO_2$ processing	20.5

According to Table 4.18, the LOI value of the neat PMMA was increased with the addition of HGM and a higher percent addition of glass particles further increased this value. Based on the table, the addition of POSS particles also enhanced the limiting oxygen index value of PMMA. The PMMA foam which was processed at 11 MPa, 35ºC for 24 h and depressurized with fast venting rate had an LOI value of 20% O_2 which was 11% higher than that of the unprocessed PMMA. The formation of pores in the PMMA matrix increased the LOI value. Composite foams with HGM and POSS addition had even higher LOI values than the neat foam. However, this values were still lower than 21% O_2 which is the concentration of oxygen in the air.

CHAPTER 5

CONCLUSIONS

PMMA foams were produced with the syntactic foam production method, $scCO_2$ foaming method and a combination of these two methods. The effects of different foaming methods on the properties of PMMA foams were investigated. The density of the PMMA reduced considerably with the syntactic foam production method whereas the mechanical properties were also decreased. However, the surface modification of the HGMs, as well as the hybrid syntactic foam production method with the selected POSS nanoparticles, compensated the reduced mechanical properties without increasing the density. The knowledge obtained from the surface modification and use of the selected POSS type to reinforce the syntactic foam matrix will contribute to the literature. With the $scCO_2$ processing, a significant reduction in the density of PMMA was obtained. The selected CO_2-philic POSS to enhance the foam morphology in terms of average pore diameter and the pore density led to production of foams with an average pore size of as small as 300 nm and pore density with the order of magnitude as high as 10^{12} cm^{-3}. The selected CO_2-phillic POSS type was used in a $scCO_2$ foaming of a polymer for the first time in the literature. The syntactic foams were processed with $scCO_2$ processing to obtain bimodal pore structure with larger pores which are formed due to the CO_2 diffusion in the matrix towards the voids between the matrix and HGM surfaces and the smaller pores which are formed in the matrix due to $scCO_2$ processing. The bimodal pore structure was achieved with this proposed method for the first time in literature. The conclusions obtained from these studies are given in the following sections.

5.1 Effects of HGM Density and Surface Modification on the Mechanical and Thermal Properties of PMMA Syntactic Foams

HGM types with three different densities were used to obtain PMMA syntactic foams. The concentrations of HGMs in the PMMA matrix were 5, 10 and 15 wt.%. The high density HGMs showed better resistance to melt processing and stayed intact, while low density HGMs were shattered. The highest reduction in the density of PMMA was attained with the incorporation of high-density HGMs. It was found that the higher percent addition of HGMs resulted in a further reduction in the density, impact and flexural strength. In order to improve the mechanical and thermal properties of PMMA syntactic foams, different approaches were taken into account. The coating of the surface of HGMs with PMMA increased the adhesion between HGM and the matrix and improved the flexural strength by 12% and the impact resistance by 17% with respect to the syntactic foams with the uncoated HGMs at the same concentration level. On the other hand, the incorporation of hollow glass microspheres into the PMMA matrix had no significant effect on the thermal degradation behavior and the glass transition temperature of PMMA. It can be concluded that the PMMA syntactic foams with decreased density and maintained mechanical and thermal properties were obtained with the using of surface coated HGMs. The coating process can offer a new and promising approach for literature on syntactic foam studies.

5.2 Effects of POSS Nanoparticle Reinforcement on the Properties of PMMA Hybrid Syntactic Foams

PMMA-POSS composites and PMMA hybrid syntactic foams with octaphenyl and octaisobutyl POSS nanoparticles were produced to understand the effects of POSS type and weight percentage on density, mechanical properties and thermal properties of PMMA and PMMA syntactic foams. While the incorporation of both types of POSS improved the mechanical properties depending on the concentration of POSS,

the incorporation of octaphenyl POSS resulted in more enhanced mechanical properties than the addition of octaisobutyl POSS in PMMA. On the other hand, incorporation of both the octaphenyl and octaisobutyl POSS did not affect the temperature at maximum wt.% loss and the glass transition temperature of PMMA. Octaphenyl POSS was selected to compose hybrid syntactic foams. While the PMMA syntactic foams with 15 wt.% HGMs had 13.3% lower density than the neat PMMA, incorporation of POSS to this composite did not have an adverse effect on the density. However, the addition of POSS nanoparticles slightly compensated the decreased flexural strength of the PMMA with the incorporation of HGMs. In addition, hybrid syntactic foams had higher specific moduli than the neat PMMA and PMMA syntactic foams. But, there was a reduction in the specific impact strength of syntactic foams with the incorporation of both microspheres and POSS. The TGA and DSC analyses showed that the thermal properties of PMMA syntactic foams were not affected by the incorporation of POSS nanoparticles. It can be concluded that the hybrid syntactic foam approach with POSS nanoparticles generally resulted in enhanced specific flexural strength and modulus, and preserved density and the thermal properties in the PMMA syntactic foams. Overall this study represents that the production of PMMA-based hybrid syntactic foams with low density, enhanced modulus and maintained thermal conductivity with respect to the neat polymer can be achieved with the hybrid syntactic foam approach using POSS nanoparticles.

5.3 Effects of scCO_2 foaming parameters and the CO_2-philic nanoparticle addition on supercritical CO_2 foaming of PMMA

PMMA and PMMA-POSS composite foams were produced to study the effects of the highly CO_2-philic octatrimethylsiloxy POSS nanoparticles addition and process conditions on the foaming performance and foam morphology. 24 h of saturation time resulted in complete foaming of specimens, while using a highly CO_2-philic POSS as a pore nucleator led to complete foaming in shorter time. Also, the addition

of POSS nanoparticles enhanced the foam morphology by increasing the pore density and decreasing the average pore diameter. Decreasing the process temperature to 35ºC, decreased the average pore diameters and increased the pore densities of the PMMA-5%POSS composite foams. Fast-venting rate enhanced the formation of smaller pores and increased the pore densities. The smallest average pore diameter (0.3 μm) and the highest pore density (6.33×10^{12} cm^{-3}) were obtained with PMMA-5% POSS composites processed at 35ºC and 32 MPa, for 24 h, and depressurized with the fast venting rate, 0.4 MPa/s. The DOE analysis stated that the most effective parameter on the average pore diameter of the PMMA/TMS5 composite foam was the temperature. The DSC analyses showed that the glass transition temperatures of the PMMA and PMMA composite foams which were saturated at low temperature were higher than the glass transition temperatures of the bulk polymer. $ScCO_2$ processing reduced the density of PMMA by about 50% compared to the unprocessed polymer. These results show that octatrimethylsiloxy POSS nanoparticles are promising pore nucleators which can be used to produce PMMA foams with $scCO_2$ processing at more economical conditions, with improved foaming performance and controlled pore morphology.

5.4 Effects of $scCO_2$ foaming parameters and the CO_2-philic nanoparticle addition on supercritical CO_2 foaming of PMMA Syntactic Foams

HGMs were used to produce PMMA syntactic foams and these syntactic foams were processed with $scCO_2$ to obtain bimodal pore structure in PMMA matrix. The effects of the processing time, pressure as well as the concentration of HGMs, and the CO_2-philic POSS nanoparticles on the foaming performance and foam morphology were investigated. The larger pores formed due to the CO_2 diffusion in the matrix towards the voids between the matrix and HGM surfaces. On the other hand, the formation of the smaller pores throughout the matrix was improved with the existence of the POSS nanoparticles in the matrix which not only formed additional nucleation sites, but also enhanced the CO_2 incorporation due to their CO_2-philic nature. The ratio of

the average pore diameters of larger and smaller pores were calculated as at least 16 which claimed the bimodal pore structure. Introduction of HGMs in PMMA-POSS composite matrix enhanced the foaming performance by decreasing the average pore diameter at lower pressure of 11 MPa due to the presence of the voids between the HGM and PMMA that formed escaping paths for the gas and enhanced transportation of CO_2 from the matrix, inhibiting the coalescence of the pores in the matrix which results in smaller average pore size. The smallest average pore diameter was 0.1 μm, which was obtained by the processing of the PMMA-5H-5P specimens at 11 MPa. HGMs had an opposite effect on the transport of the gas when they were incorporated at a higher concentration in the matrix. This was observed with a 10% increase in the concentration of the HGMs in the matrix processed at 11 MPa, leading to a 10% increase in the average pore diameter of the smaller pores. At high pressure, higher concentration of the HGMs led to the rapid transport of the CO_2 during depressurization and prevented the pores from coalescence thus increased the density of the smaller pores. There were indirect relationships between the morphology of the PMMA-POSS-HGM composite foams and certain parameters like the $scCO_2$ processing pressure, POSS concentration, and HGM concentration which allowed the morphology of these composite foams to be fine-tuned with these parameters. The densities of the foams that were processed for 24 h were lower than the unprocessed composite by about 50%.

5.5 Comparison of the Properties of the PMMA Foam Specimens Produced via Different Foaming Methods

In this part of the thesis study, we aimed to compare the two different foaming methods on the PMMA foam properties and to observe the effect of the fillers on the PMMA. For this purpose, the neat PMMA, PMMA syntactic foams (PMMA/HD-H5 and PMMA/HD-H15), PMMA-POSS composite (PMMA/TMS5), PMMA foams from the $scCO_2$ processing (PMMA foam, PMMA/TMS5 foam and the PMMA/H5/TMS5 foam) were selected and evaluated in terms of their morphologies,

densities, mechanical and thermal properties. The SEM analyses of the syntactic foams indicated that the HGMs dispersed homogeneously in the PMMA matrix and stayed intact. The SEM images of the PMMA foams which were obtained from the $scCO_2$ processing represented that the addition of POSS nanoparticles decreased the pore diameter and the addition of both HGM and POSS resulted in bimodal pore structure. Based on the density measurement it was found that while the density reduction of PMMA with syntactic foam production method had a maximum value of 13%, the $scCO_2$ foaming method decreased the density by up to 70%. The Shore D hardness values of the PMMA syntactic foams were found to be slightly higher than the neat PMMA specimen. However, the values of PMMA-POSS composite and the PMMA foams obtained via the $scCO_2$ foaming method were lower than the neat PMMA specimen. The glass transition temperature of the PMMA syntactic foams did not show differences from the neat PMMA. However, the glass transition temperatures of $scCO_2$ foams were higher than the neat PMMA possibly due to the more ordered structure of PMMA chains obtained by the supercritical CO_2 processing and the confinement effect of the smaller pores. Based on the TGA analysis it was found that neither the foaming process nor the composite type did not affect the temperature at maximum degradation values. However, temperature at 5 wt.% loss values of the foams were lower than the neat PMMA which can be explained by the heat-dissipating behavior of the particles during the earlier degradation step of the polymer. The LOI values of the composites and composite foams were found to be higher than the PMMA, however, they were still lower than the 21% oxygen.

CHAPTER 6

OUTLOOK

The primary purpose of the thesis study was to decrease the density of PMMA without reducing the mechanical properties. For this purpose, PMMA syntactic foams were produced using different types of HGMs in terms of HGM density. Although a considerable reduction in the density was obtained, the mechanical properties were also decreased. Using polymer microspheres which keep their structural integrity at the processing temperatures of PMMA may enhance the mechanical properties being more compatible with the PMMA matrix. In addition, using metallic microspheres may also enhance the mechanical properties. In this study, we carried out the surface modification of microspheres to be compatible with the PMMA matrix. The coating of the surface of the HGMs with PMMA enhanced the mechanical properties; however, other polymers might have further improved the compatibility. The silane coupling agent that was used in this study did not change the properties of the syntactic foams. Different types of silane coupling agents and silanization methods can be used to improve mechanical properties. The concentration of HGMs in the PMMA matrix was kept as a maximum of 15 wt. % due to the limitations of the extruder that was used for the production of the syntactic foams. The solvent casting method may be used to obtain syntactic foams with a higher percentage of HGMs, thus lower density.

$ScCO_2$ processing was also considered to produce PMMA foams in this thesis study. The effects of foaming parameters on the density and morphology of foams were examined with DOE analyses. The full factorial design method was selected to understand the significance of the foaming parameters on the morphology. The most effective parameters on the foam morphology were determined. Other DOE methods which provide controlling of the morphology with proposed mathematical models,

such as the surface response design method, may be applied using the determined effective parameters.

Using of different specimen dimensions such as thin samples can be beneficial to observe the CO_2 behavior in various geometries. Besides, a fixed mold may be used to obtain PMMA foams with the desired dimensions therefore the foams can be evaluated in terms of mechanical tests. The CO_2 concentration of the saturated polymer may be determined through gravimetric measurements, the CO_2 solubility in the neat polymer may be modeled, and the deviation from the modeled behvior due to the existence of POSS may be evaluated to understand the effect of CO_2-philic POSS on the solubility of CO_2 in the polymer. Similarly, the CO_2 concentration in the polymer can be obtained through gravimetric measurements after the depressurization with respect to time to evaluate the CO_2 diffusion in the polymer and understand how the CO_2-philic POSS incorporation affects the postfoaming CO_2 transport in the polymer. In this thesis study, octatrimethlysiloxy POSS was used to enhance the foam morphology as being highly CO_2-phillic. Using other CO_2-philic nanomaterials can be more effective on the morphology of the PMMA foams which may disperse more homogeneously in the PMMA matrix.

REFERENCES

1. C. C. Ibeh and M. Bubacz, “Current trends in nanocomposite foams,” J. Cell. Plast., vol. 44, no. 6, pp. 493–515, 2008.

2. D. D. Luong, V. C. Shunmugasamy, O. M. Strbik III, and N. Gupta, “High Strain Rate Compressive Behavior of Polyurethane Resin and Polyurethane/Al_2O_3 Hollow Sphere Syntactic Foams ,” J. Compos., vol. 2014, pp. 1–10, 2014.

3. A. K. Ghamsari, E. Zegeye, and E. Woldesenbet, “Viscoelastic properties of syntactic foam reinforced with short sisal fibers,” J. Compos. Mater., vol. 49, no. 1, pp. 27–34, 2015.

4. R. Maharsia, N. Gupta, and H. D. Jerro, “Investigation of flexural strength properties of rubber and nanoclay reinforced hybrid syntactic foams,” Mater. Sci. Eng. A, vol. 417, no. 1–2, pp. 249–258, 2006.

5. M. Saha, and S. Nilufar, “Nanoclay-reinforced syntactic foams: flexure and thermal behavior,” Polym. Comp., vol. 31, pp.1332-1342, 2010.

6. R. R. Maharsia and H. D. Jerro, “Enhancing tensile strength and toughness in syntactic foams through nanoclay reinforcement,” Mater. Sci. Eng. A, vol. 454–455, pp. 416–422, 2007.

7. N. Gupta and R. Maharsia, “Enhancement of energy absorption in syntactic foams by nanoclay incorporation for sandwich core applications,” Appl. Compos. Mater., vol. 12, no. 3–4, pp. 247–261, 2005.

8. S. K. Goel and E. J. Beckman, “Generation of microcellular polymeric foams using supercritical carbon dioxide. I: Effect of pressure and temperature on nucleation,” Polym. Eng. Sci., vol. 34, no. 14, pp. 1137–1147, 1994.

9. U. Ali, K. J. B. A. Karim, and N. A. Buang, “A Review of the Properties and Applications of Poly (Methyl Methacrylate) (PMMA),” Polym. Rev., vol. 55, no. 4, pp. 678–705, 2015.

10. B. Notario, J. Pinto, and M. A. Rodríguez-Pérez, “Towards a new generation of polymeric foams: PMMA nanocellular foams with enhanced physical properties,” Polymer (Guildf)., vol. 63, pp. 116–126, 2015.

11. J.-M. Yeh, K.C. Chang, C.. Peng, M.C. Lai, S.-S. Hang, H.R. Lin, S.-J. Liou, “Enhancement in Insulation and Mechanical Properties of PMMA Nanocomposite Foams Infused with Multi-Walled Carbon Nanotubes,” J. Nanosci. Nanotechnol., vol. 11, no. 8, pp. 6757–6764, 2011.

12. V. K. Kinra, and E. Ker., “Effective Elastic Moduli of a Thin-Walled Glass Microsphere/PMMA Composite,” Comp. Mater., Vol. 16, pp. 117-138, 1982.

13. W. Zhang, G. Camino, and R. Yang, “Polymer/polyhedral oligomeric silsesquioxane (POSS) nanocomposites: An overview of fire retardance,” Prog. Polym. Sci., vol. 67, pp. 77–125, 2017.

14. J.-M. Yeh, K.C. Chang, C.W. Peng, B.G. Chand, S.C. Chiou, H.H. Huang,C.Y. Lin, J.C. Yang, H.R. Lin, and C.L. Chen, “Preparation and insulation property studies of thermoplastic PMMA-silica nanocomposite foams,” vol. 30, pp. 715 – 722, 2009.

15. D. Eaves, “Handbook of Polymer Foams,” United Kingdom, 2004.

16. S.T. Lee, and C.B. Park, “Foam Extrusion: Principles and Practice,” Second Edition, United Kingdom, 2014.

17. S.T. Lee, and N.S. Ramesh, “Polymeric Foams: Mechanisms and Materials,” United Kingdom, 2004.

18. S.T. Lee, C.B. Park, and N.S. Ramesh, “Polymeric Foams Science and Technology,”, United Kingdom, 2007.

19. A.H. Landrock, “Handbook of Plastic Foams: Types, Properties, Manufacture and Applications,”. U.S.A., 1995.

20. L. J. M. Jacobs, M. F. Kemmere, and J. T. F. Keurentjes, “Sustainable polymer foaming using high pressure carbon dioxide: A review on fundamentals, processes and applications,” Green Chem., vol. 10, no. 7, pp. 731–738, 2008.

21. L. M. Matuana, O. Faruk, and C. A. Diaz, “Cell morphology of extrusion foamed poly(lactic acid) using endothermic chemical foaming agent,” Bioresour. Technol., vol. 100, no. 23, pp. 5947–5954, 2009.

22. Z. X. Xin et al., “Microcellular structure of pp/waste rubber powder blends with supercritical co 2 by foam extrusion process,” J. Cell. Plast., vol. 45, no. 6, pp. 499–514, 2009.

23. A. Ameli, M. Nofar, D. Jahani, G. Rizvi, and C. B. Park, “Development of high void fraction polylactide composite foams using injection molding: Crystallization and foaming behaviors,” Chem. Eng. J., vol. 262, pp. 78–87, 2015.

24. R. Spina, “Technological characterization of PE/EVA blends for foam injection molding,” Mater. Des., vol. 84, pp. 64–71, 2015.

25. S. Ries, A. Spoerrer, and V. Altstaedt, “Foam injection molding of thermoplastic elastomers: Blowing agents, foaming process and characterization of structural foams,” AIP Conf. Proc., vol. 1593, pp. 401–410, 2014.

26. X. Sun, and L.S. Turng, “Novel injection molding foaming approaches using gas-laden pellets with N_2, CO_2 , and N_2 + CO_2 as the blowing agents,” Polym. Eng. & Sci. vol. 54, pp. 899-913, 2014.

27. A. Ameli, D. Jahani, M. Nofar, P. U. Jung, and C. B. Park, “Development of high void fraction polylactide composite foams using injection molding: Mechanical and thermal insulation properties,” Compos. Sci. Technol., vol. 90, pp. 88–95, 2014.

28. X. Liao, H. Zhang, and T. He, “Preparation of porous biodegradable polymer and its nanocomposites by supercritical CO_2 foaming for tissue engineering,” J. Nanomater., vol. 2012, 2012.

29. “Polymer Foam Market by Resin Type (PU, PS, PO, Phenolic), Foam Type (Rigid, Flexible), End-Use Industry (Building & Construction, Packaging, Automotive, Furniture & Bedding, Footwear, Sports & Recreational), and Region - Global Forecast to 2025,” accessed August 2, 2020, https://www.marketsandmarkets.com/Market-Reports/foams-market-1011.html.

30. “Market Research Report: Polymer Foam Market Size, Share & Trends Analysis Report By Type (Polyurethane, Polystyrene, Polyolefin, Melamine, Phenolic, PVC), By Application, By Region, And Segment Forecasts, 2019 – 2025,” accessed August 2, https://www.grandviewresearch.com/industry-analysis/polymer-foam-market.

31. P. Spasojevic, M. Zrilic, V. Panic, D. Stamenkovic, S. Seslija, and S. Velickovic, “The Mechanical Properties of a Poly(methyl methacrylate) Denture Base Material Modified with Dimethyl Itaconate and Di-n-butyl Itaconate,” Int. J. Polym. Sci., vol. 2015, doi: 10.1155/2015/561012.

32. O. H. Gonçalves, T. Staudt, P. H. H. de Araújo, and R. A. F. Machado, “Foaming of poly(methyl methacrylate) particles,” Mater. Sci. Eng. C, vol. 29, no. 2, pp. 479–484, 2009.

33. L. Henri, “Thermohygroelastic Properties of Polymethylmethacrylate,” Netherlands, 2007.

34. “Reflective sheet capable of conducting plastic absorption,” accessed August 2, https://patents.google. com/patent/CN104165329A/en.

35. “Panel filled with polymeric foam,” accessed August 2, https://patents.google.com/patent/EP0716197A2/en.

36. “Heat-insulating and moistureproof corrugated board,” accessed August 2, https://patents.google.com/patent/CN202319198U/en?oq=CN202319198U.

37. “Extruded acryl composite foam board and preparation method thereof,” accessed August 2,

https://patents.google.com/patent/CN101670696B/en?oq=CN101670696B.

38. “Preparation method of polymethyl methacrylate based cell gradient material,” accessed August 2,

https://patents.google.com/patent/CN103302861B/en?oq=CN103302861B%2f

39. H. Bin Zhang, Q. Yan, W. G. Zheng, Z. He, and Z. Z. Yu, “Tough graphene-polymer microcellular foams for electromagnetic interference shielding,” ACS Appl. Mater. Interfaces, vol. 3, no. 3, pp. 918–924, 2011.

40. V. Mittal, “Polymer nanocomposite foams,” Unites Kingdom, 2014.

41. G. Li, L. Wang, H. Ni, and C. U. Pittman Jr., “Polyhedral oligomeric silsesquioxane (POSS) : a review,” J. Inorg. Organomet. Polym., vol. 11, no. 3, pp. 123–154, 2001.

42. B. X. Fu, M. Y. Gelfer, B.S. Hsiao, S. Philips, B. Viers, R. Blansky, P. Ruth “Physical gelation in ethylene-propylene copolymer melts induced by polyhedral oligomeric silsesquioxane (POSS) molecules,” Polymer (Guildf)., vol. 44, no. 5, pp. 1499–1506, 2003.

43. E. L. Heeley, D. J. Hughes, Y. El Aziz, I. Williamson, P. G. Taylor, and A. R. Bassindale, “Properties and self-assembled packing morphology of long alkyl-chained substituted polyhedral oligomeric silsesquioxanes (POSS) cages,” Phys. Chem. Chem. Phys., vol. 15, no. 15, pp. 5518–5529, 2013, doi: 10.1039/c3cp44356f.

44. E. T. Kopesky, G. H. McKinley, and R. E. Cohen, “Toughened poly(methyl methacrylate) nanocomposites by incorporating polyhedral oligomeric silsesquioxanes,” Polymer (Guildf)., vol. 47, no. 1, pp. 299–309, 2006.

45. C. Zhao, X. Yang, X. Wu, X. Liu, X. Wang, and L. Lu, “Preparation and characterization of poly(methyl methacrylate) nanocomposites containing octavinyl polyhedral oligomeric silsesquioxane,” Polym. Bull., vol. 60, no. 4, pp. 495–505, 2008.

46. H. Xu, B. Yang, J. Wang, S. Guang, and C. Li, “Preparation, tg improvement, and thermal stability enhancement mechanism of soluble poly(methyl methacrylate) nanocomposites by incorporating octavinyl polyhedral oligomeric silsesquioxanes et al., J. Polym. Sci. Part A, Polym. Chem. Vol. 32, pp. 5308-5317, 2007.

47. S. Li, G. P. Simon, J. G. Matisons, “ The effect of incorporation of POSS units on polymer blend compatibility,” J. App. Polym. Sci, vol. 115, pp. 1153-1159, 2010.

48. J. Jiao, P. Lv, L. Wang, Y. Cai, and P. Liu, “The effects of structure of POSS on the properties of POSS/PMMA hybrid materials,” Polym. Eng. & Sci., vol. 55, pp. 565-572, 2015.

49. S. Illescas and A. Arostegui, “Influence of polyhedral oligomeric silsesquioxanes on thermal and mechanical properties of melt-mixed poly(methyl methacrylate)/polyhedral oligomeric silsesquioxanes composites,” High Perform. Polym., vol. 26, no. 3, pp. 307–318, 2014.

50. C. B. Zhao, X. Wang, X. J. Yang, and W. Zhao, “Thermal and Mechanical Properties of Poly(methyl methacrylate) Nanocomposites Containing Polyhedral Oligomeric Silsesquioxane,” Adv. Mater. Res., vol. 557–559, pp. 304–308, 2012.

51. K. Tanaka , S. Adachi, and Y. Chujo, “ Structure–property relationship of octa-substituted POSS in thermal and mechanical reinforcements of conventional polymers,” J. Polym. Sci. Part A: Polym. Chem., vol. 47, pp. 5690-5697, 2009.

52. N. Gupta, R. Ye, and M. Porfiri, “Comparison of tensile and compressive characteristics of vinyl ester/glass microballoon syntactic foams,” Compos. Part B Eng., vol. 41, no. 3, pp. 236–245, 2010.

53. N. Gupta, S. E. Zeltmann, V. C. Shunmugasamy, and D. Pinisetty, “Applications of polymer matrix syntactic foams,” Jom, vol. 66, no. 2, pp. 245–254, 2014.

54. P.G. Jessop, W. Leitner, “ Chemical Synthesis Using Supercritical Fluids,” 1999.

55. A. Baiker, “Supercritical Fluids in Heterogeneous Catalysis,” Chem. Rev., vol. 99, no. 2, pp. 453–474, 2002.

56. Knez, E. Markočič, M. Leitgeb, M. Primožič, M. Knez Hrnčič, and M. Škerget, “Industrial applications of supercritical fluids: A review,” Energy, vol. 77, pp. 235–243, 2014.

57. E. Krogh, R. Nilsen, and R. Henningsen, “Liquefied CO_2 injection modelling,” Energy Procedia, vol. 23, no. 1876, pp. 527–555, 2012, doi: 10.1016/j.egypro.2012.06.022.

58. J. Z. Liang, “Mechanical properties of hollow glass bead-filled ABS composites,” J Thermoplast Compos Mater, vol 18, pp. 407-416, 2005 http://dx.doi.org/10.1177/0892705705051899.005.

59. S. N. Patankar, A. Das, and Y. A. Kranov, “Interface engineering via compatibilization in HDPE composite reinforced with sodium borosilicate hollow glass microspheres,” Compos. Part A Appl. Sci. Manuf., vol. 40, no. 6–7, pp. 897–903, 2009.

60. M. Ozkutlu, C. Dilek, and G. Bayram, “Effects of hollow glass microsphere density and surface modification on the mechanical and thermal properties of poly(methyl methacrylate) syntactic foams,” Compos. Struct., vol. 202, no. February, pp. 545–550, 2018.

61. M. Ozkutlu, C. Dilek, and G. Bayram, “Poly(methyl methacrylate) hybrid syntactic foams with hollow glass microspheres and polyhedral oligomeric silsesquioxanes,” J. Appl. Polym. Sci., vol. 137, no. 7, pp. 1–9, 2020, doi: 10.1002/app.48368.

62. E. Zegeye, A. K. Ghamsari, and E. Woldesenbet, “Mechanical properties of graphene platelets reinforced syntactic foams,” Compos. Part B Eng., vol. 60, pp. 268–273, 2014.

63. H. Mae, M. Omiya, and K. Kishimoto, “Effects of strain rate and density on tensile behavior of polypropylene syntactic foam with polymer microballoons,” Mater. Sci. Eng. A, vol. 477, no. 1–2, pp. 168–178, 2008.

64. S. N. Patankar and Y. A. Kranov, “Hollow glass microsphere HDPE composites for low energy sustainability,” Mater. Sci. Eng. A, vol. 527, no. 6, pp. 1361–1366, 2010.

65. C. Swetha and R. Kumar, “Quasi-static uni-axial compression behaviour of hollow glass microspheres/epoxy based syntactic foams,” Mater. Des., vol. 32, no. 8–9, pp. 4152–4163, 2011.

66. G. Hu and D. Yu, “Tensile, thermal and dynamic mechanical properties of hollow polymer particle-filled epoxy syntactic foam,” Mater. Sci. Eng. A, vol. 528, no. 15, pp. 5177–5183, 2011.

67. A. S. Doumbia et al., “Hollow microspheres - Poly-(propylene) blends: Relationship between microspheres degradation and composite properties,” Polym. Degrad. Stab., vol. 114, pp. 146–153, 2015.

68. N. Gupta and R. Nagorny, “Tensile properties of glass microballoon-epoxy resin syntactic foams,” J. Appl. Polym. Sci., vol. 102, no. 2, pp. 1254–1261, 2006.

69. J. Liang, “Tensile and Impact Properties of Hollow Glass Bead- Filled PVC Composites,” pp. 588–591, 2002.

70. B. R. Bharath Kumar et al., “Effect of cenosphere surface treatment and blending method on the tensile properties of thermoplastic matrix syntactic foams,” J. Appl. Polym. Sci., vol. 133, no. 35, 2016.

71. G. Li and N. Jones, “Development of rubberized syntactic foam,” Compos. Part A Appl. Sci. Manuf., vol. 38, no. 6, pp. 1483–1492, 2007.

72. M. Yi, H. Sun, H. Zhang, X. Deng, Q. Cai, and X. Yang, “Flexible fiber-reinforced composites with improved interfacial adhesion by mussel-inspired polydopamine and poly(methyl methacrylate) coating,” Mater. Sci. Eng. C, vol. 58, pp. 742–749, 2016.

73. N. Gupta, C. S. Karthikeyan, and S. Sankaran, “Physical and Mechanical Properties of Syntactic Foams With and Without Fibers C orrelation of Processing Methodology to the,” vol. 5803, no. 99, 1999.

74. C.S. Karthikeyan, S. Sankaran, M. N. Jagdish Kumar, and Kishore, “Processing and compressive strengths of syntactic foams with and without fibrous reinforcements,” J. Appl. Polym. Sci., vol. 81, no. 2, pp. 405–411, 2001.

75. C. S. Karthikeyan, S. Sankaran, and Kishore, “Elastic behaviour of plain and fibre-reinforced syntactic foams under compression,” Mater. Lett., vol. 58, no. 6, pp. 995–999, 2004.

76. C. S. Karthikeyan, S. Sankaran, and Kishore, “Influence of chopped strand fibres on the flexural behaviour of a syntactic foam core system,” Polym. Int., vol. 49, pp. 158-162, 2000.

77. C. S. Karthikeyan, S. Sankaran, and Kishore, “Flexural behaviour of fibre-reinforced syntactic foams,” Macromol. Mater. Eng., vol. 290, no. 1, pp. 60–65, 2005.

78. L. Wang, J. Zhang, X. Yang, C. Zhang, W. Gong, and J. Yu, “Flexural properties of epoxy syntactic foams reinforced by fiberglass mesh and/or short glass fiber,” Mater. Des., vol. 55, pp. 929–936, 2014.

79. C. S. Karthikeyan, S. Sankaran, and Kishore, “Investigation of bending modulus of fiber-reinforced syntactic foams for sandwich and structural applications,” Polym. Adv. Technol. Vol. 18, pp. 254–256, 2007.

80. J. A. M. Ferreira, C. Capela, and J. D. Costa, “A study of the mechanical behaviour on fibre reinforced hollow microspheres hybrid composites,” Compos. Part A Appl. Sci. Manuf., vol. 41, no. 3, pp. 345–352, 2010.

81. E. M. Wouterson, F. Y. C. Boey, X. Hu, and S. C. Wong, “Effect of fiber reinforcement on the tensile, fracture and thermal properties of syntactic foam,” Polymer (Guildf)., vol. 48, no. 11, pp. 3183–3191, 2007.

82. Y. J. Huang, L. Vaikhanski, and S. R. Nutt, “3D long fiber-reinforced syntactic foam based on hollow polymeric microspheres,” Compos. Part A Appl. Sci. Manuf., vol. 37, no. 3, pp. 488–496, 2006.

83. B. John, C. P. R. Nair, and K. N. Ninan, “Effect of nanoclay on the mechanical, dynamic mechanical and thermal properties of cyanate ester syntactic foams,” Mater. Sci. Eng. A, vol. 527, no. 21–22, pp. 5435–5443, 2010.

84. M. Dimchev, R. Caeti, and N. Gupta, “Effect of carbon nanofibers on tensile and compressive characteristics of hollow particle filled composites,” Mater. Des., vol. 31, no. 3, pp. 1332–1337, 2010.

85. R. L. Poveda, S. Achar, and N. Gupta, “Viscoelastic properties of carbon nanofiber reinforced multiscale syntactic foam,” Compos. Part B Eng., vol. 58, pp. 208–216, 2014.

86. L. Zhang and J. Ma, “Effect of carbon nanofiber reinforcement on mechanical properties of syntactic foam,” Mater. Sci. Eng. A, vol. 574, pp. 191–196, 2013.

87. M. Drdlová and M. Frank, “Mechanical Properties of Glass Microsphere / Epoxy Foams Modified by Carbon Nanotubes and Nanosilica,” J. Sci. Ind. Res., vol. 75, no. 6, pp. 365–370, 2016.

88. J. A. Reglero Ruiz, M. Dumon, J. Pinto, and M. A. Rodriguez-Pérez, “Low-density nanocellular foams produced by high-pressure carbon dioxide,” Macromol. Mater. Eng., vol. 296, no. 8, pp. 752–759, 2011.

89. S. K. Goel and E. J. Beckman, “Nucleation and growth in microcellular materials: Supercritical CO_2 as foaming agent,” AIChE J., vol. 41, no. 2, pp. 357–367, 1995.

90. Y. K. Kwon and H. K. Bae, “Production of microcellular foam plastics by supercritical carbon dioxide,” Korean J. Chem. Eng., vol. 24, no. 1, pp. 127–132, 2007.

91. S. Siripurapu, J. M. DeSimone, S. A. Khan, and R. J. Spontak, “Controlled foaming of polymer films through restricted surface diffusion and the addition of nanosilica particles or CO_2-philic surfactants,” Macromolecules, vol. 38, no. 6, pp. 2271–2280, 2005.

92. R. Li, L. Li, D. Zeng, Q. Liu, and T. Fang, “Numerical selection of the parameters in producing microcellular polymethyl methacrylate with supercritical CO_2,” Cell. Polym., vol. 35, no. 6, pp. 309–328, 2016.

93. S. Siripurapu, J. M. Desimone, R. J. Spontak, and S. A. Khan, “Generation of nanoporous thin polymer films via foaming with carbon dioxide,” Fuel Chem. Div. Prepr., vol. 48, no. 1, pp. 262–263, 2003.

94. J.A.R. Ruiz, P. Viot, and M. Dumon, “Microcellular foaming of polymethylmethacrylate in a batch supercritical CO_2 process: effect of microstructure on compression behavior,” J. App. Polym. Sci, vol. 118, pp. 320–331, 2010.

95. C. Forest, P. Chaumont, P. Cassagnau, B. Swoboda, and P. Sonntag, “CO_2 nano-foaming of nanostructured PMMA,” Polymer (Guildf)., vol. 58, pp. 76–87, 2015.

96. J. Yang et al., “A new promising nucleating agent for polymer foaming: Applications of ordered mesoporous silica particles in polymethyl methacrylate supercritical carbon dioxide microcellular foaming,” Ind. Eng. Chem. Res., vol. 52, no. 39, pp. 14169–14178, 2013.

97. L. Chen, R. Ozisik, and L. S. Schadler, “The influence of carbon nanotube aspect ratio on the foam morphology of MWNT/PMMA nanocomposite foams,” Polymer (Guildf)., vol. 51, no. 11, pp. 2368–2375, 2010.

98. C. Zeng, N. Hossieny, C. Zhang, and B. Wang, “Synthesis and processing of PMMA carbon nanotube nanocomposite foams,” Polymer (Guildf)., vol. 51, no. 3, pp. 655–664, 2010.

99. C. Zeng, N. Hossieny, C. Zhang, B. Wang, and S. M. Walsh, “Morphology and tensile properties of PMMA carbon nanotubes nanocomposites and nanocomposites foams,” Compos. Sci. Technol., vol. 82, pp. 29–37, 2013.

100. M. P. Tran, C. Detrembleur, M. Alexandre, C. Jerome, and J. M. Thomassin, “The influence of foam morphology of multi-walled carbon nanotubes/poly(methyl methacrylate) nanocomposites on electrical conductivity,” Polymer (Guildf)., vol. 54, no. 13, pp. 3261–3270, 2013.

101. Q. Shen, H. Yuan, Y. L. Xiong, G. Q. Luo, and L. M. Zhang, “The Structure and Electrical Conductivity of the CNTs/PMMA Nanocomposites Foams,” Key Eng. Mater., vol. 602–603, pp. 1048–1051, 2014.

102. Y. L. Xiong, Q. Shen, H. Yuan, F. Chen, and G. Q. Luo, “Foaming of CNTs/PMMA Nanocomposite with Supercritical Carbon Dioxide,” Key Eng. Mater., vol. 508, pp. 61–64, 2012.

103. L. Chen, L. S. Schadler, and R. Ozisik, “An experimental and theoretical investigation of the compressive properties of multi-walled carbon nanotube/poly(methyl methacrylate) nanocomposite foams,” Polymer (Guildf)., vol. 52, no. 13, pp. 2899–2909, 2011.

104. H. Yuan, Y. Xiong, Q. Shen, G. Luo, D. Zhou, and L. Liu, “Synthesis and electromagnetic absorbing performances of CNTs/PMMA laminated nanocomposite foams in X-band,” Compos. Part A Appl. Sci. Manuf., vol. 107, no. December 2017, pp. 334–341, 2018.

105. T. Li, G. Zhao, G. Wang, L. Zhang, and J. Hou, “Thermal-Insulation, Electrical, and Mechanical Properties of Highly-Expanded PMMA/MWCNT Nanocomposite Foams Fabricated by Supercritical CO_2 Foaming,” Macromol. Mater. Eng., vol. 1800789, pp. 1–14, 2019.

106. V. Realinho, M. Antunes, A. B. Martínez, and J. I. Velasco, “Influence of nanoclay concentration on the CO_2 diffusion and physical properties of PMMA montmorillonite microcellular foams,” Ind. Eng. Chem. Res., vol. 50, no. 24, pp. 13819–13824, 2011.

107. K. Goren, L. Chen, L. S. Schadler, and R. Ozisik, “Influence of nanoparticle surface chemistry and size on supercritical carbon dioxide processed nanocomposite foam morphology,” J. Supercrit. Fluids, vol. 51, no. 3, pp. 420–427, 2010.

108. D. Rende, L. S. Schadler, and R. Ozisik, “Controlling Foam Morphology of Poly(methyl methacrylate) via Surface Chemistry and Concentration of Silica Nanoparticles and Supercritical Carbon Dioxide Process Parameters,” J. Chem., vol. 2013, pp. 1–13, 2013.

109. Y. Wang, X. Liao, S. Li, Y. Luo, Q. Yang, and G. Li, “Poly(methyl methacrylate) nanocomposites based on graphene oxide: a comparative investigation of the effects of surface chemistry on properties and foaming behavior,” Polym. Int., vol. 65, no. 10, pp. 1195–1203, 2016.

110. Y. Wang, X. Liao, Y. Luo, Q. Yang, and G. Li, “Influence of Surface-functionalized Graphene Oxide on the Cell Morphology of Poly(methyl methacrylate) Composite,” J. Mater. Sci. Technol., vol. 31, no. 5, pp. 463–466, 2015.

111. M. Li, P. Cheng, R. Zhang, G. Luo, Q. Shen, and L. Zhang, “Preparation of PMMA/graphene oxide microcellular foams using supercritical carbon dioxide,” IOP Conf. Ser. Mater. Sci. Eng., vol. 87, no. 1, 2015.

112. C. Zeng, X. Han, L. J. Lee, K. W. Koelling, and D. L. Tomasko, “Polymer-Clay Nanocomposite Foams Prepared Using Carbon Dioxide,” Adv. Mater., vol. 15, no. 20, pp. 1743–1747, 2003.

113. M. Antunes, V. Realinho, G. Gedler, D. Arencón, and J. I. Velasco, "Diffusion of CO_2 in Polymer Nanocomposites Containing Different Types of Carbon Nanoparticles for Solid-State Microcellular Foaming Applications," J. Nano Res., vol. 26, pp. 63–74, 2013.

114. S. E. Zakiyan, H. Azizi, and I. Ghasemi, "Effect of cell morphology on electrical properties and electromagnetic interference shielding of graphene-poly(methyl methacrylate) microcellular foams," Compos. Sci. Technol., vol. 157, pp. 217–227, 2018.

115. M. Li, P. Cheng, L. Cheng, Q. Shen, and L. Zhang, "Effect of graphene surface functional groups on the mechanical property of pmma microcellular composite foams," Journal of Wuhan University of Technology-Mater. Sci. Ed, pp. 717-722, 2019.

116. M. Li, P. Cheng, G. Luo, Q. Shen, and L. Zhang, "Graphene nanoribbons (GNRs) by unzipping MWCNTs for the improvement of PMMA microcellular foams," J. Appl. Polym. Sci., vol. 134, no. 32, pp. 1–8, 2017.

117. A. B. Martínez, V. Realinho, M. Antunes, M. L. Maspoch, and J. I. Velasco, "Microcellular foaming of layered double hydroxide-polymer nanocomposites," Ind. Eng. Chem. Res., vol. 50, no. 9, pp. 5239–5247, 2010.

118. N. Novendra, N. Hasirci, and C. Dilek, "Supercritical processing of CO_2-philic polyhedral oligomeric silsesquioxane (POSS)-poly(L-lactic acid) composites," J. Supercrit. Fluids, vol. 117, pp. 230–242, 2016.

119. E. Ayandele, B. Sarkar, and P. Alexandridis, "Polyhedral Oligomeric Silsesquioxane (POSS)-Containing Polymer Nanocomposites," Nanomaterials, vol. 2, no. 4, pp. 445–475, 2012.

120. S. Costeux and L. Zhu, "Low density thermoplastic nanofoams nucleated by nanoparticles," Polymer (Guildf)., vol. 54, no. 11, pp. 2785–2795, 2013.

121. C. Dilek, “Supercritical carbon dioxide-soluble polyhedral oligomeric silsesquioxane (POSS) nanocages and polymer surface modification,” J. Supercrit. Fluids, vol. 73, pp. 171–177, 2013.

122. B. Kanya and C. Dilek, “Effects of functional groups on the solubilities of polyhedral oligomeric silsesquioxanes (POSS) in supercritical carbon dioxide,” J. Supercrit. Fluids, vol. 102, pp. 17–23, 2015.

123. Z. Ma, G. Zhang, Q. Yang, X. Shi, and A. Shi, “Fabrication of microcellular polycarbonate foams with unimodal or bimodal cell-size distributions using supercritical carbon dioxide as a blowing agent,” J. Cell. Plast., vol. 50, no. 1, pp. 55–79, 2014.

124. X. Xin, Q. Q. Liu, C. X. Chen, Y. X. Guan, and S. J. Yao, “Fabrication of bimodal porous PLGA scaffolds by supercritical CO_2 foaming/particle leaching technique,” J. Appl. Polym. Sci., vol. 133, no. 27, pp. 1–9, 2016.

125. A. Salerno, E. Di Maio, S. Iannace, and P. A. Netti, “Solid-state supercritical CO_2 foaming of PCL and PCL-HA nano-composite: Effect of composition, thermal history and foaming process on foam pore structure,” J. Supercrit. Fluids, vol. 58, no. 1, pp. 158–167, 2011.

126. C. Demirtas and C. Dilek, “Enhanced solubility of siloxy-modified polyhedral oligomeric silsesquioxanes in supercritical carbon dioxide,” J. Supercrit. Fluids, vol. 143, no. September 2018, pp. 358–364, 2019.

127. B. Dumanlilar and C. Dilek, “Phase Behavior of Carbon Dioxide and Polyhedral Oligomeric Silsesquioxanes with Two Different Functional Groups,” J. Supercrit. Fluids, vol. 163, p. 104860, 2020, doi: 10.1016/j.supflu.2020.104860.

128. A. Gebrekrstos, M. Sharma, S. Bahl, G. Madras, S. Suwas, and S. Bose, “Process mediated polymorphism, crystallographic texture and structure-property correlation in crystalline/amorphous blends,” Polymer (Guildf)., vol. 138, pp. 307–319, 2018, doi: 10.1016/j.polymer.2018.01.075.

129. E. Saldívar-Guerra, and E. Vivaldo-Lima, “Handbook of Polymer Synthesis, Characterization, and Processing,” U.S.A., 2013.

130. P.K. Vallittu, Curing of a silane coupling agent and its effect on the transverse strength of autopolymerizing polymethylmethacrylate-glass fibre composite, Journal of Oral Rehabilitation vol. 24, pp. 124-130, 1997.

131. H. Abbasi, M. Antunes, and J. I. Velasco, Effects of carbon nanotubes/graphene nanoplatelets hybrid systems on the structure and properties of polyetherimide-based foams, Polymers (Basel)., vol. 10, pp. 1-22, 2018, doi: 10.3390/polym10040348.

132. M. Pantoja, F. Velasco, D. Broekema, J. Abenojar, J.C. Del Real, The influence of pH on the hydrolysis process of γ-methacryloxypropyltrimethoxysilane, analyzed by FTIR, and the silanization of electrogalvanized steel, J. Adhes. Sci. Technol. vol. 24 pp. 1131–1143, 2010. https://doi.org/10.1163/016942409X12586283821559.

133. Q. Liu, J. Ding, D.E. Chambers, S. Debnath, S.L. Wunder, G.R. Baran, Filler-coupling agent-matrix interactions in silica / polymethylmethacrylate composites, (2001).

134. Duan G, Zhang C, Li A, Yang X, Lu L, Wang X. Preparation and Characterization of Mesoporous Zirconia Made by Using a Poly(methyl methacrylate) Template. Nanoscale Res Lett vol. 118 pp. 22, 2008. doi:10.1007/s11671-008-9123-7.

135. H. Kaczmarek, A. Kamińska, and A. Van Herk, “Photooxidative degradation of poly(alkyl methacrylate)s,” Eur. Polym. J., vol. 36, no. 4, pp. 767–777, 2000.

136. R.Y. Hong, H. P. Fu, Y. J. Zhang, L. Liu, J. Wang, H. Z. Li, Y. Zheng, “Surface-modified silica nanoparticles for reinforcement of PMMA,” J. App. Polym. Sci. vol. 105, pp. 2176–2184, 2007.

137. G. Tagliavia, M. Porfiri, and N. Gupta, “Analysis of flexural properties of hollow-particle filled composites,” Compos. Part B Eng., vol. 41, no. 1, pp. 86–93, 2010.

138. T. Kanie, H. Arikawa, K. Fujii, and K. Inoue, “Physical and mechanical properties of PMMA resins containing γ-methacryloxypropyltrimethoxysilane,” J. Oral Rehabil., vol. 31, no. 2, pp. 166–171, 2004, doi: 10.1111/j.1365-2842.2004.01043.x.

139. J.Z. Liang, C.B. Wu, Z.C. Wei, “Correlation between impact strength and fracture surface fractal dimension of ABS filled with hollow glass beads,” Polym Adv Technol vol.23 pp. 108-113, 2012 http://dx.doi.org/10.1002/pat.1831.

140. T.C. Lin, G. Nikhil, T. Anton, “Thermoanalytical characterization of epoxy matrix-glass microballoon syntactic foams,”. J Mater Sci vol. 1520, pp. 7, 2009 http://dx.doi.org/10. 1007/s10853-008-3074-3.

141. B. Zhu, J. Ma, J. Wang, J. Wu, and D. Peng, “Thermal, dielectric and compressive properties of hollow glass microsphere filled epoxy-matrix composites,” J. Reinf. Plast. Compos., vol. 31, no. 19, pp. 1311–1326, 2012, doi: 10.1177/0731684412452918.

142. A. Asano, K. Takegoshi, and K. Hikichi, “Inter-Polymer Interaction of Polymer Blend in Solution as Studied by NMR: Polycarbonate/Poly (methyl methacrylate).,” Polym. J., vol. 24, no. 5, pp. 473–477, 2005.

143. J. S. Meth et al., “Development of filler structure in colloidal silica-polymer nanocomposites,” Macromolecules, vol. 44, no. 20, pp. 8301–8313, 2011.J.S. Meth et al., 2011].

144. M. Kumar, V. Kumar, P. Upadhyaya, and G. Pugazhenthi, “Fabrication of poly(methyl methacrylate) (PMMA) nanocomposites with modified nanoclay by melt intercalation,” Compos. Interfaces, vol. 21, no. 9, pp. 819–832, 2014.

145. Z. Vuluga, M.C. Corobea, C. Elizetxea, M. Ordonez, M. Ghiurea, V. Raditoui, C.A. Nicolae, D. Florea, M. Lorga, R. Somoghi, and B. Trica, "Morphological and tribological properties of PMMA/halloysite nanocomposites," Polymers (Basel)., vol. 10, no. 8, pp. 816, 2018.

146. J. Gu, C. Liang, J. Dang, W. Dong, and Q. Zhang, "Ideal dielectric thermally conductive bismaleimide nanocomposites filled with polyhedral oligomeric silsesquioxane functionalized nanosized boron nitride," RSC Adv., vol. 6, no. 42, pp. 35809–35814, 2016.

147. R. Sastre et al., "Dye-doped polyhedral oligomeric silsesquioxane (poss)-modified polymeric matrices for highly efficient and photostable solid-state lasers," Adv. Funct. Mater., vol. 19, no. 20, pp. 3307–3316, 2009.

148. M. Ozkutlu, G. Bayram, C. Dilek, "Highly CO_2-philic polyhedral oligomeric silsesquioxanes (POSS) as hybrid cell nucleators for more efficient supercritical carbon dioxide foaming of poly(methyl methacrylate) (PMMA)," In 17th European Meeting on Supercritical Fluids (EMSF 2019) - 7th European Meeting on High Pressure Technology; Real, Spain, 2019.

149. J. Li, G. Zhang, H. Zhang, X. Fan, L. Zhou, Z. Shang, X. Shi, Electrical conductivity and electromagnetic interference shielding of epoxy nanocomposite foams containing functionalized multi-wall carbon nanotubes, Appl. Surf. Sci. 428 (2018) 7–16. https://doi.org/10.1016/j.apsusc.2017.08.234.

150. Y. Culhacıoglu, N. Hasirci, C. Dilek, "Highly Crystalline Poly(l-lactic acid) Porous Films Prepared with CO_2-philic, Hybrid, Liquid Cell Nucleators", Ind. Eng. Chem. Res., 58, 50, 22541-22550, 2019.

151. E. Di Maio, E. Kiran, Foaming of polymers with supercritical fluids and perspectives on the current knowledge gaps and challenges, J. Supercrit. Fluids. 134 (2018) 157–166. https://doi.org/10.1016/j.supflu.2017.11.013.

152. E. Kiran, Foaming strategies for bioabsorbable polymers in supercritical fluid mixtures. Part II. Foaming of poly(ε-caprolactone-co-lactide) in carbon dioxide and

carbon dioxide + acetone fluid mixtures and formation of tubular foams via solution extrusion, J. Supercrit. Fluids. 54 (2010) 296–307. https://doi.org/10.1016/j.supflu.2010.05.005.

153. M.T. Ngo, J.S. Dickmann, J.C. Hassler, E. Kiran, "A new experimental system for combinatorial exploration of foaming of polymers in carbon dioxide: The gradient foaming of PMMA," J. Supercrit. Fluids. vol. 109, pp. 1–19, 2015. https://doi.org/10.1016/j.supflu.2015.09.030.

154. H. M. J. Hung, R. T. O'Neill, P. Bauer, and K. Kohne, "The Behavior of the P-Value When the Alternative Hypothesis is True," Biometrics, vol. 53, no. 1, p. 11, 1997, doi: 10.2307/2533093.

155. A.R. Manninen, H.E. Naguib, A.V. Nawaby, X. Liao, M. Day, "The effect of clay content on PMMA-clay nanocomposite foams," Cell. Polym. Vol. 24, pp. 49–70, 2005. https://doi.org/10.1177/026248930502400201.

156. A.R. Manninen, H.E. Naguib, A.V. Nawaby, M. Day, "CO_2 sorption and diffusion in polymethyl methacrylate-clay nanocomposites," Polym. Eng. Sci. vol. 45 pp. 904–914, 2005. https://doi.org/10.1002/pen.20350.

157. L.J. Lee, C. Zeng, X. Cao, X. Han, J. Shen, G. Xu, "Polymer nanocomposite foams," Compos. Sci. Technol. vol. 65, pp. 2344–2363, 2005. https://doi.org/10.1016/j.compscitech.2005.06.016.

APPENDICES

A. Viscosity Average Molecular Weight Calculations

The viscosity average molecular weight of the PMMA was determine during Kramer-Huggins plot. The intersection of the reduced viscosity (η_{red}) and the inherent viscosity (η_{inh}) gave the intrinsic viscosity ([η]) of PMMA in acetone. The viscosity average molecular weight of PMMA was obtained by the help of Kraemer-Huggins equation.

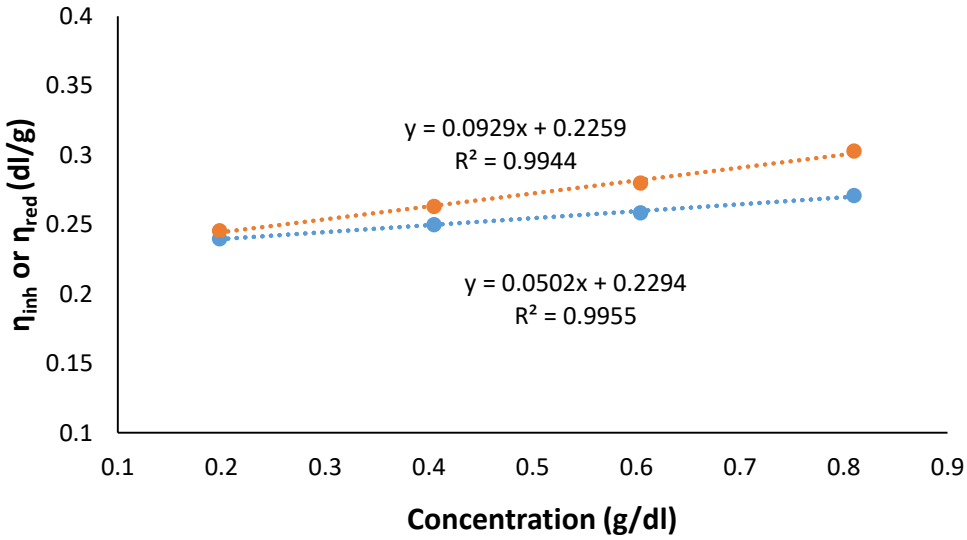

Figure A.1 Kraemer-Huggins plot for PMMA in acetone.

B. Silanization Process

Adhesion between the silane and the glass is based on two types of bonds. One of those bonds is a siloxane bridge formed by a condensation reaction between silanol groups and the silica surface. Simultaneously with this condensation reaction, the carbonyl group of the silanol molecule forms hydrogen bonds. Consequently, the condensation of the silane coupling agent is also important for the adhesion between PMMA and glass [130].

Adhesion between the silane and the glass is based on two types of bonds. One of them is the hydrogen bonding between silanol groups of MPS and silica (Form A). The other one is that the hydrogen bonding of C=O and silanol groups (Form C) and forming multilayers through hydrogen bonding (Form C). At lower silane concentrations, silane molecules will be adsorbed onto the surface of silica mainly in Form A or B. With increased silane concentration, Form C can occur. Form A will only give rise to a free C=O band in the FTIR spectrum at 1718 cm^{-1} and Form B will only give rise to a hydrogen bonded C=O band at 1700 cm^{-1}. Form C and mixed forms (Form A + form B) will give rise to bands at both 1718 and 1700 cm^{-1}. After drying at room temperature under vacuum, the surface hydrogen bonded silane (Form A) was possibly converted to covalently bonded silane through the condensation between silanol groups of the silane and surface hydroxyl group of silica [133]. Consequently, the condensation of the silane coupling agent is also important for the adhesion between PMMA and glass [130].

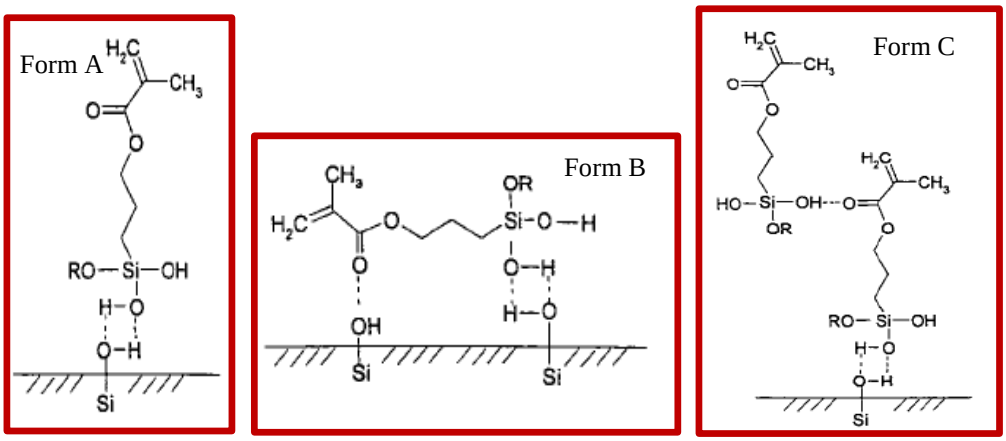

Figure B.1 Possible interactions of MPS and glass.

C. Mechanical Properties of PMMA Foams and Composites

Table C.1 Mechanical properties of PMMA syntactic foams.

Sample Code	Flexural strength (MPa)	Flexural modulus (MPa)	Impact resistance (kJ/m^2)
PMMA	107.85 ± 5.28	3207 ± 184	12.60 ± 1.67
PMMA/LD-H5	83.75 ± 3.99	3688 ± 149	11.01 ± 1.69
PMMA/LD-H10	75.86 ± 5.78	4042 ± 96	9.49 ± 1.00
PMMA/LD-H15	62.83 ± 3.66	4316 ± 173	8.82 ± 0.62
PMMA/MD-H5	82.46 ± 5.08	3613 ± 149	10.61 ± 0.42
PMMA/MD-H10	74.97 ± 5.84	3695 ± 240	9.80 ± 1.00
PMMA/MD-H15	69.80 ± 12.59	3750 ± 298	8.34 ± 0.63
PMMA/HD-H5	85.41 ± 3.77	3815 ± 97	12.18 ± 1.99
PMMA/HD-H10	79.58 ± 5.34	3845 ± 132	9.62 ± 0.58
PMMA/HD-H15	78.64 ± 2.6	3920 ± 236	8.21 ± 1.16
PMMA/HD-HC15	88.30 ± 4.56	3846 ± 375	9.63 ± 0.62
PMMA/HD-HS15	63.03 ± 4.48	3219 ± 142	11.45 ± 0.42

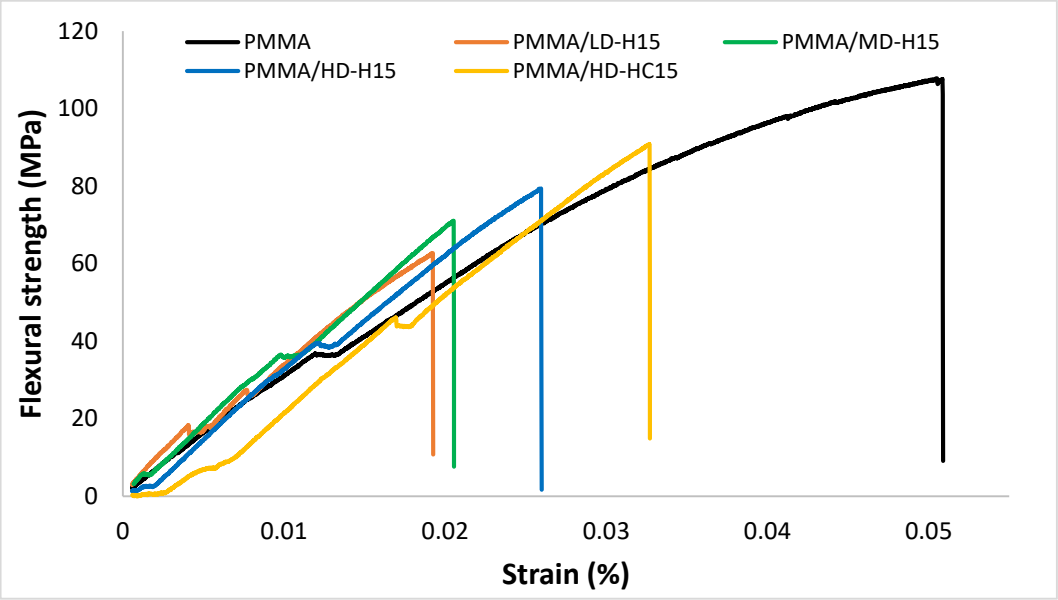

Figure C.1. Stress-strain curves of the PMMA and the PMMA syntactic foams.

Table C.2 Mechanical properties of PMMA-POSS composites.

Sample Code	Flexural strength (MPa)	Flexural modulus (MPa)	Impact resistance (kJ/m^2)
PMMA	107.85 ± 5.28	3208 ± 184	12.60 ± 1.67
PMMA/P0.25	118.60 ± 7.17	3269 ± 209	15.04 ± 1.28
PMMA/P0.5	126.78 ± 3.07	3329 ± 332	18.09 ± 2.69
PMMA/P1	126.95 ± 3.02	3547 ± 124	15.15 ± 3.21
PMMA/P3	116.00 ± 1.46	3051 ± 192	11.47 ± 1.32
PMMA/IB0.25	118.21 ± 5.12	3092 ± 129	18.21 ± 1.89
PMMA/IB0.5	116.80 ± 1.23	3197 ± 101	18.81 ± 3.00
PMMA/IB1	118.08 ±2.25	3121 ± 139	14.93 ± 1.92
PMMA/IB3	104.80 ± 1.19	2959 ± 239	14.53 ± 1.27

Table C.3 Specific mechanical properties of PMMA hybrid syntactic foams.

Sample Code	Specific flexural strength ($MPa/g.cm^{-3}$)	Specific flexural modulus ($MPa/g.cm^{-3}$)	Specific impact resistance ($kJ.m^{-2}/g.cm^{-3}$)
PMMA	102.02 ± 3.34	2643 ± 158	18.16 ± 1.54
PMMA/H5/P0	92.01 ± 1.78	3069 ± 117	17.45 ± 0.72
PMMA/H5/P0.25	97.17 ± 2.32	3329 ± 67	14.99 ± 1.02
PMMA/H5/P0.5	92.65 ± 5.09	3098 ± 140	14.31 ± 0.45
PMMA/H5/P1	89.30 ± 3.31	3194 ± 135	12.22 ± 0.65
PMMA/H10/P0	79.44 ± 3.18	3418 ± 128	10.89 ± 0.76
PMMA/H10/P0.25	76.26 ± 2.41	3384 ± 63	10.60 ± 0.94
PMMA/H10/P0.5	81.14 ± 4.50	3406 ± 108	10.04 ± 0.50
PMMA/H10/P1	84.58 ± 3.22	3547 ± 67	9.83 ± 0.18
PMMA/H15/P0	71.42 ± 3.12	3571 ± 54	10.36 ± 0.56
PMMA/H15/P0.25	78.50 ± 2.69	3637 ± 63	10.39 ± 1.03
PMMA/H15/P0.5	82.41 ± 2.51	3500 ± 113	10.74 ± 0.67
PMMA/H15/P1	78.96 ± 3.08	3494 ± 221	10.17 ± 0.49

D. Pore Densities and The Densities of The PMMA Foams

Table D.1 Pore densities of the PMMA and PMMA-POSS composite foams processed with $scCO_2$.

Experimental conditions	Pore Density (number of pores/cm^3)		
	Neat PMMA	**PMMA/TMS0.5**	**PMMA/TMS5**
35°C-24 h-11 MPa-F	6.08E+10	6.7E+10	5.45E+11
35°C-24 h-11 MPa-S	2.81E+10	1.39E+11	2.22E+11
35°C-24 h-32 MPa-F	3.1E+11	9.91E+10	6.33E+12
35°C-24 h-32 MPa-S	2.68E+08	4.54E+07	2.65E+12
100°C-2 h-32 MPa-F	-	-	1.97E+10
100°C-2 h-32 MPa-S	9.50E+04	7.44E+04	1.17E+08
100°C-24 h-11 MPa-F	7.06E+06	1.72E+07	1.26E+08
100°C-24 h-11 MPa-S	4.61E+04	8.49E+04	2.19E+06

Table D.2 Densities of the PMMA and PMMA-POSS composite foams processed with $scCO_2$.

Experimental conditions	Density (g/cm^3)		
	Neat PMMA	**PMMA/TMS0.5**	**PMMA/TMS5**
Bulk polymer	1.20	1.20	1.19
35°C-24 h-11 MPa-F	0.48 ± 0.05	0.87 ± 0.06	0.75 ± 0.05
35°C-24 h-11 MPa-S	0.52 ± 0.04	0.56 ± 0.03	0.47 ± 0.03
35°C-24 h-32 MPa-F	0.47 ± 0.01	0.38 ± 0.03	0.40
35°C-24 h-32 MPa-S	0.45 ±	0.29 ± 0.03	0.26 ± 0.01
100°C-2 h-32 MPa-F	-	-	0.20 ± 0.01
100°C-2 h-32 MPa-S	0.39 ± 0.04	0.34 ± 0.01	0.31
100°C-24 h-11 MPa-F	0.32 ± 0.02	0.26 ± 0.04	0.33 ± 0.03
100°C-24 h-11 MPa-S	0.25 ± 0.03	0.30 ± 0.05	0.31 ± 0.02

Table D.3 Densities of PMMA composites and PMMA composite foams processed with $scCO_2$.

Experimental condition	**Density (g/cm^3)**	
Unprocessed polymer		
PMMA	1.20	
PMMA/H5/TMS0	1.18	
PMMA/H5/TMS5	1.19	
PMMA/H15/TMS0	1.08	
PMMA/H15/TMS5	1.10	
Foams		
Processing time	**2h**	**24h**
PMMA/H5/TMS0 11 MPa	1.18 ± 0.01	0.93 ± 0.03
PMMA/H5/TMS5 11 MPa	1.19 ± 0.02	0.83 ± 0.08
PMMA/H15/TMS0 11 MPa	1.07 ± 0.02	1.07 ± 0.03
PMMA/H15/TMS5 11 MPa	1.07 ± 0.02	0.38 ± 0.02
PMMA/H5/TMS0 22 MPa	1.11 ± 0.03	0.55 ± 0.05
PMMA/H5/TMS5 22 MPa	1.11 ± 0.07	0.48 ± 0.04
PMMA/H15/TMS0 22 MPa	1.06 ± 0.02	0.68 ± 0.02
PMMA/H15/TMS5 22 MPa	1.1 ± 0.05	0.56 ± 0.02

E. Thermal Properties of PMMA Foams

Table E.1 Glass transition temperatures of the PMMA and PMMA composite foams processed with $scCO_2$.

Experimental conditions	Tg (°C)		
	Neat PMMA	**PMMA/TMS0.5**	**PMMA/TMS5**
Bulk polymer	116	115	120
35°C-24 h-11 MPa-F	121	121	125
35°C-24 h-11 MPa-S	121	122	122
35°C-24 h-32 MPa-F	122	122	122
35°C-24 h-32 MPa-S	123	119	123
100°C-2 h-32 MPa-F	-	-	113
100°C-2 h-32 MPa-S	118	119	118
100°C-24 h-11 MPa-F	117	116	116
100°C-24 h-11 MPa-S	114	116	120

F. JMP Output of the DOE Results

Sorted Parameter Estimates

Term		Estimate	Relative Std Error	Pseudo t-Ratio	Pseudo p-Value
Temperature(35,100)	Biased	27.588983	0.500287	1.58	0.2031
Temperature*Venting rate		-20.16102	0.516949	-1.12	0.3377
Time(2,24)	Biased	22.842373	0.707513	0.93	0.4168
Time*Venting rate		-17.00763	0.731077	-0.67	0.5483
Venting rate(1,62)		-3.411864	0.516949	-0.19	0.8609
Pressure(1600,4600)	Biased	-0.15	0.500287	-0.01	0.9936
Pressure*Venting rate		-1.78e-15	0.516949	-0.00	1.0000
Temperature*Pressure	Zeroed	0	0	.	.
Temperature*Time	Zeroed	0	0	.	.
Pressure*Time	Zeroed	0	0	.	.

Figure F.1 The sorted parameter estimates for the pore size of PMMA/TMS5 composite foams.

Sorted Parameter Estimates

Term		Estimate	Relative Std Error	Pseudo t-Ratio	Pseudo p-Value
POSS%(0,5)	Biased	-0,475	0,5	-3,62	0,0305*
HGM%*Pressure		-0,3	0,5	-2,29	0,0975
Pressure(1600,3200)	Biased	-0,1	0,5	-0,76	0,4964
HGM%(5,15)	Biased	0,075	0,5	0,57	0,6040
HGM%*POSS%		0,075	0,5	0,57	0,6040
Time(2,24)	Zeroed	0	0	.	.
HGM%*Time	Zeroed	0	0	.	.
Pressure*Time	Zeroed	0	0	.	.
Pressure*POSS%	Zeroed	0	0	.	.
Time*POSS%	Zeroed	0	0	.	.

Figure F.2 The most effective parameters on the pore size of PMMA-HGM-POSS composite foams.

CURRICULUM VITAE

PERSONAL INFORMATION

Surname, Name: Özkutlu Demirel, Merve
Nationality: Turkish (TC)
Date and Place of Birth: 11 April 1989, Edirne
Marital Status: Married
Phone: +90 505 418 30 29
email: mrv.ozkutlu@gmail.com

EDUCATION

Degree	Institution	Year of Graduation
MS	Hacettepe University Chemical Engineering	2014
BS	Ankara University Chemical Engineering	2012
High School	Milli Piyango Anadolu High School, Ankara	2007

WORK EXPERIENCE

Year	Place	Enrollment
2019-Present	Turkish Aerospace	Technology Development Engineer
2013-2019	METU Dept. of Chemical Eng.	Research Assistant
2011 August	Turkish Aerospace	Intern Eng. Student
2010 July	Petkim	Intern Eng. Student

FOREIGN LANGUAGES

Advanced English

PUBLICATIONS

1. M. Ozkutlu, C. Dilek, and G. Bayram, “Poly(methyl methacrylate) hybrid syntactic foams with hollow glass microspheres and polyhedral oligomeric silsesquioxanes,” J. Appl. Polym. Sci., vol. 137, no. 7, pp. 1–9, 2020, doi: 10.1002/app.48368.

2. M. Ozkutlu, C. Dilek, and G. Bayram, “Effects of hollow glass microsphere density and surface modification on the mechanical and thermal properties of poly(methyl methacrylate) syntactic foams,” Compos. Struct., vol. 202, no. February, pp. 545–550, 2018.

3. M. Ozkutlu, O.Y. Orhan, H.Y. Ersan, E. Alper, “Kinetic performance of ionic liquid–diethanolamine system for CO_2 absorption”, Chemical Data Collections, vol. 2, pp. 25-35, 2016. https://doi.org/10.1016/j.cdc.2016.05.001

4. M. Ozkutlu, O.Y. Orhan, H.Y. Ersan, E. Alper, “Kinetics of CO_2 capture by ionic liquid—CO_2 binding organic liquid dual systems, Chemical Engineering and Processing: Process Intensification, vol. 101, pp. 50-55, 2016. https://doi.org/10.1016/j.cep.2015.12.011

PROCEEDINGS OF INTERNATIONAL CONFERENCES

1. M. Ozkutlu, G. Bayram, C. Dilek, “Highly CO_2-philic polyhedral oligomeric silsesquioxanes (POSS) as hybrid cell nucleators for more efficient supercritical carbon dioxide foaming of poly(methyl methacrylate) (PMMA),” In 17th European Meeting on Supercritical Fluids (EMSF 2019) - 7th European Meeting on High Pressure Technology; Ciudad Real, Spain, 2019.

2. M. Ozkutlu, C. Dilek, G. Bayram, “Enhancement of properties of PMMA hybrid syntactic foams containing polyhedral oligomeric silsesquioxane (POSS),” In 21st International Conference on Composite Structures (ICCS21), Bologna, Italy, 2018.

3. M. Ozkutlu, C. Dilek, G. Bayram, “Mechanical and thermal characterization of PMMA syntactic foams,” In 20th International Conference on Composite Structures (ICCS20), Paris, France, 2017.

4. M. Ozkutlu, C. Dilek, G. Bayram, “Sentaktik PMMA köpük üretimi ve karakterizasyonu,” In 12th Ulusal Kimya Mühendisliği Kongresi, Izmir, Turkey, 2016.

HOBBIES

I have been playing guitar as an amateur since 2001 which supply me the ability of refresh and start working again. I have a curiosity on modern art especially on paintings since the perspective of modern artist on issues of our century makes me feel excited. I enjoy visiting modern art museums.